



## PhD thesis

Lisbeth Marner

# Molecular Brain Imaging of the Serotonin System: Reproducibility and Evaluation of PET Radiotracers

Academic advisor: Gitte Moos Knudsen

Submitted: 31/10/2008

### *Institute*

Neurobiology Research Unit, Rigshospitalet, Copenhagen, Denmark.

### *Supervisors*

Professor Gitte Moos Knudsen, MD, Dr.Med., Neurobiology Research Unit, The Neuroscience Centre, Copenhagen University Hospital Rigshospitalet.

Associate Professor Steen Gregers Hasselbalch, MD, Dr.Med., Neurobiology Research Unit, The Neuroscience Centre, Copenhagen University Hospital Rigshospitalet.

### *Review Committee*

Lars Friberg, MD, Dr.Med., (Chairman), Department of Clinical Physiology and Nuclear Medicine, Bispebjerg Hospital, University of Copenhagen.

Professor Richard E. Carson, PhD., Yale PET Center, Yale University School of Medicine, New Haven, USA.

Ian Law, MD, PhD, Dr.Med., Department of Clinical Physiology and Nuclear Medicine, Copenhagen University Hospital Rigshospitalet.

Front cover image: Scan with [<sup>11</sup>C]SB207145 in a human brain (male, 25 years) illustrated as standard uptake values and aligned to the MR image of the same subject. Mean of 60 to 120 min post injection normalized to Injected Dose (ID).

## Acknowledgements

I have spent the last 3.5 exciting and rich years at the Neurobiology Research Unit, which houses a number of inspiring people from various scientific backgrounds giving the place a unique and highly stimulating atmosphere.

I wish to sincerely thank my supervisors. Professor Gitte Moos Knudsen has with invaluable enthusiasm and experience guided me through the entire study. You have scientifically questioned my sometimes too hasty conclusions and been a model for the broadness of your knowledge in PET. Steen G. Hasselbalch, you have been ever present with your invariably good mood and helpfulness and I have learned much from our numerous discussions about dementia and Alzheimer's disease. Roger N. Gunn, although you have not been an official supervisor, you have nonetheless taken the task of teaching me modeling and simulations, for which I am deeply grateful for. Thank you very much. A special thank to Dorthe Givard, Pia Farup, Karin Stahr, Bente Høy, Anita Dole, and Blerta Shuka for technical and administrative assistance as well as the countless hours of your pleasant and entertaining company. David Erritzøe and Vibe Frøkjær, thank you for patiently teaching me how to perform PET scans and for all the fun hours, practical help, and fruitful discussions. I wish to thank the technicians working in the PET unit for their helpfulness and the radiochemists for their continuing high spirit in the synthesis of radiotracers. Special and sincere thanks to Nic Gillings for fruitful cooperation in solving the problems with the metabolite analysis. I thank Claus Svarer for his invaluable help and support during my time at NRU and for the enjoyable discussions. I wish to express my gratitude to my coworkers at NRU for inspiration and for practical help during the PET scans, especially Celia Kjær, Mikael Palner, Anders Bue Marcussen, Anders Ettrup, Birgitte Kornum, Lene Rottenstein, Tine Arentzen, and Haroon Arfan. I am deeply grateful to the test persons for their participation in the study and I wish to express my particular gratitude to Karine Madsen, Mette Haarh, Stina Syvänen, Bjarni Bödvarson, Jens Munk Hansen, Anetta Claussen, Jan Kalbitzer, David Elmenhorst, Lene Theil Skovgaard, Lars Pinborg, Finn Nielsen, and Esben Høgh-Rasmussen for fun and inspiring scientific discussions. A special thank to Bente Pakkenberg and Hans Jørgen G. Gundersen for introducing me to neuroscience and the value of real quantification using stereology that I will always keep in mind. I wish to thank Paul Cumming for his thorough and insightful revision of manuscripts and this thesis and for numerous interesting discussions about PET. Other current and former people at NRU, as well as coauthors are thanked for their contribution to the work.

## Lisbeth Marner: Molecular Brain Imaging of the Serotonin System

Moreover, I wish to express my gratitude to the foundations from which I received financial support: University Hospital Rigshospitalet, The Lundbeck Foundation, and The John and Birthe Meyer Foundation for donation of the PET scanner.

Last but not least, I wish to thank my family and family in law for all your support and love, especially to my children Eva and Thor for being who you are, and to you, Jacob Marner for all the years.

## Table of Contents

Institute.....	1
Supervisors .....	1
Review Committee.....	1
Acknowledgements.....	2
Table of Contents.....	4
Summary.....	6
Dansk Resumé .....	8
List of Papers .....	10
Aims of the Thesis .....	11
Background.....	12
The Serotonin System .....	12
Positron Emission Tomography .....	15
Partial Volume Effect.....	16
Radioligands.....	19
Sensitivity to Endogenously Released Neurotransmitter.....	20
Kinetic Modeling.....	21
Introduction and Hypotheses .....	27
Evaluation of PET Ligands .....	28
Hypotheses .....	29
Material and Methods .....	29
Study 1: .....	29
Study 2: .....	30
Study 3.....	33
Statistics .....	35
Results and Discussion .....	36
Study 1.....	36
Study 2.....	40
Study 3.....	45
Conclusions and Perspectives.....	51
References.....	53

# Lisbeth Marner: Molecular Brain Imaging of the Serotonin System

Abbreviations and Terminology .....	61
Appendices .....	63
Paper 1	
Paper 2	
Paper 3	

## Summary

The serotonin system is involved not only in psychiatric and neurological diseases, but also in normal behavior, personality and cognition. Positron emission tomography (PET) with selective serotonin ligands has emerged as a key technique for assessing the status of serotonin systems in healthy brain and in diverse neuropsychiatric conditions. This thesis evaluates the longitudinal stability of brain [ $^{18}\text{F}$ ]altanserin PET measurements. In addition to assessment of this well-known radiotracer for 5-HT<sub>2A</sub> receptors, the thesis also presents a thorough evaluation of the novel tracer [ $^{11}\text{C}$ ]SB207145, the first useful tracer for brain molecular imaging of the 5-HT<sub>4</sub> receptor with PET.

[ $^{18}\text{F}$ ]Altanserin-PET was used to quantify brain 5-HT<sub>2A</sub>-receptors in 12 healthy elderly subjects at baseline, and at two-year follow-up. A bolus/infusion protocol was used to achieve steady-state conditions for the simple calculation of the binding potential,  $BP_p$ . The reproducibility of the test-retest data was assessed in terms of variability and reliability (intraclass correlation coefficient,  $ICC$ ), and was used to compare inter- to intraobserver stability, and to evaluate the stability and reliability of partial volume (PV) corrections of increasing complexity.

For the evaluation of the reproducibility of the  $BP_{ND}$  estimates obtained with the novel radiotracer [ $^{11}\text{C}$ ]SB207145, six subjects were scanned twice on the same day. A further two subjects were scanned before and after blocking with a selective 5-HT<sub>4</sub>-receptor inverse agonist. Arterial blood samples were drawn for the calculation of metabolite corrected arterial input functions. Quantitative tracer kinetic modeling was investigated with one (1-TC) and two (2-TC) tissue compartment models, using plasma input functions, and the  $BP_{ND}$  was also calculated non-invasively using the simplified reference tissue model (SRTM), with cerebellum serving as the reference region.

In a separate study of seven subjects, the sensitivity of [ $^{11}\text{C}$ ]SB207145 binding to competition from endogenous released serotonin was investigated with examinations at baseline, and after infusion of citalopram, a selective serotonin reuptake inhibitor, intended to increase the concentration of serotonin in the extracellular space.

The cerebral distribution of 5-HT<sub>4</sub> receptors was reported based on sixteen healthy humans and analyzed in relation to demographical data.

Sixteen subjects (six from the test-retest part and seven from the citalopram part) were included in a study of the cerebral distribution of 5-HT<sub>4</sub> receptors in healthy humans (<45 years).

There was no change in 5-HT<sub>2A</sub> receptor binding at two-year follow-up. The variability was 12-15% and *ICC* scores were 0.45-0.67 for large cortical regions with high binding, and when applying two-tissue PV correction. Variability was 14-22% and *ICC* scores were 0.46-0.72 when no partial volume correction was applied.

[<sup>11</sup>C]SB207145 time activity data was well described by the two-tissue compartment model and all models investigated were found to have good test-retest reproducibility and reliability. The blocking study confirmed the selectivity of the radioligand for the 5-HT<sub>4</sub> receptor, and substantiated that cerebellum was a suitable reference region devoid of specific binding. The citalopram study showed that [<sup>11</sup>C]SB207145 was not discernibly sensitive to endogenous released serotonin. We found a high rank order correlation between PET results and previously published autoradiographic data, supporting the validity of [<sup>11</sup>C]SB207145. Within the sample of 16, males were found to have significantly 15% greater 5-HT<sub>4</sub> receptors availability.

In conclusion, in healthy elderly individuals, brain 5-HT<sub>2A</sub>-receptor binding remains stable over two years and has an acceptable reproducibility and reliability in larger brain regions. Furthermore, the high intra- and interobserver stability lends [<sup>18</sup>F]-altanserin for use in longitudinal studies of patients with neuropsychiatric disorders. *In vivo* imaging of cerebral 5-HT<sub>4</sub> receptors can be reliably obtained in humans with [<sup>11</sup>C]207145 PET either with arterial input or with non-invasive SRTM. [<sup>11</sup>C]207145 binding was apparently invulnerable to fluctuations in serotonin level and appeared to have a sex difference.

## Dansk Resumé

Det serotonerge transmittersystem er involveret i en række fysiologiske hjernefunktioner, såsom regulering af fødeindtag, søvn, seksualadfærd og emotioner. Det er involveret i flere psykiatriske og neurologiske lidelser, men også i adfærd, personlighed og kognition hos raske. Denne afhandling evaluerer stabiliteten af det radiomærkede sporstof [ $^{18}\text{F}$ ]altanserin, der mærker hjernens serotonin 2A (5-HT<sub>2A</sub>) receptorer og evaluerer et nyt sporstof [ $^{11}\text{C}$ ]SB207145 til molekylær billeddannelse af hjernens serotonin 4 (5-HT<sub>4</sub>) receptorer med positron emissions tomografi (PET).

Ved at skanne 12 raske ældre forsøgspersoner med [ $^{18}\text{F}$ ]altanserin, fandt vi at hjernens 5-HT<sub>2A</sub>-receptorer kan kvantiteres stabilt over to år med en acceptabel reproducerbarhed og reliabilitet i større kortikale regioner samt en høj intra- og interobservatør stabilitet. Dette muliggør brugen af [ $^{18}\text{F}$ ]altanserin i opfølgingsstudier, der strækker sig over flere år.

For at evaluere det nye sporstof [ $^{11}\text{C}$ ]SB207145 blev seks forsøgspersoner skannet to gange same dag for at måle reproducerbarheden og yderligere to blev skannet før og efter blokering af receptoren med et andet stof, der binder sig til 5-HT<sub>4</sub> receptoren. Arterielle blodprøver blev taget for at kunne udregne en metabolit korrigeret arteriel input funktion til hjernen. Kvantitative kinetiske modeller blev brugt og sammenlignet med en non-invasiv model, simplified reference tissue model (SRTM), der ikke kræver anlæggelse af arterie kanyle. Vi fandt, at den ikke-invasive model kunne bruges til at kvantificere bindingen af [ $^{11}\text{C}$ ]SB207145 med høj reproducerbarhed og reliabilitet og blokeringsstudiet bekræftede brugen af cerebellum som referenceregion.

Derudover undersøgte vi følsomheden for endogent frigivet serotonin ved at skanne 7 forsøgspersoner med og uden infusion af citalopram, en selektiv serotonin reuptake inhibitor, der øger koncentrationen af serotonin ekstracellulært. Studiet viste, at [ $^{11}\text{C}$ ]SB207145 ikke var følsom for endogent frigivet serotonin og derved stabilt overfor akutte fluktuationer i serotonin niveau.

Fordelingen af 5-HT<sub>4</sub> receptorer i raske mennesker (<45 år) blev undersøgt, og vi fandt en høj rank-order korrelation til tidligere publicerede autoradiografiske data, hvilket understøtter validiteten af [ $^{11}\text{C}$ ]SB207145. Mænd have flere tilgængelige 5-HT<sub>4</sub> receptorer i denne lidt begrænsede gruppe på ialt 16 individer. Forskellen var i gennemsnit 15% og var mest udtalt i hippocampus.

Molekylær billeddannelse af hjernens 5-HT<sub>4</sub> receptorer kan således kvantificeres tilstrækkeligt validt med [ $^{11}\text{C}$ ]207145 PET i det levende menneske med ikke-invasive modeller og

er stabilt overfor akutte fluktuationer i serotoninniveauet. Der er en mulig kønsforskel i 5-HT<sub>4</sub> receptor bindingen.

## List of Papers

The thesis is based on the following papers:

1. Lisbeth Marner, Gitte M. Knudsen, Steven Haugbøl, Søren Holm, William Baaré, and Steen G. Hasselbalch. Longitudinal assessment of cerebral 5-HT<sub>2A</sub> receptors in healthy elderly volunteers: An [<sup>18</sup>F]-altanserin PET study. (2009). *Eur J Nucl Med Mol Imaging* 36:287-293.
2. Lisbeth Marner, Nic Gillings, Robert Comley, William Baaré, Eugenii Rabiner, Alan Wilson, Marc Laruelle, Sylvain Houle, Steen G. Hasselbalch, Claus Svarer, Roger N. Gunn, Gitte M. Knudsen. Kinetic Modeling of [<sup>11</sup>C]SB207145 binding to 5-HT<sub>4</sub> receptors in the human brain *in vivo*. (*Submitted to J Nucl Med*)
3. Lisbeth Marner, Nic Gillings, Karine Madsen, David Erritzøe, William Baaré, Steen G. Hasselbalch, Gitte M. Knudsen. Brain Imaging of serotonin 5-HT<sub>4</sub> receptor in humans with [<sup>11</sup>C]SB207145-PET. (*Manuscript*)

## Aims of the Thesis

Positron Emission Tomography (PET) is a valuable tool for investigating physiological, biochemical or pharmacological processes *in vivo*. Quantification of receptor availability gives the basis for understanding the biology of neurotransmission in health and disease and can assist the dose selection in clinical trials of drugs acting at specific receptors. Although the methods for quantification of receptor availability have been improved and been refined in the past 10-15 years, a throughout validation of each new tracer is necessary to understand the possible biases and pitfalls in the quantification.

The aims of the thesis were to

1. Evaluate long-term stability for follow-up studies in the elderly of [<sup>18</sup>F]altanserin, a well-known radiotracer for PET imaging of 5-HT<sub>2A</sub> receptors
2. Perform a comprehensive evaluation in humans of [<sup>11</sup>C]SB207145, a new radiotracer for PET imaging of the serotonin 5-HT<sub>4</sub> receptor, with arterial input data
3. Test the sensitivity of [<sup>11</sup>C]SB207145 binding to endogenously released serotonin
4. Explore the distribution of 5-HT<sub>4</sub> receptors in healthy volunteers, and determine the required sample size for future studies

## Background

### *The Serotonin System*

Brain serotonin (5-hydroxytryptamine, 5-HT) has been extensively studied due to the efficacy of serotonergic agents in the treatment of neuropsychiatric conditions, including major depressive disorder, obsessive compulsive disorder, anxiety disorders, and due to post mortem findings of serotonergic pathologies in Alzheimer's disease. The pharmacology of serotonin is extremely complicated; its receptors are divided into seven major classes, most of which have multiple subtypes, e.g. 5-HT<sub>2</sub> comprises three known subtypes, 5-HT<sub>2A</sub>, 5-HT<sub>2B</sub>, and 5-HT<sub>2C</sub>. With the exception of 5-HT<sub>3</sub>, which is a ligand-gated ion-channel, the 5-HT receptors are G-protein-coupled, with signal transduction mediated by either stimulation or inhibition of cAMP synthesis (Gray and Roth 2001). Most of the receptor subtypes are exclusively located postsynaptically, on neurons, astrocytes, and vascular elements while the 5-HT<sub>1</sub> receptors in the raphe nuclei are located presynaptically on the soma, dendrites, and axon terminals of serotonin neurons, and have an autoregulatory function.

The neurons of the raphe nuclei are the main source of serotonin in the brain giving rise to descending and ascending projections to every part of the brain. Serotonin has complex effects of neuroendocrine regulation and feeding, and is implicated in the regulation of aspects of cognition, mood, aggression, and perhaps personality traits (Takano et al. 2007; Frokjaer et al. 2008). Serotonin and its metabolite can be measured in the cerebrospinal fluid (CSF) and post mortem, but there is no means of measuring serotonin directly *in vivo*. Nonetheless, the reversal of depressive symptoms after treatment with selective serotonin reuptake inhibitors (SSRI) is a major argument of the importance of serotonin in the control of mood. Several indirect measures of the status of brain serotonergic systems have been used to investigate the influence of serotonin on behavior, personality and cognition including genetic polymorphisms, positron emission tomography (PET), and *post mortem* receptor autoradiography. The interstitial serotonin concentration can be increased by pharmacological challenge, e.g. infusion of Selective Serotonin Reuptake Inhibitors (SSRI), whereas brain serotonin concentrations can be reduced by ingestion of a tryptophan-depleted mixture of amino acids; in the absence of adequate plasma levels of its precursor tryptophan, brain serotonin concentration is acutely depleted. This challenge leads to a transient relapse of depressive symptoms in depressed patients who have previously shown therapeutic response to treatment with an SSRI (Delgado et al. 1999).

Several PET studies have investigated the serotonin system in relation to personality. The personality trait, neuroticism, and especially the underlying facet depression (NEO-PI-R) is found to be positively correlated to the amount of serotonin transporters in thalamus measured by PET imaging with [<sup>11</sup>C]DASB (Takano et al. 2007). Furthermore, in a sample of 90 subjects the personality trait neuroticism was found to significantly correlate to the specific binding of the receptor antagonist [<sup>18</sup>F]altanserin to 5-HT<sub>2A</sub> receptors in frontal regions of the brain (Frokjaer et al. 2008). However, *in vivo* imaging of 5-HT<sub>2A</sub> receptors in major depression have shown either down-regulation or no change, depending on the tracer used (Messa et al. 2003); in general, 5-HT<sub>2A</sub> receptor level in depressed patients post mortem or suicide victims have shown varying results (review, see (Meltzer et al. 1998)). Therapeutically, 5-HT<sub>2A</sub> receptors are targets for medications used to treat conditions such as schizophrenia, anxiety, depression, and Parkinson's disease. Moreover, most hallucinogens mediate their effects through the 5-HT<sub>2A</sub> receptor (Berg et al. 2005).

Symptoms of depression, aggression, anxiety and disturbances in food intake and sleep are common in Alzheimer's disease and serotonergic impairment is well-documented in post mortem studies (Zarros et al. 2005). PET studies of Alzheimer's disease have shown reduced availability of 5-HT<sub>2A</sub> receptors in most cortical regions (Blin et al. 1993;Meltzer et al. 1998;Hasselbalch et al. 2008), and a decrease of 5-HT<sub>1A</sub> receptors has also been reported (Kepe et al. 2006). Other serotonin receptor types have yet to be investigated.

The serotonin 4 receptor (5-HT<sub>4</sub>) was discovered in 1988 and has been cloned from a human brain cDNA library (Van den Wyngaert et al. 1997). In autoradiographic studies of the post-mortem human brain with a selective ligand show these the receptors to have high density in the basal ganglia (striatum, globus pallidus, nucleus accumbens, and substantia nigra), with intermediate density in the hippocampal formation and the superficial layers of the neocortex, and with very low density in the cerebellum (Reynolds et al. 1995;Bonaventure et al. 2000;Varnas et al. 2003). The receptors are more associated with neurons than glia, and their activation evoked depolarization of neurons. The 5-HT<sub>4</sub> receptor is believed to act by exerting modulation of other neurotransmitter systems (Bockaert et al. 2004), in particular dopaminergic (Porras et al. 2002), GABAergic (Cai et al. 2002) and cholinergic systems, e.g. 5-HT<sub>4</sub> agonists facilitate the release of the neurotransmitter acetylcholine in frontal cortex (Yamaguchi et al. 1997) and hippocampally (Mohler et al. 2007).

The anatomic localization of 5-HT<sub>4</sub> receptors in hippocampus and the basal ganglia implies a role in memory and learning, leading to investigations of the effects of receptor stimulation on cognitive performance. In rats, the selective 5-HT<sub>4</sub> partial agonist RS67333 had procognitive effects

when injected into nucleus basalis magnocellularis, i.e. in the vicinity of the cholinergic neurons innervating the cerebral cortex and hippocampus, the same neurons degenerating in Alzheimer's disease (Orsetti et al. 2003). Enhanced delayed matching performance was found in macaques treated acutely with the 5-HT<sub>4</sub> receptor agonist RS 17017, suggesting an enhancement of memory function (Terry, Jr. et al. 1998). Peritoneal injection in rats of the 5-HT<sub>4</sub> receptor agonist VRX-03011 improved scores in the 30 seconds delay spontaneous alternation test, and had in this paradigm a synergistic effect with the acetylcholinesterase (AChE) inhibitor, galantamine (Mohler et al. 2007). Synergism with AChE inhibitors is a promising aspect of 5-HT<sub>4</sub> agents for the pharmacological treatment of Alzheimer's disease, given that AChE inhibitors are often discontinued or used at too low doses, due to gastrointestinal side effects. It is to be hoped is that supplementing low dose AChE inhibitor treatment with a 5-HT<sub>4</sub> receptor agonist will optimize the symptomatic relief of memory loss, without peripheral side effects.

Furthermore, Robert et al (2001) found that activating the 5-HT<sub>4</sub> receptor increased the secretion of the non-amyloidogenic soluble form of the amyloid precursor protein, sAPP $\alpha$ . This protein is believed to be neuroprotective and an enhancer of memory consolidation (for review see (Turner et al. 2003)); and by diverting the cleavage pathway of the amyloid precursor protein, formation of the pathologic  $\beta$ -amyloid peptide (A $\beta$ ) is precluded (Robert et al. 2001). Transgenic cortical cultures treated with RS67333 showed up to 95% lowering of the A $\beta$  concentration in a dose-dependent manner and exhibited higher neuronal survival (Cho and Hu 2007). Recently, increased levels of sAPP $\alpha$  were reported in wild-type mice following treatment with a 5-HT<sub>4</sub> agonist in vivo (Cachard-Chastel et al. 2007). In humans, the involvement of 5-HT<sub>4</sub> receptors in Alzheimer's disease has only been studied post-mortem, and has given conflicting results (Wong et al. 1996;Lai et al. 2003)..

5-HT<sub>4</sub> receptor directed drugs are indicated for functional gastro-intestinal disorders such as irritable bowel syndrome. However, at the moment there are no licensed drugs acting at 5-HT<sub>4</sub> receptors which pass the blood brain barrier. However, clinical trials (phase IIb) with a partial agonist are currently underway for the treatment of Alzheimer's disease. In addition to potential benefits for treating Alzheimer's disease, centrally-acting agonists at 5-HT<sub>4</sub> receptor could be applicable for rapid-onset treatment of depression (Lucas et al. 2007b), and for the alleviation of epilepsy (Compan et al. 2004), and eating disorders (Compan et al. 2004;Jean et al. 2007).

## Positron Emission Tomography

PET is a functional imaging method that allows for studying physiological, biochemical or pharmacological processes *in vivo*. A chemical structure designed to bind to the biological molecule of interest is labeled with a positron-emitting isotope, i.e.  $^{11}\text{C}$ ,  $^{13}\text{N}$ ,  $^{15}\text{O}$ ,  $^{18}\text{F}$ ,  $^{68}\text{Ga}$ , or  $^{82}\text{Rb}$ . As oxygen, carbon and nitrogen are included in most organic molecules, it is in principle possible to label the majority of natural substrates chemically indistinguishable from their unlabeled counterpart; in practice, the brief physical half life of PET isotopes can preclude complex radiosynthesis. The radionuclide decay mode of a positron-emitting isotope is illustrated in figure 1.

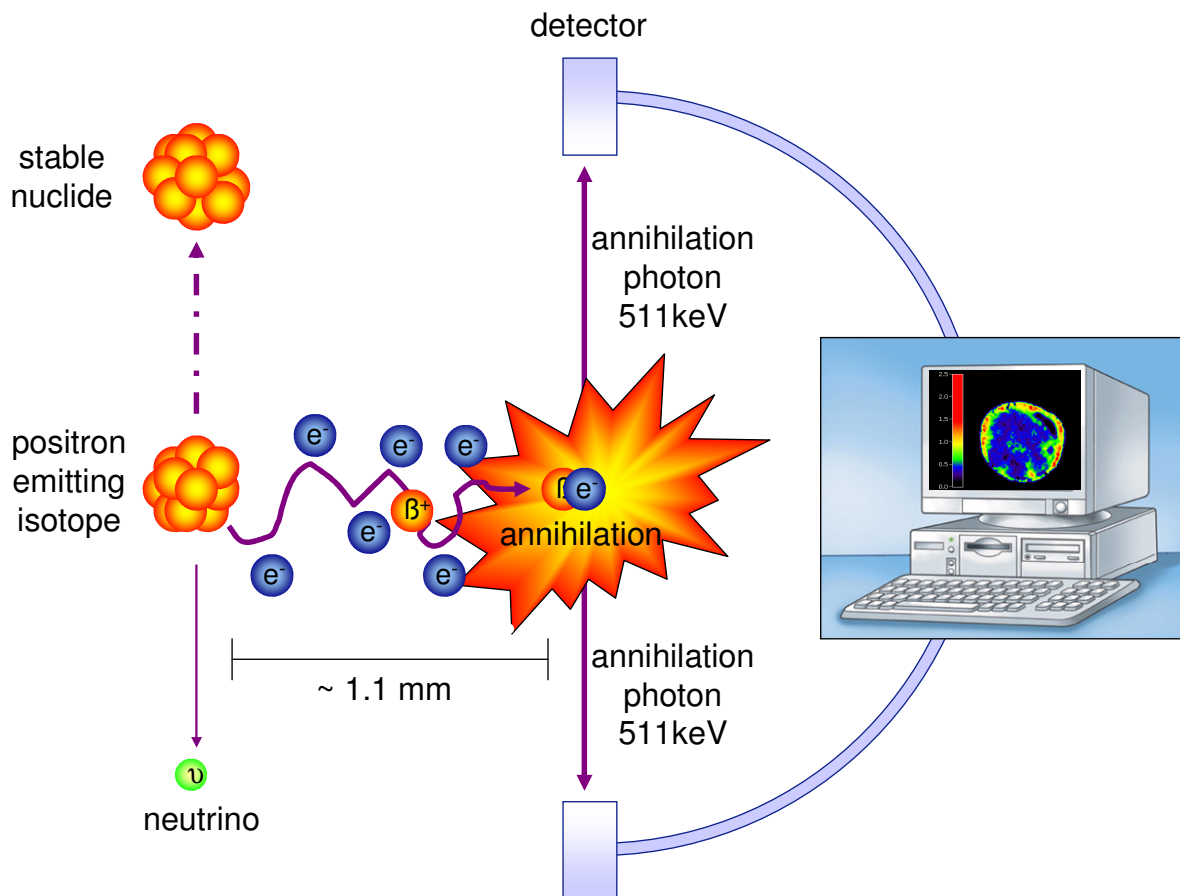


Figure 1. The unstable parent nucleus has a surplus of protons and the extra proton is converted to a neutron, a positron (a positive electron) and a neutrino. The positron and the neutrino are immediately emitted from the nucleus, and the positron subsequently annihilates on contact with an electron after travelling a short distance (on average 1-2 mm) within the body. The annihilation produces two 511 keV photons travelling in opposite directions and these photons may be detected by the PET tomograph (drawing kindly provided by Ronald Boellard, PhD).

A PET apparatus consist of rings of detectors surrounding the subject. The electronics of the individual detectors are linked so that the detections of two photons occurring within a certain time window (10 ns) can be registered as a coincident event, most likely arising from the same annihilation. Each coincident event is assigned to a line of response joining the two relevant detectors. A 3D image of the distribution of the isotope can subsequently be made by estimating the original source distribution by a process known as back-projection (FBP), or alternatively using an iterative algorithm. Several sources of noise and bias are present in the recordings; most can be corrected before and during the reconstruction of the PET image. However, high amounts of statistical noise distort the final image, such that a filtering process is included in the reconstruction, at the FBP stage.

The PET investigation can be static or dynamic. In static recordings, the distribution of radiotracer is recorded in one time frame, and a single 2D or 3D image for the whole investigation period is obtained. In dynamic recordings, the data is divided into a number of successive time frames, resulting in a series of images over time, resulting, in the case of 3D PET in a 4D image. PET images can be hard to assign anatomically; the usual practice is to align the PET image to a magnetic resonance (MR) image, in which anatomical regions are clearly defined, or available as templates. Then, regional time-activity curves can be extracted from the dynamic PET recording, and used for subsequent kinetic modeling (see below).

The development of dual modality scanners (PET-CT) has enabled sequential imaging of both function and structure in a single session, thus constituting a major advance in medical imaging technology. The clinical use of diagnostic PET has increased widely the last years, especially the use of [ $^{18}\text{F}$ ]FDG (2- $^{18}\text{F}$ fluoro-2-deoxy-D-glucose), a radiolabeled analog of glucose, which was first employed for brain energetics studies, but has found widespread clinical use for identifying corporal regions of high glucose consumption, e.g. cancer metastases.

### *Partial Volume Effect*

Filtering, movement artifacts, and statistical noise all decrease the resolution of the PET image. Even with high-resolution research tomographs (HRRT) for human brain, the spatial resolution is at best 2.3-3.2 mm full width at half maximum (FWHM) in the transaxial direction and 2.5-3.4 mm FWHM in the axial direction (van Velden et al. 2008). Today, most PET instruments have a resolution around 6-8 mm in the transaxial plane. The gray matter of the cerebral cortex has a thickness of 2.5-3 mm (Pakkenberg and Gundersen 1997). Thus, radioactivity from CSF, gray,

and white matter will appear merged and averaged in the final PET image, and will be contaminated by intrusion of radioactivity from adjacent areas. Together, these phenomena are known as the partial volume (PV) effect. When obtaining quantitative measures of the brain, the PV effects give false values, and are especially prone to bias PET outcome measures in studies of subjects in whom gray matter atrophy is to be expected, e.g. Alzheimer's disease patients (Pelvig et al. 2003). Some of the bias arising from a pure gray matter volume loss could theoretically be accounted for by having gray matter volume, as assessed with the MR scan, as a covariate in the final analysis. Unfortunately, such a correction is by no means simple. Even if one is able to segment the MR image correctly into gray and white matter, the white matter loss may be more pronounced, leading to conformational changes with enlarged sulci in the brain, as is certainly the case in normal aging (Pakkenberg and Gundersen 1997). Enlarged sulci will increase the apparent surface of the brain, and even if gray matter volume was unaffected, considerably more spill-over from cortical gray matter to CSF would occur.

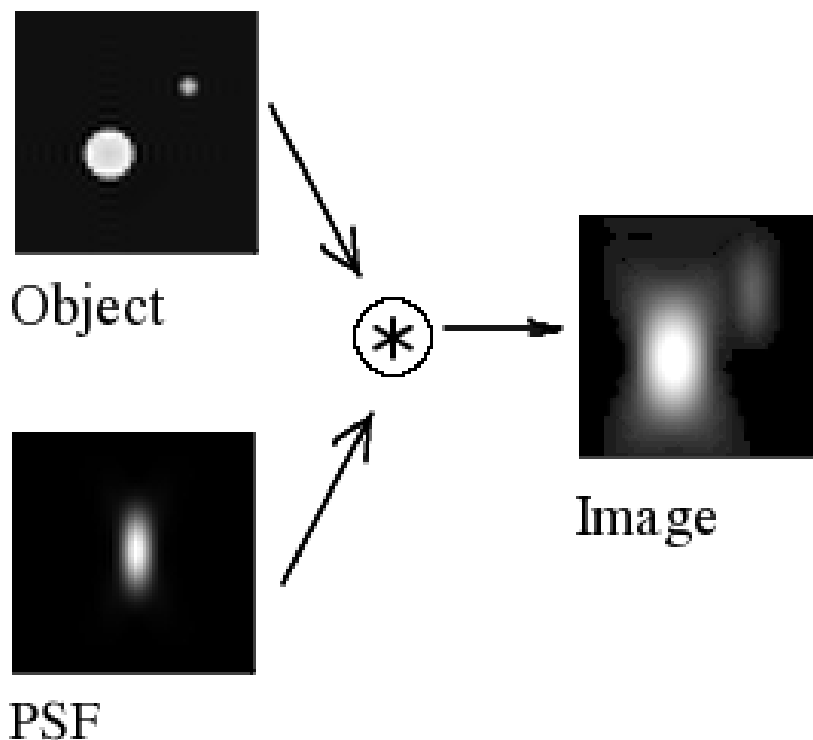


Figure 2. The Point Spread Function (PSF) describes the response of an imaging system to a point source or point object. When the PSF of the scanner is known, the obtained blurred image of any object can be simulated by convoluting ( $\otimes$ ) the object and the PSF (drawing from Wikipedia, The Free Encyclopedia).

In order to correct for the partial volume effects, the segmentation of gray matter and white matter in the brain can be obtained in an aligned MR. An algorithm that corrects the gray matter radioactivity concentrations for spill-over and spill-in to CSF can be used (Meltzer et al. 1990), or alternately a more complex algorithm that corrects the gray matter values for spill-over and spill-in to both CSF and white matter (Muller-Gartner et al. 1992). If a Point Spread Function (*PSF*) (see figure 2) of the scanner (including head-motion artifacts) is estimated from measurement (e.g, 8 mm), then the observed image  $I_{obs}$  will be a function of the “true” gray matter image,  $I_{GM}$ , the true white matter image,  $I_{WM}$ , and the true CSF image  $I_{CSF}$ :

$$I_{obs} = I_{GM} \otimes PSF + I_{WM} \otimes PSF + I_{CSF} \otimes PSF \quad (\text{Equation 1})$$

where  $\otimes$  is the operation of convolution. If one assumes uniform activity in white matter and CSF, then  $I_{WM}$  and  $I_{CSF}$  can be approximated by:

$$I_{WM} \approx \bar{I}_{WM} X_{WM} \quad \text{and} \quad I_{CSF} \approx \bar{I}_{CSF} X_{CSF} \quad (\text{Equation 2})$$

with  $X_{WM}$  and  $X_{CSF}$  being the spatial location of the white matter and CSF voxels from the MR image, e.g.  $X_{WM}=1$  for white matter voxels and zero otherwise (or alternatively a probability map) and  $\bar{I}_{WM}$  and  $\bar{I}_{CSF}$  being the (uniform) activity within all the white matter or CSF voxels. Then:

$$I_{GM} \otimes PSF = I_{obs} - \bar{I}_{WM} X_{WM} \otimes PSF - \bar{I}_{CSF} X_{CSF} \otimes PSF \quad (\text{Equation 3})$$

For typical cortical PET imaging scenarios with almost uniform gray matter activity, an approximation of PV corrected activity in each gray matter voxel (Muller-Gartner et al. 1992),  $\tilde{I}_{GM}$ , is:

$$\tilde{I}_{GM} = \frac{I_{obs} - \bar{I}_{WM} X_{WM} \otimes PSF - \bar{I}_{CSF} X_{CSF} \otimes PSF}{X_{GM} \otimes PSF} \quad (\text{Equation 4})$$

Note, however, that the approximation in the algorithm assumes only minor variations in gray matter activity and relies on correct segmentation of the MR image as well as alignment of PET and MR images. These requirements and assumptions result in the introduction of noise, and perhaps also bias. Alternative methods for correction for the partial volume effect exist; these may more reliably allow for estimation of regional gray matter radiotracer activity if the activity can be assumed to be uniform within a limited set of gray matter defined regions (Rousset et al. 1998).

## *Radioligands*

The radionuclides commonly used in PET have relatively short half-lives ( $^{15}\text{O}$ : 2.03 min,  $^{11}\text{C}$ : 20.3 min, and  $^{18}\text{F}$ : 109.8 min). Thus, the PET instrument (with the exception of  $^{18}\text{F}$ , which can be transported considerable distances) is usually situated in close proximity to the cyclotron producing the isotopes. Furthermore, as noted above, the time required for tracer synthesis time has to be short. When studying receptor systems of the brain, several requirements of the radioligand are of importance. In particular, a radioligand should:

- Bind selectively to the receptor with high affinity (nM range), and only to a minor degree to other receptor subtypes.
- Have a sufficiently high lipophilicity in order to cross the blood brain barrier
- Have low non-specific binding, so as to obtain a high signal-to-noise ratio, i.e. the lipophilicity should not be too high.
- Have rather fast kinetics, such that equilibrium between association to and dissociation from the receptor can occur within the time of endurable scan duration (and not more than six to eight half lives of the isotope).
- Be non-toxic, and not accumulating in body-parts especially sensitive to radioactivity, e.g. gonads
- Be obtainable in injectable form via a reliable and fast radiosynthesis.

Additional requirements of a good tracer include, low plasma protein binding, peripheral metabolism not resulting in lipophilic metabolites capable of entering the brain, and poor substrate affinity for the brain efflux transporter, P-glycoprotein (Syvanen et al. 2006). Furthermore, the existence of a receptor-devoid reference region in the brain presents distinct advantages for widespread use of a radioligand.

When measuring receptors in the brain, it is important not to change the system while measuring. Large amounts of a ligand will significantly occupy the receptor sites, decreasing the apparent amount of receptors, potentially desensitizing or down-regulating the receptor, and most catastrophically, potentially poisoning the subject by exerting pharmacological effects. To avoid pharmacologically perturbing the system, the ligand should always be used at a tracer dose, i.e. ever occupying no more than 5% of the receptors.

### *Sensitivity to Endogenously Released Neurotransmitter*

PET can in some cases be used to measure acute fluctuations in a neurotransmitter's interstitial concentration in the living brain. It was shown in 1997 that *in vivo* occupancy of the dopamine D<sub>2</sub> receptor by endogenous dopamine can be quantitatively assessed by imaging with the D<sub>2</sub> receptor agonist SPECT ligand [<sup>123</sup>I]IBZM first at baseline, and again during dopamine depletion, which results in an increase in receptor availability (Laruelle et al. 1997). Conversely, a decrease in specific binding can be detected when subjects are treated with amphetamine that is known to release dopamine. The competition paradigm allowed for functional studies on dopamine release. In numerous studies of dopamine D<sub>2</sub> receptors with the single photon emission tomography (SPET) ligand [<sup>123</sup>I]IBZM and the PET ligand [<sup>11</sup>C]raclopride, pharmacological challenge has been used to reveal, for example dopamine release in drug-users (Martinez et al. 2007), and patients with schizophrenia (Soares and Innis 1999). The new functional information derived from these experiments has increased our understanding of the pathophysiologies underlying these disorders.

The precise mechanism behind the decreased binding of D<sub>2</sub> ligands following amphetamine treatment is not yet entirely clear. The simple occupancy model has been widely accepted, but cannot explain all observations. According to his model, there occurs simple competition between the released dopamine and the radioligand for binding to the same receptors. However, it is also possible that internalization of the active receptors evoked by high concentrations of dopamine results in a lower affinity and thereby lower binding (Laruelle 2000), although this qualification has been challenged on the basis of *in vitro* data (Jiang et al. 2006). It has been the experience of PET researchers that most classes of receptor ligands have not proven sensitive to endogenous released neurotransmitter. An explanation could be that most tracers bind not only to the extracellular receptors available to the endogenous neurotransmitter, but bind also to inactive intracellular receptors, such that only a fraction of the receptors available to the radiotracer can ever be occupied by the endogenous neurotransmitter in living brain.

To test for sensitivity of the 5-HT<sub>2A</sub> ligand [<sup>18</sup>F]altanserin to endogenous released serotonin, an experimental paradigm was employed with intravenous infusion of citalopram during *steady state* binding conditions (Pinborg et al. 2004). Citalopram, an SSRI, inhibits the serotonin reuptake by serotonin terminals, thereby increasing the interstitial concentration of serotonin. This treatment will also have pre-synaptic effects tending to confound the competition model. In particular,

activation of autoregulatory presynaptic 5-HT<sub>1A</sub> receptors will tend to inhibit further serotonin release during acute treatment with citalopram. Indeed, simultaneous blockade of these autoreceptors has been proposed as a means to overcome the autoregulation of serotonin release during SSRI treatment, so as to enhance the early-onset of antidepressant efficacy (Blier 2003). The  $\beta$ -blocker pindolol is a combined 5-HT<sub>1A</sub> partial agonist and  $\beta$ -adrenoceptor antagonist and was used to enhance the serotonin release during citalopram infusion in the PET study of serotonin competition against [<sup>18</sup>F]altanserin binding (Pinborg et al. 2004). The combined treatment with citalopram and the 5-HT<sub>1A</sub> antagonist WAY100635 has been shown by cerebral microdialysis in rats to increase interstitial levels of serotonin by a factor of 4-5 in the forebrain (Hjorth et al. 1997). Plasma prolactin is a well-known biomarker of serotonin release in the hypothalamus, an effect that is mediated through 5-HT<sub>2A</sub> and 5-HT<sub>1A</sub> receptors in hypothalamic paraventricular nucleus (Pinborg et al. 2004). Plasma cortisol also increases with increasing brain serotonin levels, but in a less specific manner, since sensitivity to stress blurs the cortisol response.

### *Kinetic Modeling*

Obtaining precise quantitative measures of receptor concentrations in the brain *in vivo* in humans is a challenging task. The measured binding of the ligand to the receptor will depend not only on the receptor concentration ( $B_{max}$ ), and also on the dissociation coefficient of the ligand from the receptor ( $K_D$ ). The two parameters can be measured independently *in vivo* only through a complex experimental design with serial injection of tracer at two or more concentrations, including a non-tracer dose resulting in partial receptor occupancy. Generally, one carries out single PET examinations using a single tracer dose, and calculates the so-called binding potential ( $BP$ ), which is defined as the ratio of  $B_{max}$  to  $K_D$  (Innis et al. 2007).

Binding potential quantifies the equilibrium concentration of specific binding as a ratio to a reference concentration; the specific type of binding potential is designated according to the chosen reference tissue concentration (Innis et al. 2007):

- free plasma concentration (free, non-protein bound), we measure  $BP_F$
- total plasma concentration (not corrected for protein binding), we measure  $BP_P$
- non-displaceable uptake (concentration in reference region), we measure  $BP_{ND}$

In invasive PET studies with arterial blood sampling, we can calculate the total volume of distribution ( $V_T$ ) at equilibrium, relative to the blood input. This concept originates from clinical pharmacology and refers in the context of PET to the volume of plasma needed to account for the

radioligand in a brain region. Thus, if the concentration at equilibrium is five times the concentration in plasma, then  $V_T=5$ , as five times as much plasma would be needed to contain the same amount of radioligand. It must be noted that  $V_T$  is a sum of distribution volumes of free ligand in tissue water, specifically bound ligand, and nonspecifically bound ligand. The magnitude of  $BP_{ND}$  can be calculated indirectly from  $V_T$  as:

$$BP_{ND} = \frac{V_T - V_{ND}}{V_{ND}} = \frac{V_T}{V_{ND}} - 1 \quad (\text{Equation 5})$$

where  $V_{ND}$  is the non-displaceable binding, i.e. the binding in a receptor-void reference region. Valid use of  $BP_{ND}$  requires that we have a true receptor-void reference region and homogenous non-specific binding throughout the brain.

In *steady state* conditions, equilibrium conditions prevail and the distribution volumes can be assessed directly by measuring plasma and brain concentrations. Then  $BP_P$  can be calculated as:

$$BP_P = V_T - V_{ND} = \frac{C_T - C_{ND}}{C_P} \quad (\text{Equation 6})$$

where  $C_P$  is the plasma concentration of unmetabolized radiotracer,  $C_T$  is the concentration in the target region, and  $C_{ND}$  the concentration in the reference region. However, it is often the case that *steady state* conditions are not readily attained, in which event kinetic modeling is used to calculate the magnitudes of  $V_T$  or  $BP_{ND}$ . In general, the kinetic models are simple extension of a cerebral blood flow (CBF) model, with additional terms for the binding to and dissociation of radioligand from receptors. Transport across the blood brain barrier, except when mediated by a carrier (e.g. FDG) is not saturable, and binding to receptors does not become saturated at tracer doses, and is thus only dependent on the unbound concentration of the tracer in brain (which is itself determined by the permeability of the blood brain barrier and blood flow). In the special case of substrates for the P-glycoprotein efflux transporter, self-competition or inhibition by other substrates can enhance the net tracer uptake in brain.

The general kinetic model contains one, two or three tissue compartments, as well as a plasma compartment. Traditionally, the first tissue compartment is the free ligand, the second the specific binding, and the third is composed of the non-specific binding (see figure 3). The unidirectional blood-brain clearance ( $K_1$ ) has units of cerebral blood flow ( $\text{mL g}^{-1} \text{min}^{-1}$ ), and the other defined processes ( $k_2, k_3, k_4, k_5, k_6$ ;) are fractional rate constants ( $\text{min}^{-1}$ ). In most cases it is not possible, given the noise properties of PET recordings, to separately determine the masses occupying the

three tissue compartments. Therefore, the free and non-specific compartments are often regarded as a single compartment, and only four rate constants are used to describe the biological system. Thus, the number of compartments should not be viewed strictly in biological terms, since the number of rate constants to be measured depends on what can in actual practice be separated kinetically. Thus, for example, the reference tissue may have two compartments (free and non-specific compartments), while the tracer kinetics in the high binding tissue maybe best described with only one.

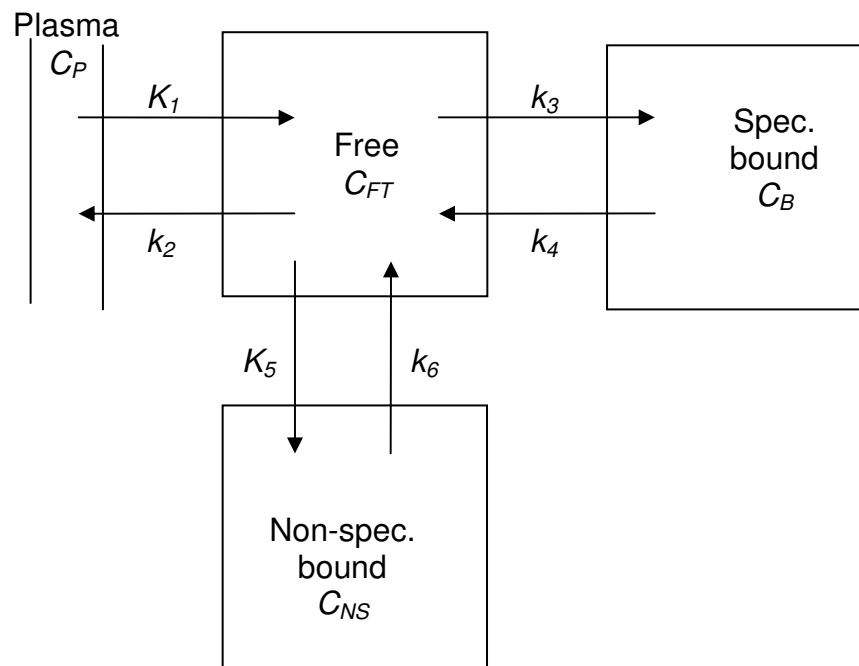


Figure 3. The possible compartments in a kinetic model. The rate constants  $K_1$ ,  $k_2$ ,  $k_3$ ,  $k_4$ ,  $k_5$  and  $k_6$  describe the transport of tracer between plasma and the three tissue compartments (free, specifically bound and non-specifically bound). In most applications, a maximum of only two tissue compartments can be distinguished kinetically.

In order to derive the distribution volume and binding potential, the plasma concentration and tissue concentration have to be measured serially during the emission recoding, at sufficiently short intervals. The PET image shows the sum (total concentration,  $C_T$ ) of the radioactivity, both bound and free:

$$C_T = C_{FT} + C_S \quad (\text{Equation 7})$$

where  $C_{FT}$  is the free tissue concentration and  $C_S$  is the concentration of specifically bound tracer.

*Derivation of distribution volume from rate constants*

In the following text, the relationship between rate constants and distribution volume will be derived (Laruelle et al. 2002): If a two tissue compartment model is assumed, then the changes in concentrations can be described by the differential equations (differentiated with respect to time,  $t$ ):

$$\frac{dC_{FT}}{dt} = K_1 C_P - k_2 C_{FT} - k_3 C_{FT} + k_4 C_S \quad (\text{Equation 8})$$

$$\frac{dC_S}{dt} = k_3 C_{FT} - k_4 C_S \quad (\text{Equation 9})$$

At equilibrium, there will be no net transport of ligand and  $dC_{FT}/dt$  and  $dC_S/dt$  will thus be zero.

From:

$$0 = k_3 C_{FT} - k_4 C_S \quad (\text{Equation 10})$$

It follows that

$$C_S = \frac{k_3}{k_4} C_{FT} \quad (\text{Equation 11})$$

Therefore:

$$V_T = \frac{C_T}{C_P} = \left( \frac{C_{FT} + C_S}{C_P} \right) = \left( 1 + \frac{k_3}{k_4} \right) \frac{C_{FT}}{C_P} \quad (\text{Equation 12})$$

Adding equation 8 and 9, we obtain at equilibrium:

$$\frac{dC_{FT}}{dt} + \frac{dC_S}{dt} = K_1 C_P - k_2 C_{FT} = 0 \quad (\text{Equation 13})$$

It follows that:

$$\frac{C_{FT}}{C_P} = \frac{K_1}{k_2} \quad (\text{Equation 14})$$

And  $V_T$  then simplifies to:

$$V_T = \left( \frac{K_1}{k_2} \right) \left( 1 + \frac{k_3}{k_4} \right) \quad (\text{Equation 15})$$

Similarly, if a three tissue model is used:

$$V_T = \left( \frac{K_1}{k_2} \right) \left( 1 + \frac{k_3}{k_4} + \frac{k_5}{k_6} \right) \quad (\text{Equation 16})$$

Thus, determining the rate constants from the non-equilibrium situation, i.e. a dynamic study, we can calculate the distribution volume (at equilibrium).

The radioactive plasma time-activity curve (corrected for radiolabeled metabolites of the tracer) defines the input to the brain, and the unidirectional blood-brain clearance and rate constants together define the brain output, i.e. the time-activity curves derived from the dynamic PET scan. The solution to Equation 8 and 9 can be written as the arterial input function convoluted to a sum of exponentials (Laruelle et al. 2002). Thus, when measuring the plasma input curve, regional rate constants can be fitted to the regional PET time-activity curves and distribution volumes and binding potentials can be derived (figure 4). It must be stressed that the individual rate constants are microparameters, and not as robust as the macroparameter,  $V_T$ .

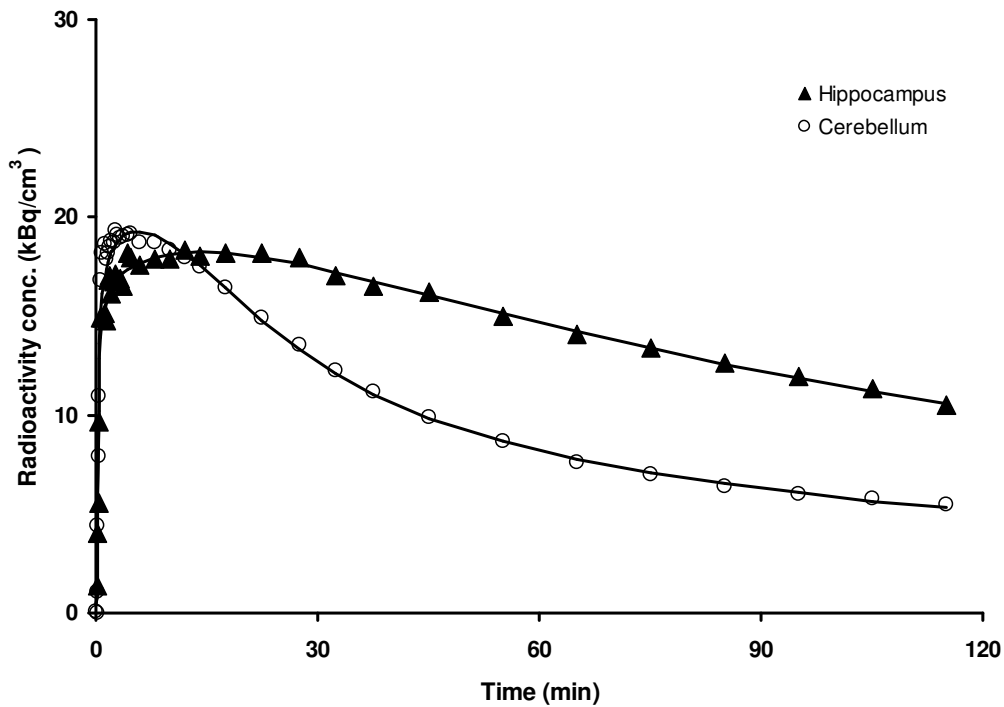


Figure 4. The time activity curve from hippocampus and cerebellum using the 5-HT<sub>4</sub> tracer [<sup>11</sup>C]SB207145 (female, 36 years). Two-tissue compartment models are fitted to the data. The derived rate constants for cerebellum are:  $K_1= 0.38 \text{ mL cm}^{-3} \text{ min}^{-1}$ ,  $k_2=0.06 \text{ min}^{-1}$ ,  $k_3=0.02 \text{ min}^{-1}$ , and  $k_4=0.02 \text{ min}^{-1}$ , and the distribution volume is  $13.9 \text{ mL cm}^{-3}$ . For hippocampus:  $K_1= 0.35 \text{ mL cm}^{-3} \text{ min}^{-1}$ ,  $k_2=0.07 \text{ min}^{-1}$ ,  $k_3=0.11 \text{ min}^{-1}$ , and  $k_4=0.03 \text{ min}^{-1}$ , and the distribution volume is  $25.1 \text{ mL cm}^{-3}$ . Thus, the binding potential for hippocampus is:

$$BP_{ND} = \frac{V_T}{V_{ND}} - 1 = \frac{25.1}{13.9} - 1 = 0.81.$$

*Simplified Reference Tissue Model*

Measuring the plasma input curve to the brain requires invasive arterial cannulation and labor-intensive measuring of radiolabeled metabolites, which often introduces noise into the measurements. However, if a true reference tissue exists, demonstrably devoid of specific binding, and with similar non-specific binding as the rest of the brain, use of a non-invasive reference tissue model becomes feasible (Hume et al. 1992). Fitting the region of interest with the reference region serving as an indirect input function, provides robust estimates for  $BP_{ND}$ ,  $k_2$  and  $RI = K_1/K_1'$  (relative delivery,  $K_1'$  is the rate constant of the reference tissue). The widely-used simplified reference tissue model (SRTM) (Lammertsma and Hume 1996) assumes:

- 1) that the non-displaceable distribution volume ( $V_{ND}$ ) is the same in region of interest and reference tissue is the same, i.e.  $K_1'/k_2' = K_1/k_2$
- 2) that tracer kinetics in the target region (as well as the reference tissue) are such that it is difficult to distinguish between free and specific compartments, i.e. can be fitted satisfactorily with a one-tissue compartment model, without distinct  $k_3$  and  $k_4$  terms.

The SRTM is expressed as:

$$C_T(t) = R_1 C_{ND}(t) + \left( k_2 - R_1 \frac{k_2}{1 + BP_{ND}} \right) C_{ND}(t) \otimes e^{\frac{-k_2 t}{1 + BP_{ND}}} \quad (\text{Equation 13})$$

where  $t$  is time, and  $\otimes$  denotes convolution. It has been shown for the case of [ $^{11}$ C]raclopride that, even when the second assumption is not met, i.e. kinetics in the target tissue is best described by a two-tissue compartment model, the SRTM remains sensitive to changes in binding potential in human brain (Lammertsma and Hume 1996). However, when the assumption of one-tissue compartment kinetics in the reference tissue is not met, a bias appears especially in high-binding regions (Slifstein et al. 2000), resulting in estimates of  $BP_{ND}$  which are low relative to estimates based upon an arterial input (assuming of course that it is possible to fit a  $K_1/k_2/k_3/k_4$  model to the data).

The SRTM or other reference methods (Ichise et al. 2003) are very useful, as they obviate the need for labor-intensive blood sampling, and have lower levels of noise in the estimated parameters make, such that pharmacologically-evoked changes in binding potential can be more readily detected. However, the end point, i.e. binding potential relative to non-displaceable binding ( $BP_{ND}$ ) is vulnerable to changes in non-displaceable binding, the outcome parameter can change, even with the specific binding is actually unchanged (Slifstein et al. 2000). Thus, the risk of biased estimates is higher with SRTM than with arterial input models.

## Introduction and Hypotheses

Recently, a new radioligand, [ $^{11}\text{C}$ ]SB207145, was introduced for PET imaging of the 5-HT<sub>4</sub> receptor (Gee et al. 2008). It has high affinity to the 5-HT<sub>4</sub> receptor, with a low  $K_D$  *in vitro* of about 0.40 nM (Kornum et al. 2008) and binds with considerable selectivity, although with some binding at the 5-HT<sub>3</sub> receptor, and slight binding at the dopamine D<sub>1</sub>, D<sub>2</sub>, D<sub>4</sub>, histamine H<sub>2</sub>, and  $\alpha_{2B}$ -adrenergic receptors. PET studies in pigs showed that the radiotracer readily entered the brain, giving rise to a heterogeneous distribution consistent with known regional pattern of 5-HT<sub>4</sub> density (striatum > thalamus > cortical regions > cerebellum) (Gee et al. 2008). In the minipig, [ $^{11}\text{C}$ ]SB207145 time activity curves were described equally well by one-tissue compartment (1-TC) and two-tissue compartment (2-TC) kinetics, and in all brain regions the simplified reference tissue model (SRTM2) with fixed  $k_2'$  provided stable and precise estimates of the binding potential, which furthermore was highly correlated to *in vitro* binding, as measured in the same pigs' brains (Kornum et al. 2008). Preliminary data in six human subjects showed slower tissue kinetics compared to the pig, and the same rank order of brain tissues as reported *in vitro* (Gee et al. 2008). The radioligand metabolism was, however, not reliably assessed in this initial study, due to a continuing metabolism of tracer in plasma samples on the bench, apparently due the activity of plasma esterases (figure 5). This phenomenon interfered with quantification of the human data. In the present study, the continuing tracer metabolism in plasma was blocked by treating the vials with Dichlorvos®, a pesticide that is known to inhibit plasma esterases.

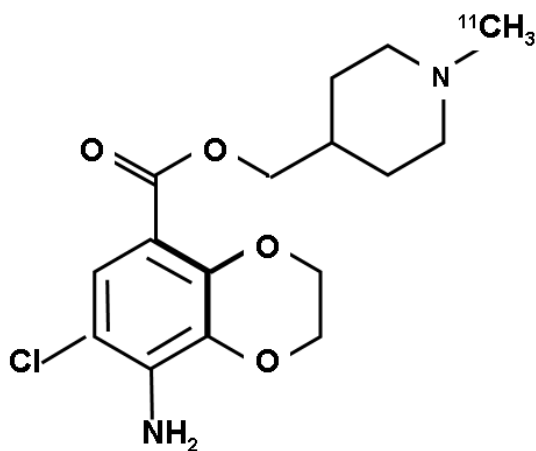


Figure 5. [ $^{11}\text{C}$ ]SB207145 is an ester and is readily degraded in human plasma.

## *Evaluation of PET Ligands*

To obtain reliable quantitative measures of receptor binding, a throughout evaluation of the several approaches to data analysis is necessary. Compartmental modeling with the assessment of distribution volumes is regarded the gold standard, and other methods of quantification should be validated against the results of compartmental modeling. However, this approach requires arterial plasma radioactivity measurements corrected for the *in vivo* metabolism of the tracer. The changing fraction of unmetabolized tracer as a function of circulation time can be measured with high performance liquid chromatography (HPLC), but this method is labor intensive and prone to bias and noise. Thus, a primary obstacle to compartmental modeling can be imposed by the need for accurate measurement of the input function in circulation, especially for tracers which are rapidly metabolized.

Compartmental modeling requires determining the appropriate number of compartments in the model. To quantitatively assess this, the Akaike Information Criterion (*AIC*) is used:

$$AIC = N \ln(SS) + 2P \quad (\text{Equation 14})$$

N= number of frames

P=number of parameters in model, i.e. two-tissue compartment model=4

SS= residual sum of squares

The fit with the lowest *AIC* is considered the “best” fit. Adding additional parameters result in a penalty in the precision and reliability of the several parameters, a problem known as over-specification.

As noted above, the calculation of binding potentials entails the use of a proper reference tissue, devoid of specific binding and with non-displaceable binding representative of that in the target tissues. Cerebellum is kinetically and anatomically fairly representative of the cerebrum as a whole, and is devoid, or nearly devoid of many types of neuroreceptors. This can be verified *in vitro*, but *in vivo* blocking studies with high doses of drugs that selectively bind to the receptor in question may be required for definitive assessment of the homogeneity of the non-specific binding. Comparison of *in vivo* and *in vitro* measurements can be used to verify that the distribution of receptors is correctly attributed in the PET study.

For reasons described above, compartmental modeling will often prove too labor-intensive, and prone to noisy or biased estimates. Furthermore, compartmental modeling is not generally suitable for extensive clinical studies. Thus a comparison with other, more convenient, methods of quantification will be warranted. The comparison will include comparison of output parameters in

terms of bias, performance on test-retest data, and stability for different scan durations. By this means, the stability of the model and the scan duration can be optimized. The distribution of parameter estimates in a larger sample allows the calculation of inter-subject variability and correlation to *in vitro* data, as required for validation of a new ligand.

Further validation of the ligand may include quantification in an elderly population. Test-retest data over a longer time scale are useful to assess the stability of baseline measures obtained months or years earlier. This is especially important in longitudinal studies, and when including data obtained previously, i.e. using a historical control group, as is sometimes necessary in order to obtain sufficiently large sample sizes. This complete validation was not possible for [<sup>11</sup>C]SB207145 investigated in this thesis. Instead, the validation of longitudinal stability was tested in the case of [<sup>18</sup>F]altanserin, a well-characterized ligand.

## *Hypotheses*

The following hypotheses were the basis of the studies:

- Longitudinal assessment of 5-HT<sub>2A</sub> receptors with [<sup>18</sup>F]altanserin extending for two years is reliable in a healthy elderly population
- Test-retest variability of [<sup>11</sup>C]SB207145-PET is in the same order of magnitude as other well-accepted tracers, i.e. 10%
- [<sup>11</sup>C]SB207145 binding is not sensitive to endogenous released serotonin
- 5-HT<sub>4</sub> receptor binding decreases with age, and is without important sex differences.

## **Material and Methods**

For detailed information of the methods used, please refer to the papers in Appendices.

### *Study 1:*

[<sup>18</sup>F]altanserin is a highly selective antagonist for the 5-HT<sub>2A</sub> receptor, but suffers from that liability that its radiolabeled metabolites cross the blood brain barrier and contribute to the total amount of non-displaceable radioactivity. Thus, calculation of binding potentials relative to non-displaceable binding ( $BP_{ND}$ ) is not valid with this tracer, as the non-displaceable binding will vary

depending on the extent of tracer metabolism. To circumvent this problem, binding potential relative to plasma ( $BP_P$ ) is the preferred end point. A *steady state* method has been developed for the easy and reliable assay of  $BP_P$  (Pinborg et al. 2003), giving high test-retest reproducibility at an interval of two weeks (Haugbol et al. 2007).

In brief, pairs of [ $^{18}\text{F}$ ]altanserin PET recordings were obtained in 12 subjects (7 men, age-range 63-79 years) with two years in between (range 23-28 months). Data from the test-retest analysis over two weeks (Haugbol et al. 2007) were included for comparison to the two-year follow-up data. The [ $^{18}\text{F}$ ]-altanserin was administered as a combination of a bolus injection and continuous infusion (ratio of 1.75 hours) so as to obtain tracer *steady state* in plasma and tissue within two hours. Emission scans (five frames of eight minutes each) were acquired with an eighteen-ring GE-Advance scanner operating in 3D-acquisition mode, with an approximate in-plane resolution of 6 mm. Venous blood samples were drawn at mid frame times during the emission scan for measurements of plasma activity, and the fraction of unmetabolized tracer in venous plasma. Structural brain imaging with MR was conducted in all subjects on a 1.5 T Vision scanner, followed by alignment of PET and MR images. The MR images were segmented into gray matter, white matter, and cerebrospinal fluid (CSF) with Statistical Parametric Mapping (SPM2) using the MNI template (Montreal Neurological Institute, Canada), and the result was visually inspected with manual image editing to remove remaining non-brain tissue. The 12 baseline scans were processed three times to evaluate inter- and intraobserver variability; one observer processed the data twice. A total of 19 bilateral regions were automatically delineated (Svarer et al. 2005) on each subject's MR image. Partial volume (PV) correction with a one-tissue method using brain and non-brain segmentation (Meltzer et al. 1990) and a two-tissue method using gray matter, white matter, and non brain segmentation (Muller-Gartner et al. 1992) were performed and compared to uncorrected PET data. The outcome parameter,  $BP_P$ , was calculated from Equation 6 with cerebellum as reference region since it represents non-specific binding only (Pinborg et al. 2003). This ensures subtraction of radiolabeled metabolites together with non-specific binding.

## *Study 2:*

### *Test-retest*

Six healthy subjects were included in the test-retest study (age-range 21-44 years, 3 males) that was performed at Copenhagen University Hospital, Rigshospitalet, Copenhagen. [ $^{11}\text{C}$ ]-SB207145 was synthesized as described in paper 2, appendices. Subjects received via a venous

catheter a 20 second bolus injection of  $572 \pm 33$  MBq [ $^{11}\text{C}$ ]SB207145, upon which a two-hour dynamic emission recording consisting of 36 frames was initiated. Arterial blood samples for measurement of the radioactivity concentration in whole blood and plasma were drawn at 5-10 second intervals during the first 2 min and subsequently at the mid frame times, using a catheter placed earlier in the radial artery of the non-dominant hand. In addition, seven arterial blood samples were acquired for metabolite measurements. Following withdrawal, the blood samples were immediately heparinized and Dichlorvos® (1  $\mu\text{g}/\text{mL}$  blood) added to avoid further de-esterification of the radiotracer in plasma. The fraction of unmetabolized tracer in arterial plasma was determined using a column-switching HPLC method (Gillings et al. 2007). Structural MR imaging was conducted on a 3 T Trio scanner (Siemens, Erlangen, Germany).

### *Blocking*

The blocking part included two healthy male subjects (aged 37 and 29), and was performed at the Vivian M. Rakoff PET Centre in Toronto. Subjects underwent a baseline [ $^{11}\text{C}$ ]SB207145 PET examination, followed by a second otherwise identical recording the same day beginning approximately four hours after receiving an oral dose of 150 mg of a selective 5-HT<sub>4</sub> inverse agonist. The PET scans were performed as described above using a Siemens-Biograph HiRez XVI PET tomograph. MR scans were performed using a GE medical system Signa Excite HD 1.5T scanner system.

PET recordings from all eight subjects were processed the same way. PET- and MR-images were co-registered using a single five-minute long frame (15-20 min after injection), selected on the basis of its CBF-like tracer distribution. Registration was accomplished through manually-guided translation and rotation of the PET image to fit the MR image. The MR images were segmented into gray matter, white matter, and cerebrospinal fluid by means of Statistical Parametric Mapping (SPM2). A total of 19 bilateral regions were automatically delineated (Svarer et al. 2005) on each subject's MR image.

To fit the measured unmetabolized [ $^{11}\text{C}$ ]SB207145 fractions as a function of circulation time, we used a bi-exponential function, with the slowest exponential constrained to the difference between the washout time-constants measured in plasma and in the reference region. The parent arterial plasma input function was then calculated as the total measured plasma activity multiplied by the fitted parent fraction, and constrained to be equal to a sum of exponentials following the peak. Using the test-retest PET data, three kinetic models were investigated. We estimated the  $BP_{ND}$

$BP_P$  using the 1-TC and 2-TC models, with blood volume fixed at 0.05 mL/mL. As a non-invasive reference tissue method, we chose the simplified reference tissue model (SRTM) (Lammertsma and Hume 1996), which does not suffer to the same extent from with noise-induced bias as does Logan's graphical analysis. All modeling was performed using in-house software at GlaxoSmithKline implemented with Matlab. The different models were compared using the Akaike Information Criterion, test-retest reproducibility and reliability, and time stability.

A time stability analysis was performed to determine the minimal scanning duration for reliable estimation of the outcome measures of interest. The distribution volumes ( $V_T$ ) or  $BP_{ND}$  were calculated for a range of truncated data sets using 1-TC, 2-TC, and SRTM. Estimation was performed on data sets corresponding to durations of 120, 110, 100, 90, 80, 70, 60 and 50 min. Hippocampus and striatum time activity curves (TAC's) were used for this analysis, as they were deemed representative of moderate- and high-binding regions, respectively. The outcome parameters were normalized to the value obtained with the full 120 min scan and mean outcome values and standard deviations ( $SD$ ) for all test-retest scans were plotted as a function of scan length.

In order to assess the potential impact of regional cerebral blood flow (rCBF) alterations on the outcome parameters,  $V_T$  or  $BP_{ND}$ , simulations of rCBF changes were done by calculating noise-free TACs using the population means of the estimates of  $K_1$ ,  $k_2$ ,  $k_3$ , and  $k_4$  in cerebellum, striatum, and hippocampus using the 2-TC model, and using the population mean arterial inputs for the test-retest scans. To simulate stepwise changes in rCBF lasting for the entire duration of the scan, we multiplied  $K_1$  and  $k_2$  by 1.3 (30% increase) or 0.7 (30% decrease), and constructed new time-activity curves in the three brain regions specified above, all based on the common input function. Gaussian noise was added using the  $SD$ 's of the residuals from the 2-TC modeling of the measured data. Kinetic modeling of the resulting noisy time-activity curves was done with 2-TC modeling and  $BP_{ND}$ 's were calculated for striatum and hippocampus with increased and decreased CBF in the target regions, as well as in the reference region. To estimate the bias of SRTM-generated binding potentials caused by CBF changes in striatum and hippocampus noise-free TAC's were used. The  $BP_{ND}$ 's were calculated with SRTM using cerebellar TAC's that were unaltered as well as scaled to simulate up to  $\pm 30\%$  blood flow. The correlation between changes in binding potential in the regions and the simulated change in CBF was tested.

### Study 3

#### *Sensitivity to Endogenously Release of Serotonin*

Seven healthy subjects were included in the intervention part of the study (4 men, age-range 21-44 years), as well as a control group of six subjects, who had participated in study 2. The study was a modification of an earlier study of the sensitivity of [<sup>18</sup>F]altanserin binding to endogenous release of serotonin (Pinborg et al. 2004). The previous study had been performed with infusion of citalopram during *steady state* binding conditions, which was not possible with [<sup>11</sup>C]SB207145 due to the slow tissue kinetics, as well as the short half-life of <sup>11</sup>C. Instead, a baseline and a pharmacologically-stimulated PET recording were acquired for measurement of significant differences, as well as comparison to test-retest scans (study 2, n=6).

Four subjects had cannulation of a radial artery, performed under local anesthesia, for sampling of the arterial input curve. All subjects were scanned twice on the same day. In order to blind the subjects, they received a 40 ml intravenous saline-infusion over a period of one hour, starting 30 min prior to tracer administration for the baseline scan, and an infusion 40 mg Seropram® (citalopram, a selective serotonin reuptake inhibitor, Lundbeck Pharma A/S, Denmark) in 40 ml of saline, also delivered over a period of one hour, starting 30 min before tracer infusion.

The experimental design was intended to impose a high concentration of serotonin in the interstitial space during the initial part of the scan, with citalopram dose and infusion time based upon earlier reports that prolactin levels, a well-known biomarker of hypothalamic serotonin release, could be increased for up to three hours (Smith et al. 2002;Goldberg et al. 2004). Investigators were not blinded as this would have required a randomization of baseline and challenge scans, which was inappropriate as citalopram (Seropram®) has a plasma half-life of 36 hours, such that a delay of one week would be required to return to baseline conditions. To circumvent the autoregulation of the extracellular serotonin concentration mediated by presynaptic 5-HT<sub>1A</sub> autoreceptors in nucleus raphe, increasing doses (3 x 2.5 mg increasing to 3 x 7.5 mg) of the 5-HT<sub>1A</sub> partial agonist/ $\beta$ -adrenoceptor antagonist Hexapindol (Sandoz) were given the last three days before the PET session, and on the morning of the PET recording (Pinborg et al. 2004).

The two PET recordings were made on the same day. Subjects received a bolus injection over 20 seconds of [<sup>11</sup>C]SB207145 (mean dose 317  $\pm$ 112 MBq at first scan and 381  $\pm$ 108 MBq at second scan, the specific activity was 133 GBq/ $\mu$ mol (range 13.5-494) at first scan and 104 GBq/ $\mu$ mol (range 7.7-245) at second scan followed by a two-hour dynamic emission scan as described in paper

2. Venous blood samples were drawn at the times 32 and 55 min after injection for measurements of total plasma radioactivity concentration and parent compound and its metabolites.

Automatic on-line sampling (Allogg AB, Mariefred, Sweden) of arterial blood for measurements of the radioactivity concentration was performed the first 10 min in four of the subjects followed by manual sampling. The on-line system was cross-calibrated to the scanner beforehand and calibrated to the manual samples during data analysis. All blood samples were heparinized and dichlorvos was added to the vials to avoid further decomposition of the tracer in plasma. The manual samples were analyzed as described in paper 2. Structural brain imaging (T1 and T2 weighted) with MR was conducted in all subjects on a 3.0 T Trio scanner. Using AIR, a flow-weighted mean emission image of the first 20 min was automatically aligned to the T1-weighted MR image, which had been segmented into gray matter, white matter, and CSF using SPM2 with the T2 weighted images serving for brain masking. The segmentation was subsequently used for partial volume (PV) correction (Muller-Gartner et al. 1992) and for masking the voxels in the volumes of interest. A total of 24 bilateral region of interest were automatically delineated on each subject's MR image in a user-independent fashion with the Pvelab software package (Svarer et al. 2005).

TAC's were extracted for each region with and without PV correction. Volume weighted averaged TAC in the right and left hemisphere were constructed and kinetic modeling was performed using the research tool PMOD (version 2.95, PMOD Inc, Zürich, Switzerland) with the SRTM using cerebellum as reference region.

For the four subjects with arterial sampling a further processing was performed as described in study 2. Regions of interest chosen for sensitivity to endogenous released serotonin were: Nucleus caudatus, putamen (average of putamen and globus pallidum), insula, and hippocampus, as these regions showed the smallest required sample size for detecting significant differences between groups (see below) and PV correction was applied.

#### *5-HT<sub>4</sub> quantification in a healthy young population*

Sixteen healthy subjects were included in the study (mean age: 28.5 years  $\pm$  7.92, range 20-45 years, 8 males). In six of the subjects (3 males), two scans were obtained for the test-retest study (paper 2). For these subjects, one of the two scans was randomly selected for inclusion in the normal material. Seven subjects (four males) had been treated with the partial 5-HT<sub>1A</sub> agonist/ $\beta$ -adrenoceptor antagonist, pindolol as described above and the baseline of these scans were used in this part. The scanning and data analysis was performed as described above.

## Statistics

For the descriptive analysis of the test-retest data, a relative test-retest difference was calculated per region as either:

$$\text{Variability (paper 1):} = \frac{|retest\_value - test\_value|}{average(test\_value, retest\_value)} \cdot 100\% \quad (\text{Equation 15})$$

$$\text{Relative change (paper 1 and 2)} = \frac{2 \cdot (retest\_value - test\_value)}{test\_value + retest\_value} \cdot 100\% \quad (\text{Equation 16})$$

and the mean and *SD* of these metrics reported across subjects. The *SD* of the relative change is another measure of reproducibility, which is independent of systematic changes between first and second scan. It is the measure used for the calculation of sample size or power but is more sensitive to outliers than the variability as the relative changes are squared before averaging in the calculation of the *SD*.

Reliability was assessed using the intraclass correlation coefficient (*ICC*), determined as:

$$ICC = \frac{MSS_{Between} - MSS_{Within}}{MSS_{Between} + MSS_{Within}} \quad (\text{Equation 17})$$

$MSS_{Between}$  is the mean sum of squares between subjects and  $MSS_{Within}$  is the mean sum of squares within subjects. An *ICC* score of  $-1$  denotes no reliability and  $+1$  denotes maximum reliability.

To statistically compare the difference in variability and *ICC* (paper 1) in the chosen regions between inter- and intraobserver processing, between two-week and two-year follow-up, and between different levels of PV correction, Wilcoxon signed-rank tests were performed.

Spearman's rank correlations were used to evaluate the correlation between binding potentials *in vivo* and literature values for *post mortem* specific binding across regions (paper 3). A non-parametric test was used because the distribution of  $BP_{ND}$  did not follow the normal distribution. The required sample sizes to detect group differences of 15% or 20% with a power of 0.8 were calculated using the regional mean and *SD* of  $BP_{ND}$  across subjects. Sex differences were evaluated using a linear mixed effect model. Mixed models allow data to vary at more than one level and are well suited for nested or clustered data. To include repeated measures from several regions for each subject, region was used as a within-subject factor and sex and age as between-subject factors. Here, we used logarithmic transformation of  $BP_{ND}$  to improve the normal distribution, since the magnitude extended over a large range (from 0.4 in prefrontal cortex to 2.3 in nucleus caudatus). Eight bilateral regions were selected for the analysis (cingulate cortex (average of anterior and

posterior), insula, nucleus caudatus, putamen (average of putamen and globus pallidum), temporal cortex (average of superior and medial inferior temporal cortices), prefrontal cortex (average of dorsolateral and ventrolateral), hippocampus and amygdala) to reflect various functional brain areas and receptor densities. The analysis was repeated for PV corrected binding potentials to ensure that the observed sex differences were not due to larger size of the male brains. Student's t-test was used to compare the area under curve (AUC) for the cerebellum time activity normalized the dose per kg bodyweight. We used the statistical software SAS and adopted a significance level of 0.05 throughout.

## Results and Discussion

### Study 1

In the longitudinal study of healthy elderly individuals, we found no change in regional 5-HT<sub>2A</sub> receptor levels at two-year follow-up regardless of application of PV correction (table 1).

Cortical Regions	No PV correction			1-tissue PV correction			2-tissue PV correction		
	Mean Baseline $BP_p$ (CV)	Mean 2-year follow-up $BP_p$ (CV)	Relative diff. (SD)	Mean Baseline $BP_p$ (CV)	Mean 2-year follow-up $BP_p$ (CV)	Relative diff. (SD)	Mean Baseline $BP_p$ (CV)	Mean 2-year follow-up $BP_p$ (CV)	Relative diff. (SD)
Orbito-frontal Ctx.	0.83 (38%)	0.79 (42%)	2.2% (0.38)	1.35 (30%)	1.31 (34%)	1.2% (0.30)	1.85 (27%)	1.84 (27%)	3.8% (0.25)
Parietal Cortex	0.88 (27%)	0.80 (28%)	-6.9% (0.23)	1.86 (23%)	1.76 (20%)	-2.8% (0.21)	3.10 (22%)	2.98 (20%)	-1.6 (0.20)
Temporal Cortex	1.02 (27%)	0.97 (26%)	-2.9% (0.18)	1.59 (24%)	1.56 (21%)	0.0% (0.17)	2.25 (22%)	2.23 (17%)	1.3% (0.16)
Ant.-cing. Cortex	0.93 (36%)	0.81 (36%)	-9.6% (0.25)	1.23 (34%)	1.11 (32%)	-4.6% (0.28)	1.85 (27%)	1.70 (25%)	-3.8% (0.27)
Occipital Cortex	1.04 (28%)	1.04 (24%)	2.2% (0.19)	1.56 (28%)	1.57 (22%)	4.0% (0.19)	2.90 (28%)	2.95 (19%)	5.2% (0.19)
Frontal Cortex	0.81 (30%)	0.76 (28%)	-4.0% (0.21)	1.75 (22%)	1.71 (19%)	0.1% (0.20)	2.72 (21%)	2.67 (15%)	1.1% (0.19)

Table 1: Binding potential as a function of increasing complexity of the PV correction. The mean binding potentials ( $BP_p$ ) and Coefficient of Variations ( $CV= SD/mean$ ) for baseline and two-year follow-up are shown for six cortical regions with no, one-tissue (Meltzer et al. 1990) and two-tissue (Muller-Gartner et al. 1992) PV correction and the relative differences =  $(scan2-scan1)/scan1$  with standard deviations ( $SD$ ) are reported.

The variability was 12-15% and the *ICC* scores were 0.45-0.67 for larger cortical regions with relatively high binding, when applying two tissue partial volume corrections. Corresponding variability was 14-22%, with *ICC* scores of 0.46-0.72 when no partial volume correction was applied. The orbito-frontal and anterior cingulate cortices showed higher variability and lower reliability, and therefore cannot be recommended as primary volumes of interest in studies requiring high test-retest performance. The higher variability and lower reliability in anterior cingulate cortex is probably due to the small size, while the orbito-frontal cortex shows high variability due to the proximity to the air-containing sinuses around orbita, making this brain region more prone to noise from alignment of PET and MR.

Test-retest within two weeks showed higher reproducibility (4.8-12.7%,  $p=0.031$ ) and reliability (0.78-0.94,  $p=0.031$ ) compared to test-retest within two years. This could be due to the greater age of the subjects enrolled in the two-year follow-up. Correcting for an expected two-year decline in 5-HT<sub>2A</sub> receptors of 1.7% (Meltzer et al. 1998; Adams et al. 2004) did not, however, seem to diminish variability. We found a significant reduction of gray matter volume in the two-year follow-up that may be partly explained by an age-related atrophy of gray matter and partly by a lowering of the water content in the gray matter with age (Neeb et al. 2006), resulting in a change of the segmentation into gray and white matter. The use of the MNI template consisting of young subjects with higher MR contrast compared to elderly may call into question the reliability of the present segmentation. However, we found a high robustness in test-retest gray matter volume with *ICC* scores of 0.74-0.87, and the segmentation did not seem to bias our findings, as no change in binding potentials over two years are observed, regardless of application of the PV correction. Thus, the observed variability between the MR images at baseline and two-year follow-up can only account for some of the greater variability in the two-year follow-up, compared to the two week follow-up, which made use of the same MR image. It is to be expected that coregistration to slightly different MR images must increase variability in the PET end-point.

Figure 6 shows an increasing reproducibility (mean 18% for the large regions, 24% for orbito-frontal cortex, and 8% for anterior cingulate cortex) and decreasing reliability (mean 12% for the large regions, 21% for orbito-frontal cortex, and 26% for anterior cingulate cortex) with increasing complexity of the PV correction. This is in accordance with earlier findings (Haugbol et al. 2007). The lower variability does not favor applying PV correction, as we found that the reliability was also diminished. The variability of non-PV corrected and PV corrected binding

potentials are not directly comparable, given that the between-subject variability decreased with increasing complexity of the PV correction.

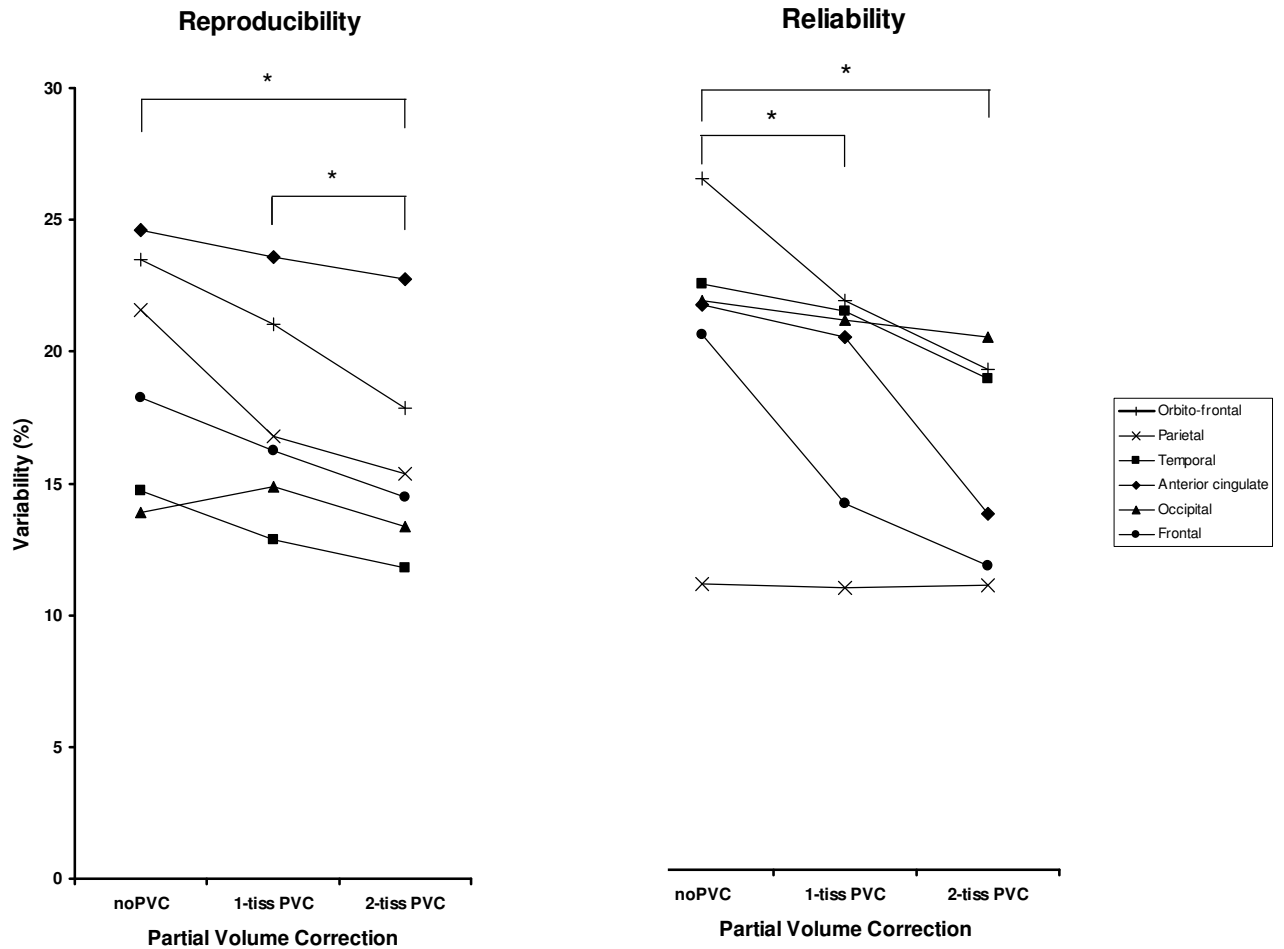


Figure 6. The effect of no, one-tissue (Meltzer et al. 1990) and two-tissue (Muller-Gartner et al. 1992) partial volume correction on two-year test-retest variability<sup>1</sup> (the lower the better) (left) and intraclass correlation coefficients ( $ICC^2$ ) (the higher the better) (right). Both two-year test-retest variability ( $p=0.016$ ) and  $ICC$  ( $p=0.047$ ) are seen to significantly decline with increasing partial volume correction (Wilcoxon signed-rank test), thereby contradicting each other.

\*  $p < 0.05$

<sup>1</sup> Test-retest variability =  $|scan2 - scan1| / \text{mean}(scan1, scan2)$ .

<sup>2</sup>  $ICC = (MSS_{Between} - MSS_{Within}) / (MSS_{Between} + MSS_{Within})$ , where  $MSS_{Between}$  is the mean sum of squares between subjects and  $MSS_{Within}$  is the mean sum of squares within subjects.

When applying PV correction, the target region and the reference region are affected differently. According to equation 4, the PV-corrected gray matter activity in a given voxel is calculated by dividing by  $X_{GM} \otimes PSF$  (the segmented gray matter image (gray matter voxels = 1, non-gray matter voxels = 0) convolved with the point spread function of the scanner). A cortical region such as the parietal cortex is only 2-3 mm thick, as compared to a PSF of 8 mm, resulting in a small  $X_{GM} \otimes PSF$  (on average 0.27). When dividing by  $X_{GM} \otimes PSF$ , the PV-corrected gray matter activity, i.e. the concentration ( $C_T$ ) in parietal cortex, increases by  $0.27^{-1}=3.7$ . Cerebellum has an apparent gray matter thickness in the order of magnitude of one cm, and  $X_{GM} \otimes PSF$  is consequently less affected (on average 0.83), such that the PV corrected concentration ( $C_{ND}$ ) only increases by a factor  $0.83^{-1}=1.2$ . If  $C_T$  and  $C_{ND}$  were affected equally by the PV correction, then  $BP_P$  would have been simply scaled and therefore the relative differences between regions and individuals would have been unchanged. However, the  $C_{ND}$ , which is subtracted from  $C_T$  in the calculation of  $BP_P$  (equation 6), remains essentially constant, such that the PV correction is not a simple scaling, and the relative differences between regions and individuals decrease. Thus, with increasing complexity of PV correction, both within-subject and between-subject variability decreases. The lower reliability when applying PV correction is most likely due in part to the lower between-subject variability (when  $MSS_{Between}$  goes down,  $ICC$  goes down as well, Equation 17), and also to the increase in noise arising from the greater sensitivity to PET-MR alignment. However, low between-subject variability and consequent diminished reliability does not by itself decrease the chance of detecting differences in radioligand binding between groups, even though the expected differences are most likely relatively smaller after PV correction. Thus, when planning future studies with this ligand, the anticipated relative binding difference between groups should be dependent on whether PV correction is applied. In studies requiring high test-retest performance, PV correction is not to be recommended, but its use should, on the other hand, be considered in studies of neurodegenerative diseases, with anticipated differences in the volume of gray matter. PV correction is still the only method that allows for a distinction between  $BP_P$  changes due to atrophy and due to real changes in receptors concentration.

Our findings indicate a stable 5-HT<sub>2A</sub> receptor level over two years in healthy aged subjects, which is in accordance with a report in monozygotic twins, in whom there was a higher degree of covariability of 5-HT<sub>2A</sub> receptor density than in dizygotic twins (Pinborg et al. 2008). Stable assay of 5-HT<sub>2A</sub> receptor binding in the elderly, with high intra- and interobserver reproducibility, is a

prerequisite for future use of [ $^{18}\text{F}$ ]altanserin in longitudinal studies of elderly with presumed neuropsychiatric disorders.

## Study 2

[ $^{11}\text{C}$ ]SB207145 readily crosses the blood brain barrier in humans and yields a heterogeneous brain distribution consistent with the known 5-HT<sub>4</sub> receptor localization. The radioligand has reversible binding kinetics, which were well-described in all regions by a two tissue compartment (2-TC) plasma input model, as judged by the Akaike Information Criteria (table 2).

	Regions	$K_1$ (mL cm <sup>-3</sup> min <sup>-1</sup> )	$k_2$ (min <sup>-1</sup> )	$k_4$ (min <sup>-1</sup> )	$V_T$ (mL/cm <sup>3</sup> )	$BP_{ND}$	Akaike Inf. Criteria	Average diff $BP_{ND}$ (%)	ICC $BP_{ND}$
<b>1-TC model</b>	Cerebellum	0.19 ±0.07	0.023 ±0.003	-	7.86 ±2.23	-	586 ±20	-	-
	Parietal ctx	0.19 ±0.07	0.016 ±0.003	-	11.8 ±3.26	0.51 ±0.10	542 ±26	13.2	0.82
	Sup. fr. ctx	0.19 ±0.07	0.016 ±0.003	-	11.3 ±3.17	0.43 ±0.10	541 ±23	12.5	0.87
	Hippocampus	0.17 ±0.06	0.010 ±0.002	-	16.2 ±4.59	1.07 ±0.21	569 ±13	13.0	0.80
	Striatum	0.23 ±0.08	0.006 ±0.002	-	40.4 ±11.7	4.20 ±0.93	536 ±27	8.2	0.84
<b>2-TC model</b>	Cerebellum	0.24 ±0.08	0.056 ±0.009	0.018 ±0.003	9.50 ±2.58	-	510 ±28	-	-
	Parietal ctx	0.23 ±0.08	0.054 ±0.019	0.050 ±0.023	12.3 ±3.42	0.30 ±0.08	506 ±30	13.6	0.80
	Sup. fr. ctx	0.22 ±0.08	0.057 ±0.021	0.050 ±0.023	11.7 ±3.32	0.23 ±0.08	504 ±26	19.4	0.79
	Hippocampus	0.23 ±0.07	0.110 ±0.032	0.026 ±0.008	17.3 ±5.01	0.82 ±0.19	517 ±21	12.9	0.82
	Striatum	0.27 ±0.09	0.066 ±0.032	0.060 ±0.063	41.4 ±12.0	3.38 ±0.72	519 ±31	7.9	0.68
<b>SRTM</b>	Cerebellum	-	0.016 ±0.012	-	-	-	-	-	-
	Parietal ctx	-	0.069 ±0.011	-	-	0.36 ±0.06	449 ±25	13.6	0.77
	Sup. fr. ctx	-	0.067 ±0.008	-	-	0.30 ±0.07	467 ±20	12.6	0.84
	Hippocampus	-	0.037 ±0.005	-	-	0.70 ±0.13	517 ±14	9.92	0.88
	Striatum	-	0.054 ±0.004	-	-	2.21 ±0.21	496 ±28	6.06	0.76

Table 2. Summary of parameter estimation for the test-retest part (n=6) for five selected brain regions using the 1-TCM, 2-TCM, and SRTM kinetic models.  $K_1$ ,  $k_2$ , and  $k_4$  are the rate constants,  $V_T$  is the total volume of distribution,  $BP_{ND}$  is the binding potential relative to non-displaceable binding, the (minimum) Akaike Information Criterion indicates a more statistically appropriate model. For  $BP_{ND}$  estimates, the mean test-retest difference, which is the standard deviation ( $SD$ ) of the relative difference ( $\Delta\%$ ), is reported. The intraclass correlation coefficient ( $ICC$ ) indicates the reliability. The outcome parameters and Akaike Information Criteria are given as mean  $\pm$   $SD$ . A paired Student's t-test was performed to evaluate for systematic differences between first and second scan. \*  $p < 0.05$ , \*\*  $p < 0.01$ .

Ctx. = cortex.

In addition, the SRTM with cerebellum input was suited to quantitation of radiotracer binding, albeit with a certain bias in striatum, the region with the slowest approach to equilibrium binding; We observed a bias of 20-43% in the striatum (figure 7) arising as a result of violations of SRTM assumptions, in particular due to the likely requirement of 2-TC kinetics in cerebellum (Slifstein et al. 2000). Given this, care should be exercised in the choice between 2-TC (blood sampling) and SRTM (no blood sampling) approaches, depending on the particular application in question. The SRTM yielded low test-retest differences (6-10% in moderate- to high-binding regions and 12-14% in low-binding regions), high reliability ( $ICC$ : 0.76-0.88), and good time stability. The low-binding cortical regions had binding potentials in the range of 0.3-0.4, which were nonetheless measured with good reproducibility and reliability, favoring the investigation of cortical binding potentials in future clinical studies.

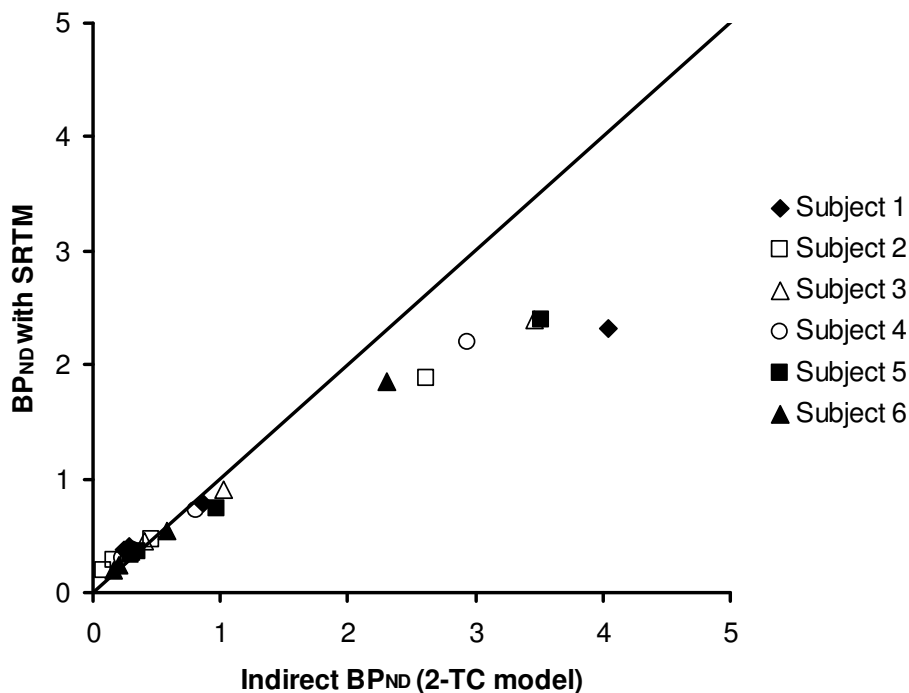


Figure 7.  $BP_{ND}$  estimated with the SRTM compared to  $BP_{ND}$  determined by arterial input (2-TC model) from the test scans of the test-retest data set. The graph shows that a bias is introduced in areas of high binding with SRTM (on average 30%, range 20-43%). The solid line is the line of identity.

The time stability analysis allows for an assessment of the stability of the model and the selection of optimal scan duration. For acquisitions of 100 min or longer, all three models yielded

relatively stable outcome parameters (figure 8) in terms of bias and variance, although there was a slight bias present at 100 min for hippocampus when using SRTM. Thus, 100 min of dynamic data is suitable for quantitative assessment of 5-HT<sub>4</sub> receptors when using an arterial input, however, 120 min acquisition is recommended when SRTM is to be employed.

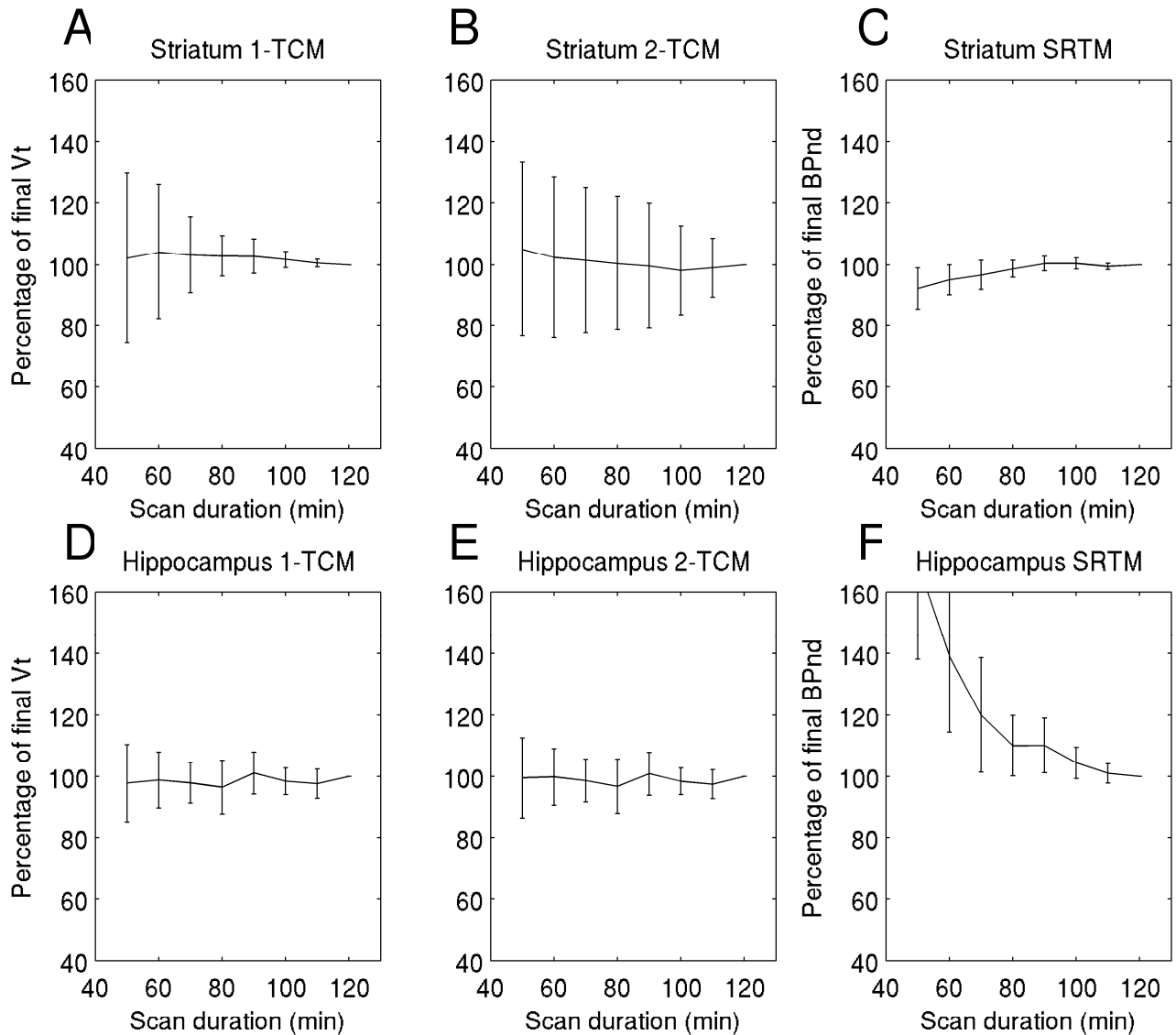


Figure 8. Time stability using the 1-TC model (A), 2-TC model (B), and SRTM (C) for striatum and for hippocampus (D, E, F) for the six test and retest scans. Error bars represent one standard deviation.

Following blocking with a structurally dissimilar selective 5-HT<sub>4</sub> inverse agonist, the distribution volumes in all regions were reduced to that seen in the cerebellum in the baseline condition, whereas  $V_D$  in cerebellum was unchanged (figure 9). These data support the use of the cerebellum as a reference region, and the validity of assuming homogeneous non-specific binding. In addition, the blocking study confirms the selectivity of the specific signal for the 5-HT<sub>4</sub> receptor.

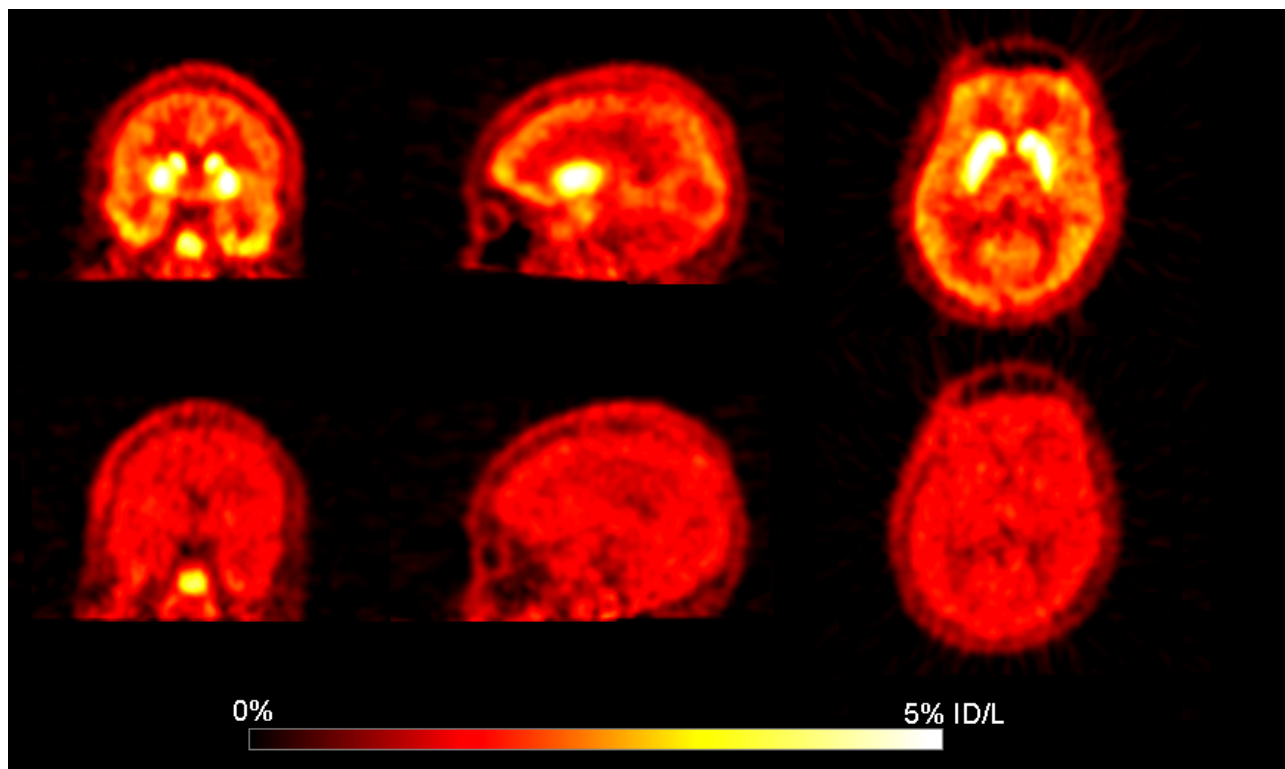


Figure 9. Baseline (A) and a blocked (B) [<sup>11</sup>C]SB207145 scan (male, 29 years) before and after oral administration of the selective inverse 5-HT<sub>4</sub> agonist. The mean images from 30 to 120 min after injection are normalized to injected dose to obtain a standard uptake value (% ID/L= percentage of injected dose per liter). The chosen orthogonal sections pass through the highest binding region of the striatum.

When we simulated CBF-changes in the region of interest by scaling  $K_1$  and  $k_2$ , we saw no significant bias with 2-TC modeling. In contrast, we observed a +12% bias in  $BP_{ND}$  with 30% increased rCBF, versus a bias of -19% with 30% decreased rCBF, when cerebellum blood flow remained constant (figure 10). The finding was less marked for global CBF changes, where the corresponding biases were +7% and -11%. Thus, rCBF changes as seen for example in Alzheimer's disease patients, in whom there occurs hypoperfusion of cerebral cortex and stable cerebellar

perfusion, will result in increased bias in the estimate of  $BP$ , especially when the SRTM is employed. Medication-induced CBF changes are more likely to be global, and will thus result in less bias. The simulated changes of 30% were chosen to evaluate the worst case scenario, since only the most severely-affected patients Alzheimer's disease patient (clinical dementia rating, CDR=3) have CBF reductions of 25-30% (Kobayashi et al. 2008) in comparison to healthy elderly subjects. Nevertheless, the impact of rCBF on the estimation of  $BP_{ND}$  should be considered whenever rCBF is expected to differ between groups.

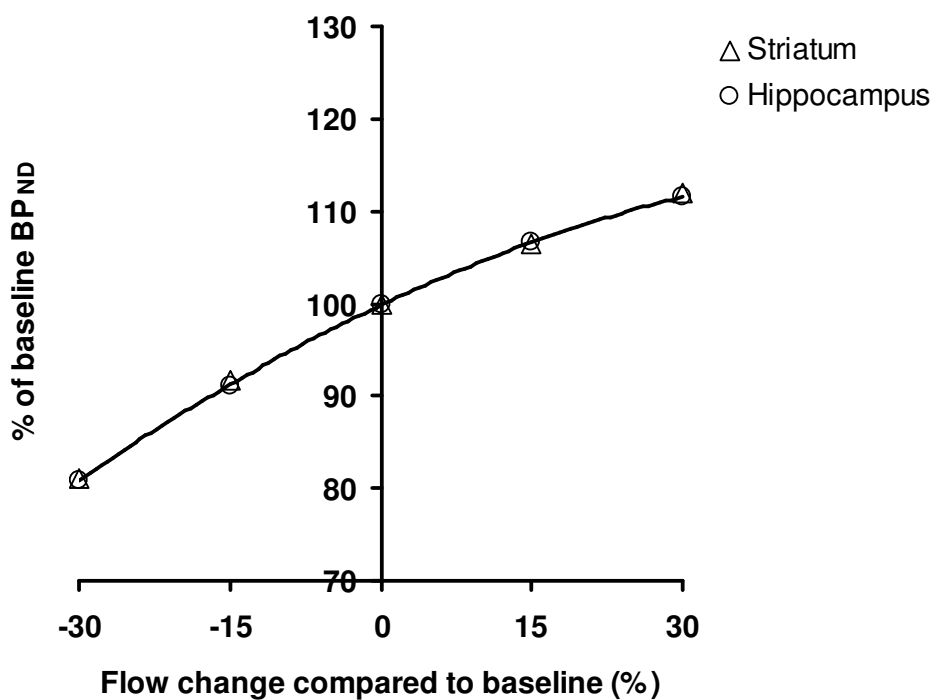


Figure 10. Relative change in SRTM  $BP_{ND}$  (baseline =100%) with changes in cerebral blood flow (CBF) for striatum and hippocampus. The effects of CBF changes are simulated using noise-free time-activity curves to be able to estimate the bias. A second order polynomial had a better fit ( $p=0.0003$ ) compared to a linear fit ( $p=0.001$ ). A positive bias of 12% is commensurate with a CBF increase of 30% and a negative bias of 19% is commensurate with CBF decrease of 30%. When the CBF change is global, i.e. cerebellum CBF changes accordingly, the bias is smaller.

### Study 3

#### *Sensitivity to Endogenous Released Serotonin*

The subjects tolerated the 5-HT<sub>1A</sub> antagonist treatment and citalopram infusion well. Three subjects experienced nausea after half an hour of infusion, and one subject also experienced hot flushes. We deduced a significant release of hypothalamic serotonin, as revealed by altered plasma prolactin and cortisol levels during the entire PET recording (figure 11).

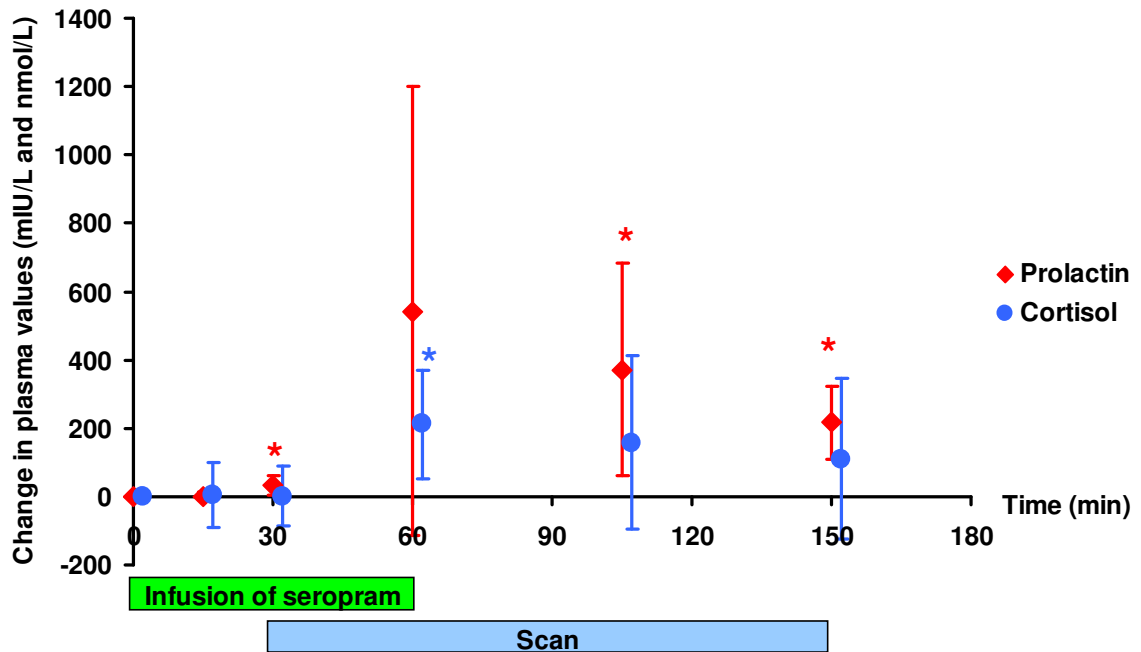


Figure 11. The release of serotonin as measured with plasma prolactin and cortisol (n=7). The plasma values have been subtracted the value at time point 0. Significant and highly varying increases in prolactin and cortisol levels were observed. Error bars represent one standard deviation. \* p<0.05.

The neuroendocrine response was highly variable, with an increase of prolactin of 543 mIU/L (range 59-1511), and an increase of cortisol of 212 nmol/L (range 68-676). [<sup>11</sup>C]SB207145 binding showed no sensitivity to endogenous released serotonin evoked by the treatment. In particular,  $BP_{ND}$  was unaffected in nucleus caudatus, putamen, insula, and hippocampus, both with and without PV correction (figure 12) and we found no correlation between change in  $BP_{ND}$  and change (relative to baseline or absolute values) in plasma prolactin levels.

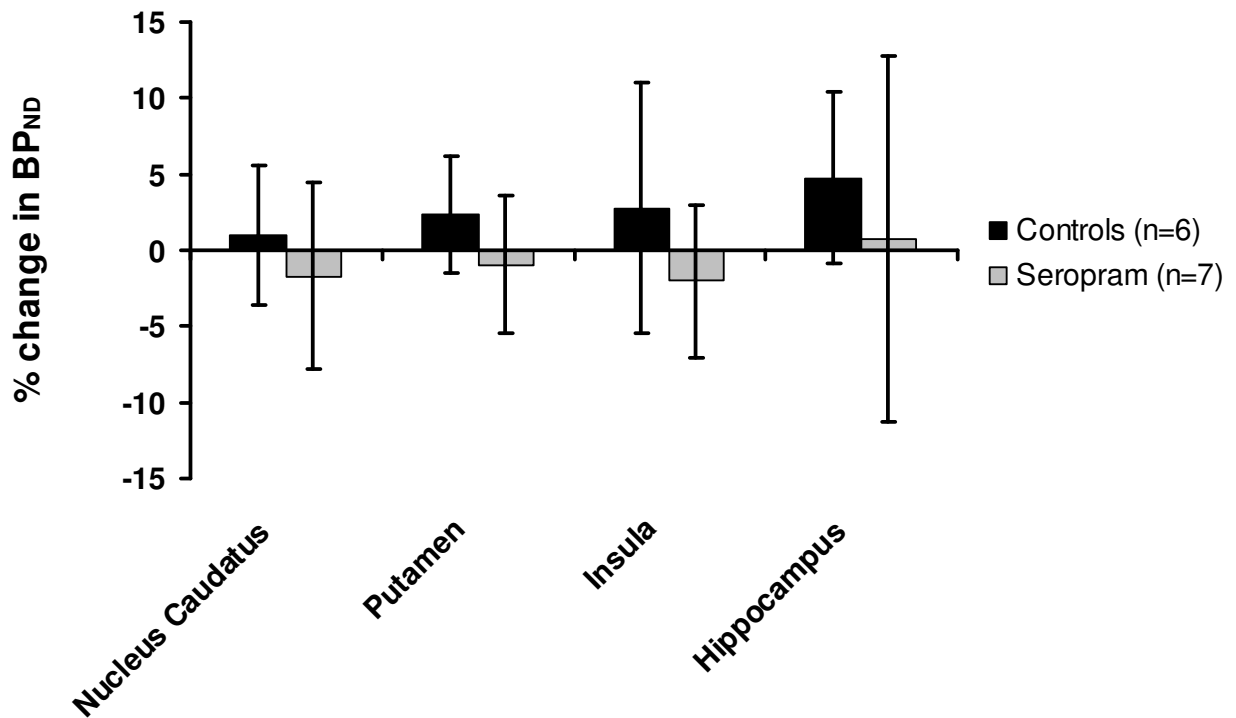


Figure 12. The relative change in non-PV corrected  $BP_{ND}$  between first and second scan is shown for the controls with identical scans and for the cases that received placebo during first scan and 40 mg intravenous citalopram (Seropram, Lundbeck Pharma A/S, Denmark) during second scan. Error bars indicate 95% confidence intervals.

To test for local changes in CBF lasting the entire scan length, we compared the relative delivery of radiotracer, ( $R_I = K_I/K_I'$ ), which was derived from the SRTM. The magnitude of  $R_I$  was unchanged during the citalopram infusion PET recording relative to baseline in nucleus caudatus (paired t-test,  $p = 0.32$ ), putamen ( $p = 0.57$ ), and insula ( $p = 0.15$ ). However, in hippocampus the magnitude of  $R_I$  decreased from  $0.87 \pm 0.04$  to  $0.84 \pm 0.03$  ( $p = 0.02$ ). Transient and focal CBF changes during the scan could, however, have affected the measured  $BP_{ND}$ . We found no global CBF changes, as measured by the differences in  $K_I$  between first and second PET recordings for the three subjects in whom the arterial input was obtained, and for whom compartmental modeling was successful.

The lack of sensitivity to endogenously released serotonin was not unexpected, since this phenomenon has not yet been clearly demonstrated for any serotonin ligand. Based on the confidence intervals depicted in figure 12, we could have overlooked a decrease in [ $^{11}\text{C}$ ]SB207145

binding smaller than 5%, but given the presumably large increases in cerebral 5-HT levels invoked by the pharmacological treatment, we consider that at more physiological (smaller) alterations in cerebral 5-HT levels, a change in binding below 5% is irrelevant in the context of neuroimaging. Although acute changes did not seem to influence binding of [<sup>11</sup>C]SB207145, subacute or chronic changes in cerebral serotonin levels are shown to have a profound effect on the 5-HT<sub>4</sub> receptor levels (Compan et al. 1996) (Licht, personal communication). Accordingly, it will be interesting to investigate if more chronic alterations in cerebral 5-HT levels are associated with inverse changes in [<sup>11</sup>C]SB207145 binding *in vivo*.

No studies have yet evaluated the cellular localization of 5-HT<sub>4</sub> receptors, so it could be conjectured that our negative result is influenced by the presence of large pool of intracellular 5-HT<sub>4</sub> receptors binding to [<sup>11</sup>C]SB207145. If this were the case, then the binding potential obtained with [<sup>11</sup>C]SB207145 is a measure not only of functional receptors presented on the plasma membrane, but also a pool of intracellular receptors, given that the lipophilicity of this tracer predicts easy transit across the plasma membrane. It is not known to what extent the hypothetical intracellular receptor pool reflects functional receptors, or if apparent changes in receptor binding would be due to internalization of receptors. However, it can be assumed that there must be tight control of the number of non-functional receptors; the energy requirement for producing, storing, and degrading receptors must be considerable. Therefore, acute changes in receptor availability as measured with [<sup>11</sup>C]SB207145 would surely reflect disturbances in serotonergic transmission via 5-HT<sub>4</sub> receptors. While [<sup>11</sup>C]SB207145 thus fails as a probe for serotonin release *in vivo*, it proves well-suited for stable assay of receptor availability in healthy individuals. Further studies on the cellular location of the 5-HT<sub>4</sub> receptor may elucidate the binding properties of [<sup>11</sup>C]SB207145, leading to an optimal employment in future molecular imaging studies.

#### *5-HT<sub>4</sub> quantification in a healthy young population*

The regional estimates of  $BP_{ND}$  follow a similar rank order as earlier reports of specific binding *post mortem* (Reynolds et al. 1995; Bonaventure et al. 2000; Varnas et al. 2004). The Spearman's rank correlations between regional autoradiographic data and  $BP_{ND}$  showed significant correlations to PV-corrected  $BP_{ND}$  ( $p=0.0003$ ), but not to non-PV corrected  $BP_{ND}$  estimates ( $p=0.10$ ) (figure 13). This may arise because the PV error distorts rank order of PET binding in regions which seem similar without PV correction.

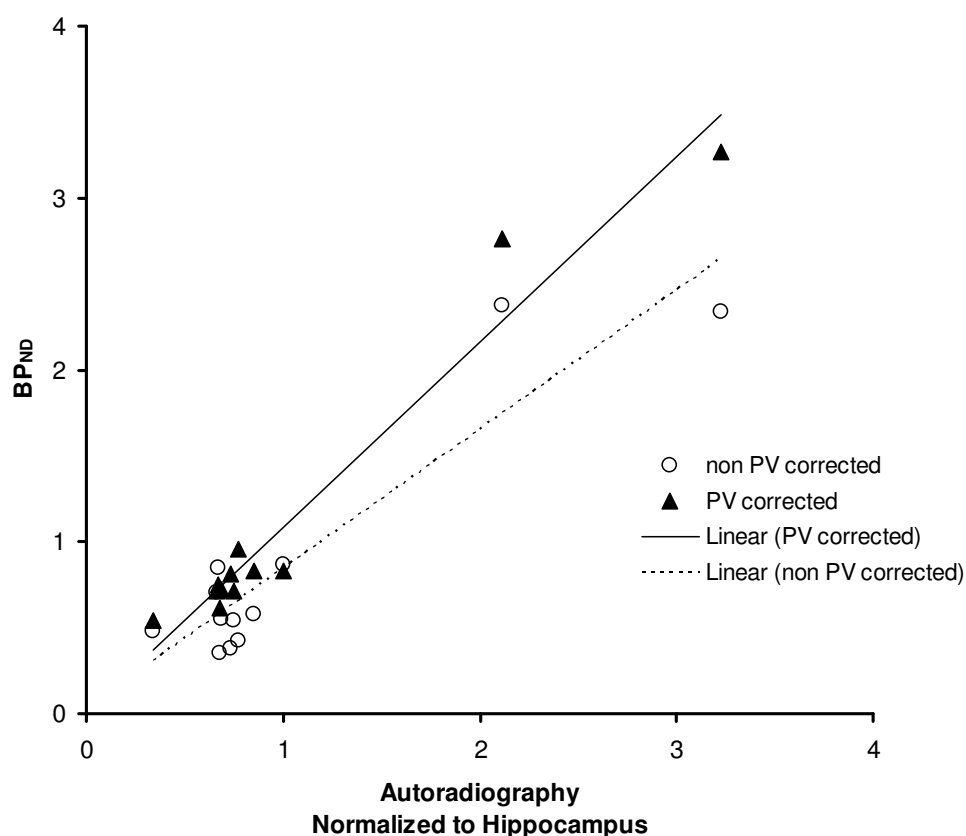


Figure 13. The binding assessed with autoradiography in eleven selected regions: occipital cortex, frontal cortex, temporal cortex, parietal cortex, insula, anterior cingulate, posterior cingulate, amygdala, hippocampus, thalamus, putamen, and nucleus caudatus. Values are averaged from three *post mortem* studies of the human brain with [<sup>125</sup>I]SB207710 (Varnas et al. 2004) (mean of cortical layers, n=3-7), [<sup>3</sup>H]Prucalopride and [<sup>3</sup>H]R116712 (Bonaventure et al. 2000) (n=3), and [<sup>3</sup>H]R116712 (Reynolds et al. 1995). To be able to average, the regional binding in each study was normalized to the value of Hippocampus. The autoradiographic measures of specific binding were correlated to the mean [<sup>11</sup>C]SB207145 binding potential for males (n=8) in the same regions both with and without PV correction (Spearman rank correlation, non-PV corrected:  $r=0.50$ ,  $p=0.095$ , PV corrected:  $r=0.86$ ,  $p=0.0003$ ).

The regional analysis of PET results (table 3) shows that nucleus caudatus and putamen are the highest binding regions, the temporal lobe, hippocampus, and insula are intermediate-binding regions, while anterior and posterior cingulate, prefrontal cortex, parietal cortex and thalamus are low-binding regions. Although, binding in amygdala and hypothalamus are of comparable

magnitude to that of other regions, the small volumes of these latter structures resulted in high variance of the estimates, and correspondingly larger predicted sample sizes for detecting a 15% change. Sensorimotor cortex and occipital cortex proved to have too little binding for reliable quantification. Given the age composition of the present group (<45 years), we cannot predict the corresponding sample sizes needed for elderly subjects. The power calculations are based on non-PV corrected  $BP_{ND}$ 's, to avoid a spurious lowering of the inter-subject variation, as explained above in study 1.

Region	Without PV correction				With PV correction		
	Males (n=8) $BP_{ND}$ ( $\pm SD$ )	Females (n=8) $BP_{ND}$ ( $\pm SD$ )	All (n=16) $BP_{ND}$ ( $\pm SD$ )	Sample Size 2-sample (n=16) 15%/20%	Sample Size Paired (n=6) 15%	Males (n=8) $BP_{ND}$ ( $\pm SD$ )	Females (n=8) $BP_{ND}$ ( $\pm SD$ )
Temporal cortex	0.58 $\pm$ 0.05	0.49 $\pm$ 0.09*	0.54 $\pm$ 0.08	18 / 11	4	0.83 $\pm$ 0.07	0.77 $\pm$ 0.08
Parietal cortex	0.43 $\pm$ 0.03	0.39 $\pm$ 0.09	0.41 $\pm$ 0.07	20 / 12	5	0.96 $\pm$ 0.10	0.89 $\pm$ 0.10
Occipital cortex	0.35 $\pm$ 0.03	0.31 $\pm$ 0.08	0.33 $\pm$ 0.06	27 / 15	4	0.61 $\pm$ 0.10	0.57 $\pm$ 0.07
Sensorimotor cortex	0.25 $\pm$ 0.04	0.22 $\pm$ 0.06	0.24 $\pm$ 0.05	39 / 22	9	0.73 $\pm$ 0.11	0.67 $\pm$ 0.07
Prefrontal cortex	0.38 $\pm$ 0.03	0.35 $\pm$ 0.06	0.36 $\pm$ 0.05	14 / 9	4	0.81 $\pm$ 0.07	0.79 $\pm$ 0.06
Insula	0.71 $\pm$ 0.06	0.62 $\pm$ 0.11	0.66 $\pm$ 0.10	17 / 10	7	0.72 $\pm$ 0.10	0.65 $\pm$ 0.10
Thalamus	0.48 $\pm$ 0.03	0.44 $\pm$ 0.08	0.46 $\pm$ 0.06	13 / 8	6	0.54 $\pm$ 0.05	0.50 $\pm$ 0.08
Anterior Cingulate	0.54 $\pm$ 0.05	0.47 $\pm$ 0.11	0.51 $\pm$ 0.09	24 / 14	14	0.71 $\pm$ 0.11	0.64 $\pm$ 0.12
Putamen	2.37 $\pm$ 0.10	2.14 $\pm$ 0.32	2.26 $\pm$ 0.26	11 / 7	4	2.77 $\pm$ 0.17	2.53 $\pm$ 0.33
Hippocampus	0.87 $\pm$ 0.05	0.69 $\pm$ 0.13**	0.78 $\pm$ 0.13	21 / 13	5	0.83 $\pm$ 0.10	0.69 $\pm$ 0.14*
Posterior Cingulate	0.55 $\pm$ 0.06	0.47 $\pm$ 0.10	0.51 $\pm$ 0.09	24 / 14	3	0.72 $\pm$ 0.08	0.66 $\pm$ 0.09
Caudate Nucleus	2.34 $\pm$ 0.31	2.17 $\pm$ 0.38	2.25 $\pm$ 0.34	18 / 11	4	3.27 $\pm$ 0.21	3.05 $\pm$ 0.31
Amygdala	0.71 $\pm$ 0.09	0.57 $\pm$ 0.09**	0.64 $\pm$ 0.12	24 / 14	8	0.75 $\pm$ 0.13	0.61 $\pm$ 0.17
Hypothalamus	0.57 $\pm$ 0.10	0.50 $\pm$ 0.12	0.53 $\pm$ 0.11	33 / 17	12	1.11 $\pm$ 0.21	1.01 $\pm$ 0.18

Table 3. [ $^{11}\text{C}$ ]SB207145  $BP_{ND}$  ordered in very large (>50 cm<sup>3</sup>), large (10-50 cm<sup>3</sup>), intermediate (5-10 cm<sup>3</sup>), and small regions (<5 cm<sup>3</sup>). Sample size estimates for group wise comparisons (2-sample) were based on mean and standard deviation ( $SD$ ) of all 16 subjects, a power of 0.80 and a group difference of 15% or 20%, while the estimates for paired tests were based on mean and  $SD$  of the difference between first and second scan for the 6 subjects with test-retest data. \* $p$ <0.05, \*\* $p$ <0.01 (Student's t-test).

We found a trend for [ $^{11}\text{C}$ ]SB207145  $BP_{ND}$  to decrease with age ( $p$ =0.056). Several monaminergic receptors decline with age (Wang et al. 1998; Inoue et al. 2001; Tauscher et al. 2001; Adams et al. 2004), so it seems plausible that the 5-HT<sub>4</sub> receptor binding should likewise decline with age. However, the age span in our sample was not large enough for sensitively

detecting age-related changes, which might have been evident in a cohort including healthy elderly subjects.

Males were found to have significantly higher  $BP_{ND}$  in three of the eight selected regions (figure 14). The mixed model showed an overall significant sex effect ( $t=-2.49$ ,  $df=13$ ,  $p=0.027$  when age was included in the analysis and  $t=-2.57$ ,  $df=14$ ,  $p=0.022$  when age was not included). PV correction did not change this finding significantly, and the sex effect seemed to be global as no sex  $\times$  region effect could be demonstrated and.

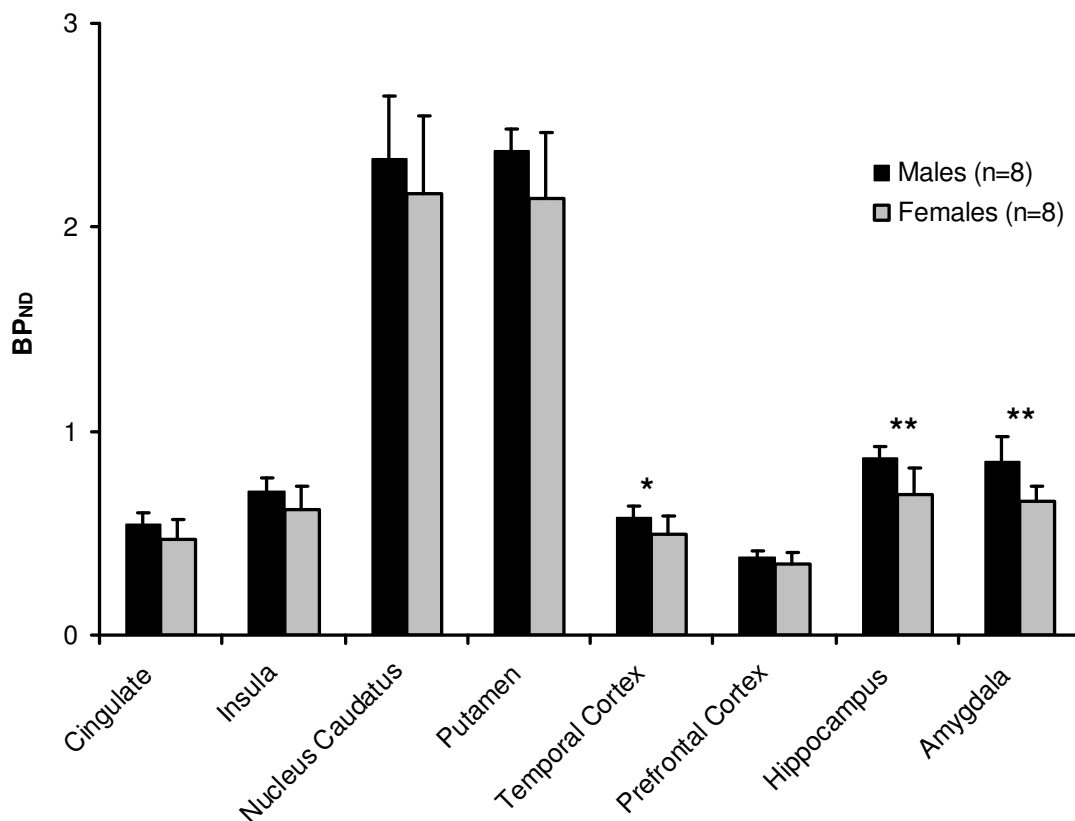


Figure 14. The mean [ $^{11}\text{C}$ ]SB207145 binding potential in eight selected regions for males and females. The binding potentials are not partial volume corrected. Error bars represent one standard deviation. \* $<0.05$ , \*\* $<0.005$ .

The use of hormonal contraception, time of cycle, smoking, education, handedness, relative delivery, or brain size did not seem to influence the binding results in the present group of 16 subjects. In addition to the limited power, there are several possible limitations to the interpretation of the observed sex difference. First, the level of presumably non-displaceable [ $^{11}\text{C}$ ]207145 binding in the cerebellum AUC normalized to the percentage injected dose per kg body weight were  $116 \pm$

12 g min mL<sup>-1</sup> in males and 132 ± 29 g min mL<sup>-1</sup> in females (p=0.17), perhaps reflecting sex differences in tracer metabolism. As the outcome measure is calculated relative to this non-displaceable binding, a greater cerebellum AUC would propagate to lower  $BP_{ND}$ . However, non-significant *positive* correlations (r=0.26 in males and r=0.48 for in females) between hippocampal binding (the region with the most pronounced sex difference) and cerebellum AUC were observed, suggesting that other factors may account for the lower  $BP_{ND}$  in females. Also, the present sample size is rather limited for detection of subtle sex differences, and firm conclusions on sex differences in the 5-HT<sub>4</sub> receptor availability will require studies of larger groups. Possible sex differences in 5-HT<sub>4</sub> binding are highly interesting due to the involvement of serotonin in affective and anxiety disorders, which are much more prevalent in females. Future investigations of sex difference in the serotonin system are likely to aid the understanding of these common disorders.

## Conclusions and Perspectives

In conclusion, no change in 5-HT<sub>2A</sub>-receptor binding was found during two-year follow-up of healthy elderly subjects, indicating a stable serotonin system in these individuals. The variability in  $BP_P$  was 12-15% in large brain regions with high binding, but the variability should be interpreted with care when PV correction is applied, and cannot be compared to the case of test-retest studies without PV correction. PV correction diminishes the reliability of  $BP_P$ , but allows for the important distinction between atrophy and changes in abundance of receptors. Further, the rank order between regions may be more identical to autoradiographic data when PV correction is applied (figure 13). A lowering of the inter-subject variability and thereby of the reliability in cortical regions when applying PV correction is likely to occur for most tracers when cerebellum is used as the reference region. Thus, the decision to apply PV correction results in a trade-off between accuracy and precision; after PV correction, binding estimates approach the “true” value, but reliability and most likely the sensitivity to detect subtle changes in binding potentials are decreased. Test-retest reliability with ICC scores of 0.45-0.67 in healthy volunteers is acceptable and provides the basis for future longitudinal studies of elderly patients with neuropsychiatric disorders.

[<sup>11</sup>C]SB207145 can be used for quantitative PET measurements of 5-HT<sub>4</sub> receptors in the human brain. The distribution volumes and binding potentials can be reliably estimated using 2-TC modeling with arterial input measurements. Use of the SRTM to avoid the need for invasive arterial cannulation gives high reproducibility and reliability at scan times of 120 min, but resulted in

downward bias in high binding regions, and was associated with sensitivity to rCBF changes. Especially in striatum, temporal cortex, and hippocampus, the estimates of  $BP_{ND}$  exhibit low inter-subject variation, and had a rank order in accordance with autoradiographic findings *in vitro*.

[<sup>11</sup>C]SB207145 specific binding is not sensitive to endogenous release of serotonin, and the stability of its binding in the presence of acute fluctuations in serotonin release is a useful property for future studies of 5-HT<sub>4</sub> receptor availability in health and disease. The stable serotonin system shown in paper 1 and the high test-retest reproducibility shown in paper 2 furthermore hold promise for studies in elderly and for longitudinal studies using [<sup>11</sup>C]SB207145.

The present findings can provide the basis for investigations of the relationship between 5-HT<sub>4</sub> binding in cerebral cortex and cognitive function. In particular, evaluating the state of 5-HT<sub>4</sub> receptors in Alzheimer's disease may have implications for future disease-modifying treatments. Finally, 5-HT<sub>4</sub> receptor agonists acting in the brain could become of relevance for rapid-onset treatment of depression (Lucas et al. 2007a), epilepsy (Compan et al. 2004), or eating disorders (Compan et al. 2004; Jean et al. 2007). We anticipate that the use of [<sup>11</sup>C]SB207145 PET in occupancy studies will be a superior tool for dose selection in future clinical trials of drugs acting on the 5-HT<sub>4</sub> receptor.

## References

- Adams KH, Pinborg LH, Svarer C, Hasselbalch SG, Holm S, Haugbol S, Madsen K, Frokjaer V, Martiny L, Paulson OB, Knudsen GM (2004) A database of [(18)F]-altanserin binding to 5-HT(2A) receptors in normal volunteers: normative data and relationship to physiological and demographic variables. *Neuroimage* 21:1105-1113
- Berg KA, Harvey JA, Spampinato U, Clarke WP (2005) Physiological relevance of constitutive activity of 5-HT<sub>2A</sub> and 5-HT<sub>2C</sub> receptors. *Trends Pharmacol Sci* 26:625-630
- Blier P (2003) The pharmacology of putative early-onset antidepressant strategies. *Eur Neuropsychopharmacol* 13:57-66
- Blin J, Baron JC, Dubois B, Crouzel C, Fiorelli M, ttar-Levy D, Pillon B, Fournier D, Vidailhet M, Agid Y (1993) Loss of brain 5-HT<sub>2</sub> receptors in Alzheimer's disease. In vivo assessment with positron emission tomography and [18F]setoperone. *Brain* 116:497-510
- Bockaert J, Claeysen S, Compan V, Dumuis A (2004) 5-HT<sub>4</sub> receptors. *Curr Drug Targets CNS Neurol Disord* 3:39-51
- Bonaventure P, Hall H, Gommeren W, Cras P, Langlois X, Jurzak M, Leysen JE (2000) Mapping of serotonin 5-HT<sub>4</sub> receptor mRNA and ligand binding sites in the post-mortem human brain. *Synapse* 36:35-46
- Cachard-Chastel M, Lezoualc'h F, Dewachter I, Delomenie C, Croes S, Devijver H, Langlois M, Van LF, Sicsic S, Gardier AM (2007) 5-HT<sub>4</sub> receptor agonists increase sAPP $\alpha$  levels in the cortex and hippocampus of male C57BL/6j mice. *Br J Pharmacol* 150:883-892
- Cai X, Flores-Hernandez J, Feng J, Yan Z (2002) Activity-dependent bidirectional regulation of GABA(A) receptor channels by the 5-HT<sub>4</sub> receptor-mediated signalling in rat prefrontal cortical pyramidal neurons. *J Physiol* 540:743-759
- Cho S, Hu Y (2007) Activation of 5-HT<sub>4</sub> receptors inhibits secretion of beta-amyloid peptides and increases neuronal survival. *Exp Neurol* 203:274-278

- Compan V, Daszuta A, Salin P, Sebben M, Bockaert J, Dumuis A (1996) Lesion study of the distribution of serotonin 5-HT<sub>4</sub> receptors in rat basal ganglia and hippocampus. *Eur J Neurosci* 8:2591-2598
- Compan V, Zhou M, Grailhe R, Gazzara RA, Martin R, Gingrich J, Dumuis A, Brunner D, Bockaert J, Hen R (2004) Attenuated response to stress and novelty and hypersensitivity to seizures in 5-HT<sub>4</sub> receptor knock-out mice. *J Neurosci* 24:412-419
- Delgado PL, Miller HL, Salomon RM, Licinio J, Krystal JH, Moreno FA, Heninger GR, Charney DS (1999) Tryptophan-depletion challenge in depressed patients treated with desipramine or fluoxetine: implications for the role of serotonin in the mechanism of antidepressant action. *Biol Psychiatry* 46:212-220
- Frokjaer VG, Mortensen EL, Nielsen FA, Haugbol S, Pinborg LH, Adams KH, Svarer C, Hasselbalch SG, Holm S, Paulson OB, Knudsen GM (2008) Frontolimbic Serotonin 2A Receptor Binding in Healthy Subjects Is Associated with Personality Risk Factors for Affective Disorder. *Biol Psychiatry* 63:569-576
- Gee AD, Martarello L, Passchier M, Wishart C, Parker J, Matthews R, Comley R, Hopper R, Gunn R (2008) Synthesis and Evaluation of [<sup>11</sup>C]SB207145 as the First *In Vivo* Serotonin 5-HT<sub>4</sub> Receptor Radioligand for PET Imaging in Man. *Current Radiopharmaceuticals* 1:
- Gillings N, Marner L, Knudsen GM (2007) A Rapid, Robust and Fully Automated Method for Analysis of Radioactive Metabolites in Plasma Samples from PET Studies [abstract]. *J Label Compd Radiopharm* 50:S503
- Goldberg S, Smith GS, Barnes A, Ma Y, Kramer E, Robeson K, Kirshner M, Pollock BG, Eidelberg D (2004) Serotonin modulation of cerebral glucose metabolism in normal aging. *Neurobiol Aging* 25:167-174
- Gray JA, Roth BL (2001) Paradoxical trafficking and regulation of 5-HT<sub>2A</sub> receptors by agonists and antagonists. *Brain Res Bull* 56:441-451
- Hasselbalch SG, Madsen K, Svarer C, Pinborg LH, Holm S, Paulson OB, Waldemar G, Knudsen GM (2008) Reduced 5-HT<sub>2A</sub> receptor binding in patients with mild cognitive impairment. *Neurobiol Aging* 29:1830-1838

- Haugbol S, Pinborg LH, Arfan HM, Frokjaer VM, Madsen J, Dyrby TB, Svarer C, Knudsen GM (2007) Reproducibility of 5-HT<sub>2A</sub> receptor measurements and sample size estimations with [(18)F]altanserin PET using a bolus/infusion approach. *Eur J Nucl Med Mol Imaging* 34:910-915
- Hjorth S, Westlin D, Bengtsson HJ (1997) WAY100635-induced augmentation of the 5-HT-elevating action of citalopram: relative importance of the dose of the 5-HT<sub>1A</sub> (auto)receptor blocker versus that of the 5-HT reuptake inhibitor. *Neuropharmacology* 36:461-465
- Hume SP, Myers R, Bloomfield PM, Opacka-Juffry J, Cremer JE, Ahier RG, Luthra SK, Brooks DJ, Lammertsma AA (1992) Quantitation of carbon-11-labeled raclopride in rat striatum using positron emission tomography. *Synapse* 12:47-54
- Ichise M, Liow JS, Lu JQ, Takano A, Model K, Toyama H, Suhara T, Suzuki K, Innis RB, Carson RE (2003) Linearized reference tissue parametric imaging methods: application to [11C]DASB positron emission tomography studies of the serotonin transporter in human brain. *J Cereb Blood Flow Metab* 23:1096-1112
- Innis RB, Cunningham VJ, Delforge J, Fujita M, Gjedde A, Gunn RN, Holden J, Houle S, Huang SC, Ichise M, Iida H, Ito H, Kimura Y, Koeppe RA, Knudsen GM, Knuuti J, Lammertsma AA, Laruelle M, Logan J, Maguire RP, Mintun MA, Morris ED, Parsey R, Price JC, Slifstein M, Sossi V, Suhara T, Votaw JR, Wong DF, Carson RE (2007) Consensus nomenclature for in vivo imaging of reversibly binding radioligands. *J Cereb Blood Flow Metab* 27:1533-1539
- Inoue M, Suhara T, Sudo Y, Okubo Y, Yasuno F, Kishimoto T, Yoshikawa K, Tanada S (2001) Age-related reduction of extrastriatal dopamine D<sub>2</sub> receptor measured by PET. *Life Sci* 20;69:1079-1084
- Jean A, Conductier G, Manrique C, Bouras C, Berta P, Hen R, Charnay Y, Bockaert J, Compan V (2007) Anorexia induced by activation of serotonin 5-HT<sub>4</sub> receptors is mediated by increases in CART in the nucleus accumbens. *Proc Natl Acad Sci U S A* 104:16335-16340
- Jiang M, Guo W, Scheiren R, Narendran R, Javitch J, Rayport S, Laruelle M (2006) Agonist-mediated internalization of dopamine D<sub>2</sub> receptors does not appear to mediate the decrease

in benzamides binding potential observed after dopamine surge [abstract]. *Neuroimage* 31:T32

Kepe V, Barrio JR, Huang SC, Ercoli L, Siddarth P, Shoghi-Jadid K, Cole GM, Satyamurthy N, Cummings JL, Small GW, Phelps ME (2006) Serotonin 1A receptors in the living brain of Alzheimer's disease patients. *Proc Natl Acad Sci U S A* 103:702-707

Kobayashi S, Tateno M, Utsumi K, Takahashi A, Saitoh M, Morii H, Fujii K, Teraoka M (2008) Quantitative analysis of brain perfusion SPECT in Alzheimer's disease using a fully automated regional cerebral blood flow quantification software, 3DSRT. *J Neurol Sci* 264:27-33

Kornum BR, Lind NM, Gillings N, Marner L, Andersen F, Knudsen GM (2008) Evaluation of the novel 5-HT(4) receptor PET ligand [(11)C]SB207145 in the Göttingen minipig. *J Cereb Blood Flow Metab*

Lai MK, Tsang SW, Francis PT, Esiri MM, Hope T, Lai OF, Spence I, Chen CP (2003) [3H]GR113808 binding to serotonin 5-HT(4) receptors in the postmortem neocortex of Alzheimer disease: a clinicopathological study. *J Neural Transm* 110:779-788

Lammertsma AA, Hume SP (1996) Simplified reference tissue model for PET receptor studies. *Neuroimage* 4:153-158

Laruelle M (2000) Imaging synaptic neurotransmission with in vivo binding competition techniques: a critical review. *J Cereb Blood Flow Metab* 20:423-451

Laruelle M, D'Souza CD, Baldwin RM, bi-Dargham A, Kaner SJ, Fingado CL, Seibyl JP, Zoghbi SS, Bowers MB, Jatlow P, Charney DS, Innis RB (1997) Imaging D2 receptor occupancy by endogenous dopamine in humans. *Neuropsychopharmacology* 17:162-174

Laruelle M, Slifstein M, Huang Y (2002) Positron emission tomography: imaging and quantification of neurotransmitter availability. *Methods* 27:287-299

Lucas G, Rymer VV, Du J, Mnie-Filali O, Bisgaard C, Manta S, Lambas-Senas L, Wiborg O, Haddjeri N, Pineyro G, Sadikot AF, Debonnel G (2007a) Serotonin(4) (5-HT(4)) receptor agonists are putative antidepressants with a rapid onset of action. *Neuron* 55:712-725

- Lucas G, Rymar VV, Du J, Mnie-Filali O, Bisgaard C, Manta S, Lambas-Senas L, Wiborg O, Haddjeri N, Pineyro G, Sadikot AF, Debonnel G (2007b) Serotonin(4) (5-HT(4)) receptor agonists are putative antidepressants with a rapid onset of action. *Neuron* 55:712-725
- Martinez D, Narendran R, Foltin RW, Slifstein M, Hwang DR, Broft A, Huang Y, Cooper TB, Fischman MW, Kleber HD, Laruelle M (2007) Amphetamine-induced dopamine release: markedly blunted in cocaine dependence and predictive of the choice to self-administer cocaine. *Am J Psychiatry* 164:622-629
- Meltzer CC, Leal JP, Mayberg HS, Wagner HN, Jr., Frost JJ (1990) Correction of PET data for partial volume effects in human cerebral cortex by MR imaging. *J Comput Assist Tomogr* 14:561-570
- Meltzer CC, Smith G, DeKosky ST, Pollock BG, Mathis CA, Moore RY, Kupfer DJ, Reynolds CF, III (1998) Serotonin in aging, late-life depression, and Alzheimer's disease: the emerging role of functional imaging. *Neuropsychopharmacology* 18:407-430
- Messa C, Colombo C, Moresco RM, Gobbo C, Galli L, Lucignani G, Gilardi MC, Rizzo G, Smeraldi E, Zanardi R, Artigas F, Fazio F (2003) 5-HT(2A) receptor binding is reduced in drug-naive and unchanged in SSRI-responder depressed patients compared to healthy controls: a PET study. *Psychopharmacology (Berl)* 167:72-78
- Mohler EG, Shacham S, Noiman S, Lezoualc'h F, Robert S, Gastineau M, Rutkowski J, Marantz Y, Dumuis A, Bockaert J, Gold PE, Ragozzino ME (2007) VRX-03011, a novel 5-HT4 agonist, enhances memory and hippocampal acetylcholine efflux. *Neuropharmacology* 53:563-573
- Muller-Gartner HW, Links JM, Prince JL, Bryan RN, McVeigh E, Leal JP, Davatzikos C, Frost JJ (1992) Measurement of radiotracer concentration in brain gray matter using positron emission tomography: MRI-based correction for partial volume effects. *J Cereb Blood Flow Metab* 12:571-583
- Neeb H, Zilles K, Shah NJ (2006) Fully-automated detection of cerebral water content changes: study of age- and gender-related H2O patterns with quantitative MRI. *Neuroimage* 29:910-922

- Orsetti M, Dellarole A, Ferri S, Ghi P (2003) Acquisition, retention, and recall of memory after injection of RS67333, a 5-HT<sub>4</sub> receptor agonist, into the nucleus basalis magnocellularis of the rat. *Learn Mem* 10:420-426
- Pakkenberg B, Gundersen HJ (1997) Neocortical neuron number in humans: effect of sex and age. *J Comp Neurol* 384:312-320
- Pelvig DP, Pakkenberg H, Regeur L, Oster S, Pakkenberg B (2003) Neocortical glial cell numbers in Alzheimer's disease. A stereological study. *Dement Geriatr Cogn Disord* 16:212-219
- Pinborg LH, Adams KH, Svarer C, Holm S, Hasselbalch SG, Haugbol S, Madsen J, Knudsen GM (2003) Quantification of 5-HT<sub>2A</sub> receptors in the human brain using [18F]altanserin-PET and the bolus/infusion approach. *J Cereb Blood Flow Metab* 23:985-996
- Pinborg LH, Adams KH, Yndgaard S, Hasselbalch SG, Holm S, Kristiansen H, Paulson OB, Knudsen GM (2004) [18F]altanserin binding to human 5HT<sub>2A</sub> receptors is unaltered after citalopram and pindolol challenge. *J Cereb Blood Flow Metab* 24:1037-1045
- Pinborg LH, Arfan H, Haugbol S, Kyvik KO, Hjelmberg JV, Svarer C, Frokjaer VG, Paulson OB, Holm S, Knudsen GM (2008) The 5-HT<sub>2A</sub> receptor binding pattern in the human brain is strongly genetically determined. *Neuroimage* 40:1175-1180
- Porras G, Di Matteo V, De Deurwaerdere P, Esposito E, Spampinato U (2002) Central serotonin<sub>4</sub> receptors selectively regulate the impulse-dependent exocytosis of dopamine in the rat striatum: in vivo studies with morphine, amphetamine and cocaine. *Neuropharmacology* 43:1099-1109
- Reynolds GP, Mason SL, Meldrum A, De KS, Parnes H, Eglen RM, Wong EH (1995) 5-Hydroxytryptamine (5-HT)<sub>4</sub> receptors in post mortem human brain tissue: distribution, pharmacology and effects of neurodegenerative diseases. *Br J Pharmacol* 114:993-998
- Robert SJ, Zugaza JL, Fischmeister R, Gardier AM, Lezoualc'h F (2001) The human serotonin 5-HT<sub>4</sub> receptor regulates secretion of non-amyloidogenic precursor protein. *J Biol Chem* 276:44881-44888

- Rousset OG, Ma Y, Evans AC (1998) Correction for partial volume effects in PET: principle and validation. *J Nucl Med* 39:904-911
- Slifstein M, Parsey RV, Laruelle M (2000) Derivation of [(11)C]WAY-100635 binding parameters with reference tissue models: effect of violations of model assumptions. *Nucl Med Biol* 27:487-492
- Smith GS, Ma Y, Dhawan V, Gunduz H, Carbon M, Kirshner M, Larson J, Chaly T, Belakhleff A, Kramer E, Greenwald B, Kane JM, Laghrissi-Thode F, Pollock BG, Eidelber D (2002) Serotonin modulation of cerebral glucose metabolism measured with positron emission tomography (PET) in human subjects. *Synapse* 45:105-112
- Soares JC, Innis RB (1999) Neurochemical brain imaging investigations of schizophrenia. *Biol Psychiatry* 46:600-615
- Svarer C, Madsen K, Hasselbalch SG, Pinborg LH, Haugbol S, Frokjaer VG, Holm S, Paulson OB, Knudsen GM (2005) MR-based automatic delineation of volumes of interest in human brain PET images using probability maps. *Neuroimage* 24:969-979
- Syvanen S, Blomquist G, Sprycha M, Hoglund AU, Roman M, Eriksson O, Hammarlund-Udenaes M, Langstrom B, Bergstrom M (2006) Duration and degree of cyclosporin induced P-glycoprotein inhibition in the rat blood-brain barrier can be studied with PET. *Neuroimage* 32:1134-1141
- Takano A, Arakawa R, Hayashi M, Takahashi H, Ito H, Suhara T (2007) Relationship Between Neuroticism Personality Trait and Serotonin Transporter Binding. *Biol Psychiatry* 62:588-592
- Tauscher J, Verhoeff NP, Christensen BK, Hussey D, Meyer JH, Kecojevic A, Javanmard M, Kasper S, Kapur S (2001) Serotonin 5-HT<sub>1A</sub> receptor binding potential declines with age as measured by [(11)C]WAY-100635 and PET. *Neuropsychopharmacology* 24:522-530
- Terry AV, Jr., Buccafusco JJ, Jackson WJ, Prendergast MA, Fontana DJ, Wong EH, Bonhaus DW, Weller P, Eglen RM (1998) Enhanced delayed matching performance in younger and older macaques administered the 5-HT<sub>4</sub> receptor agonist, RS 17017. *Psychopharmacology (Berl)* 135:407-415

- Turner PR, O'Connor K, Tate WP, Abraham WC (2003) Roles of amyloid precursor protein and its fragments in regulating neural activity, plasticity and memory. *Prog Neurobiol* 70:1-32
- Van den Wyngaert I, Gommeren W, Verhasselt P, Jurzak M, Leysen J, Luyten W, Bender E (1997) Cloning and expression of a human serotonin 5-HT<sub>4</sub> receptor cDNA. *J Neurochem* 69:1810-1819
- van Velden FH, Kloet RW, van Berckel BN, Wolfensberger SP, Lammertsma AA, Boellaard R (2008) Comparison of 3D-OP-OSEM and 3D-FBP reconstruction algorithms for High-Resolution Research Tomograph studies: effects of randoms estimation methods. *Phys Med Biol* 53:3217-3230
- Varnas K, Halldin C, Hall H (2004) Autoradiographic distribution of serotonin transporters and receptor subtypes in human brain. *Hum Brain Mapp* 22:246-260
- Varnas K, Halldin C, Pike VW, Hall H (2003) Distribution of 5-HT<sub>4</sub> receptors in the postmortem human brain--an autoradiographic study using [<sup>125</sup>I]SB 207710. *Eur Neuropsychopharmacol* 13:228-234
- Wang Y, Chan GL, Holden JE, Dobko T, Mak E, Schulzer M, Huser JM, Snow BJ, Ruth TJ, Calne DB, Stoessl AJ (1998) Age-dependent decline of dopamine D1 receptors in human brain: a PET study. *Synapse* 30:56-61
- Wong EH, Reynolds GP, Bonhaus DW, Hsu S, Eglen RM (1996) Characterization of [<sup>3</sup>H]GR 113808 binding to 5-HT<sub>4</sub> receptors in brain tissues from patients with neurodegenerative disorders. *Behav Brain Res* 73:249-252
- Yamaguchi T, Suzuki M, Yamamoto M (1997) Evidence for 5-HT<sub>4</sub> receptor involvement in the enhancement of acetylcholine release by p-chloroamphetamine in rat frontal cortex. *Brain Res* 772:95-101
- Zarros AC, Kalopita KS, Tsakiris ST (2005) Serotonergic impairment and aggressive behavior in Alzheimer's disease. *Acta Neurobiol Exp (Wars)* 65:277-286

## Abbreviations and Terminology

- 1-TC model = one tissue compartment model
- 2-TC model = two tissue compartment model
- 3D = three Dimensional
- 5-HT = 5-Hydroxy-Tryptophan, serotonin
- AChE inhibitor = acetylcholinesterase inhibitor, main pharmacological treatment of Alzheimer's Disease
- AUC = area under curve
- $BP_{ND}$  = binding potential relative to Non-Displaceable binding
- $BP_P$  = binding potential relative to Plasma concentration
- $C_{ND}$  = concentration of ligand in reference tissue
- $C_P$  = Plasma concentration of ligand
- $C_S$  = concentration of Specifically bound ligand
- $C_{FT}$  = concentration of ligand in Free Tissue water
- CBF=Cerebral blood flow
- Convolution  $\otimes$  is a mathematical operation on two functions. It is defined as the integral of the product of the two functions after one is reversed and shifted.
- CSF cerebrospinal fluid
- HPLC = high pressure liquid chromatography
- $K_1, k_2, k_3, k_4, k_5$  and  $k_6$  = rate constants for transport between brain compartments ( $\text{g mL}^{-1} \text{min}^{-1}$  and  $\text{min}^{-1}$ )
- keV = kilo electron volt
- ligand = the radio labeled molecule used for imaging, synonymous with tracer
- MR = magnetic resonance
- PET = positron emission tomography
- PV = partial volume, averaging of adjacent tissue activity due to low resolution
- $R_1=(K_1/K_1')$  relative tracer delivery. The ' denotes the reference tissue.
- SRTM = simplified reference tissue model
- SRTM2 = simplified reference tissue model with fixed  $k_2'$
- SSRI = Selective serotonin reuptake inhibitors, e.g. citalopram, antidepressant medication
- $SD$  = standard deviation

## Lisbeth Marner: Molecular Brain Imaging of the Serotonin System

- TAC = Time activity curve = the radioactive concentration in a region or plasma as a function of time
- tracer = the radio labeled molecule used for imaging, synonymous with ligand
- $V_T$  = Total distribution volume
- $V_{ND}$  = Non-Displaceable distribution volume

## Appendices

1. Longitudinal assessment of cerebral 5-HT<sub>2A</sub> receptors in healthy elderly volunteers: An [<sup>18</sup>F]-altanserin PET study.
2. Kinetic Modeling of [<sup>11</sup>C]SB207145 binding to 5-HT<sub>4</sub> receptors in the human brain *in vivo*
3. Brain Imaging of serotonin 5-HT<sub>4</sub> receptor in humans with [<sup>11</sup>C]SB207145-PET

*Paper 1*

# Longitudinal assessment of cerebral 5-HT<sub>2A</sub> receptors in healthy elderly volunteers: an [<sup>18</sup>F]-altanserin PET study

Lisbeth Marner · Gitte M. Knudsen · Steven Haugbøl · Søren Holm · William Baaré · Steen G. Hasselbalch

Received: 21 June 2008 / Accepted: 23 August 2008 / Published online: 1 October 2008  
© Springer-Verlag 2008

## Abstract

**Purpose** The serotonin 2A (5-HT<sub>2A</sub>) receptor is of interest in several psychiatric and neurological diseases. In the present study we investigated the longitudinal stability of 5-HT<sub>2A</sub> receptors and the stability of the quantification procedure in the elderly in order to be able to study elderly patients with neuropsychiatric diseases on a longitudinal basis.

**Methods** [<sup>18</sup>F]-Altanserin PET was used to quantify 5-HT<sub>2A</sub> receptors in 12 healthy elderly individuals at baseline and at 2 years in six volumes of interest. A bolus/infusion protocol was used to achieve the binding potential, BP<sub>p</sub>. The reproducibility as assessed in terms of variability and the reliability as assessed in terms of intraclass correlation coefficient (ICC) were used to compare inter- and intra-observer stability and to evaluate the effects of increasing complexity of partial volume (PV) corrections. We also compared the stability of our measurements over 2 years

with the stability of data from an earlier study with 2-week test–retest measurements.

**Results** BP<sub>p</sub> was unaltered at follow-up without the use of PV correction and when applying two-tissue PV correction, test–retest reproducibility was 12–15% and reliability 0.45–0.67 in the large bilateral regions such as the parietal, temporal, occipital and frontal cortices, while orbitofrontal and anterior cingulate cortical regions were less stable. The use of PV correction decreased the variability but also decreased the between-subject variation, thereby worsening the reliability.

**Conclusion** In healthy elderly individuals, brain 5-HT<sub>2A</sub> receptor binding remains stable over 2 years, and acceptable reproducibility and reliability in larger regions and high intra- and interobserver stability allow the use of [<sup>18</sup>F]-altanserin in longitudinal studies of patients with neuropsychiatric disorders.

**Keywords** Brain · Serotonin · Test–retest · Reproducibility · Partial volume correction · 5-HT

L. Marner (✉) · G. M. Knudsen · S. Haugbøl · S. G. Hasselbalch  
Neurobiology Research Unit, N9201,  
University Hospital Rigshospitalet,  
Blegdamsvej 9,  
DK-2100 Copenhagen O, Denmark  
e-mail: lisbeth.marner@nru.dk

S. Holm  
PET and Cyclotron Unit,  
Department of Clinical Physiology and Nuclear Medicine,  
Rigshospitalet,  
Copenhagen, Denmark

W. Baaré  
Danish Research Center for Magnetic Resonance,  
Hvidovre Hospital,  
Copenhagen, Denmark

S. G. Hasselbalch  
Memory Disorders Research Unit, The Neuroscience Center,  
Copenhagen, Denmark

## Introduction

Serotonin transmission contributes to the expression of normal behaviour, personality and cognition across the human life-span. The advent of positron emission tomography (PET) has enabled the investigation of various aspects of serotonin transmission. A well-documented decrease in serotonin 2A (5-HT<sub>2A</sub>) receptor binding is seen in Alzheimer's disease [1, 2], and a decrease of 6–8% per decade is seen during normal ageing [3, 4].

Quantification of 5-HT<sub>2A</sub> receptors with [<sup>18</sup>F]-altanserin, a highly selective 5-HT<sub>2A</sub> receptor antagonist, can be performed with a bolus/infusion protocol where steady-state tracer levels are obtained in blood and brain [5]. The

reproducibility of the method was tested in six normal male subjects (age range 33–67 years) with a 2-week scan interval. The median difference between the measurements ranged from 6% in high binding regions to 17% in low binding regions [6]. However, the stability of the method on a longer time-scale and in older individuals must be ascertained to validate the use of [ $^{18}\text{F}$ ]-altanserin for long-term follow-up examinations in studies of neuropsychiatric disorders. We obtained [ $^{18}\text{F}$ ]-altanserin PET recordings in 12 healthy elderly subjects at baseline and at 2 years to compare 2-year to 2-week reproducibility, to compare inter- to intraobserver variability, and to evaluate variability with increasing complexity of partial volume (PV) corrections.

## Material and methods

Included in the study were 17 healthy subjects, of whom 12 (7 men, age range 63–79 years) were re-examined after 2 years (range 23–28 months); the remaining 5 subjects did not wish to participate in the follow-up part. The study was approved by the Danish Ethics Committee ((KF)12-113/00) and subjects were recruited from newspaper advertisements. Exclusion criteria were a history of or present neurological or psychiatric disease, abuse of alcohol or drugs (including sedatives), head trauma, family history of mental illness in first-degree relatives, use of a drug known to act on the serotonergic/noradrenergic system within the last 3 months, neurological signs suggesting a neurological disorder, or abnormal performance on the cognitive test battery (for details see [1]). Data from test–retest analysis over 2 weeks [6] with PV correction and with other regions were used and compared to the 2-year follow-up data. Furthermore, to exclude the presence of time-associated bias in our PET measurements, we included data from a large group of healthy individuals ( $n=84$ , 51 men, age range 18–74 years) who had undergone the same examination program during 2000–2005 [6].

The 5-HT<sub>2A</sub> receptors were imaged with [ $^{18}\text{F}$ ]-altanserin PET using a previously described method [5]. Subjects received a maximum dose of 3.7 MBq/kg body weight [ $^{18}\text{F}$ ]-altanserin with a chemical purity greater than 99%. At baseline the average dose was 267 MBq (range 189–340 MBq,  $n=11$ ) with a specific activity at the time of injection of 72.2 GBq/ $\mu\text{mol}$  (range 41–121 GBq/ $\mu\text{mol}$ ,  $n=9$ ), and at the 2-year follow-up the average dose was 256 MBq (range 130–303 MBq,  $n=8$ ) and the specific activity was 51.2 GBq/ $\mu\text{mol}$  (range 22–109 GBq/ $\mu\text{mol}$ ,  $n=12$ ). The amount of injected unlabelled substance was 4.79 nmol (range 2.58–8.34 nmol,  $n=7$ ) at baseline and 7.87 nmol (range 2.08–13.5 nmol,  $n=9$ ) at the 2-year follow-up. Two hours after bolus/infusion of tracer (bolus/infusion ratio of 1.75), steady-state conditions were reached

and emission scans (five frames of 8 min) were acquired with an 18-ring GE-Advance scanner (GE, Milwaukee, WI) operating in 3-D acquisition mode with an approximate in-plane resolution of 6 mm. The frames were reconstructed using 2-D filtered back projection (6 mm transaxial Hann filter and 8.5 mm axial ramp filter) into a sequence of 128×128×35 voxel matrices, each voxel measuring 2.0×2.0×4.25 mm. Corrections for dead time, scatter and attenuation were performed using a transmission scan corrected for tracer activity using a 5-min emission scan. Venous blood samples were drawn at the mid-point of each frame during the emission scan. The plasma activity was measured at five time points and the fraction of unmetabolized tracer in venous plasma was determined at three time points (4, 20 and 36 min) using high-performance liquid chromatography [5]. The degree of protein binding was estimated by measurement of the free fraction,  $f_p$ , of [ $^{18}\text{F}$ ]-altanserin using equilibrium dialysis. Plasma in aliquots of 500  $\mu\text{l}$  together with 500  $\mu\text{l}$  of buffer was dialyzed using a semipermeable cellulose membrane retaining proteins of >10 kDa in Teflon-coated dialysis chambers (Harvard Bioscience, Amika, Holliston, MA) at 37°C for 3 h [3]. The buffer consisted of 135 mM NaCl, 3.0 mM KCl, 1.2 mM CaCl<sub>2</sub>, 1.0 mM MgCl<sub>2</sub>, and 2.0 mM phosphate (pH 7.4). Structural brain imaging was conducted using MRI in all subjects on a 1.5-T Vision scanner (Siemens, Erlangen, Germany).

## Processing and quantification

The five frames of the PET scan were aligned and averaged to correct for motion artefacts using the AIR routines (alignlinear combined reconcile; Air version 5.2.5) [7]. PET and MR images were coregistered using an in-house program based on Matlab (Mathworks, Natick, MA) with manual translation and rotation of the PET image. The automated methods were found unstable for altanserin as the steady-state protocol does not provide early frames with flow-like tracer uptake. The MR images were segmented into grey matter, white matter, and cerebrospinal fluid (CSF) with Statistical Parametric Mapping (SPM2; Wellcome Department of Cognitive Neurology, London, UK) using the MNI template (Montreal Neurological Institute, Canada) and the result was visually inspected with manual removal of remaining non-brain tissue. Each voxel was designated as the tissue class with the highest probability. The segmentation was used for the PV correction and for masking the voxels in the volumes of interest (VOI). The 12 baseline scans were processed three times to evaluate inter- and intraobserver variability; one observer processed the data twice and a second observer once. A total of 37 VOIs were automatically delineated [8] on each subject's MR image in a user-independent fashion with the Pvelab software package (freely available at [www.nru.dk/downloads](http://www.nru.dk/downloads)) [9]. Six cortical

regions were constructed as volume-weighted bilateral averages of the smaller 37 VOIs: orbitofrontal, parietal, temporal, anterior cingulate, occipital, and frontal cortices. An earlier cross-sectional study of age effects showed no tendencies to regional differences in age changes [3]. Thus the VOIs included in this study were selected to represent regions of varying size and binding. The orbitofrontal cortex was not included in the frontal cortex, but was analysed separately due to the higher noise in this volume. As no right–left differences were expected, binding potentials from both hemispheres were averaged to reduce noise.

PV correction uses the anatomical information from the MR image to correct for the spill-in and spill-out from neighbouring tissue in the smoothed PET image. Both a one-tissue method using brain and non-brain segmentation [10] and a two-tissue method using grey matter, white matter, and non-brain segmentation [11] were performed in a modified method [9] and compared to uncorrected data.

The outcome parameter was the binding potential of specific tracer binding ( $BP_P$ ) in grey matter. The cerebellum was used as the reference region since it represents nonspecific binding only [5]. In steady state,  $BP_P$  is defined as:

$$BP_P = \frac{C_T - C_{ND}}{C_P} = f_P \cdot \frac{B_{max}}{K_D}$$

where  $C_T$  and  $C_{ND}$  denote steady-state mean radiotracer concentrations in the VOI and in the reference region, respectively, and  $C_P$  denotes the steady-state concentration of unmetabolized radiotracer in plasma. Parametric images of  $BP_P$  were calculated and transferred into standard space using the nonlinear transformation matrix derived from the spatial normalization of the individual's MR image to the MNI template with SPM2.

### Statistics

The reproducibility of the measurements was examined by the variability [ $= |scan2 - scan1| / \text{mean}(scan1, scan2) \times 100\%$ ] and the reliability was examined by the intraclass correlation coefficient, ICC [ $= (MSS_{\text{Between}} - MSS_{\text{Within}}) / (MSS_{\text{Between}} + MSS_{\text{Within}})$ ], where  $MSS_{\text{Between}}$  is the mean sum of squares between subjects and  $MSS_{\text{Within}}$  is the mean sum of squares within subjects. An ICC score of  $-1$  denotes no reliability and a score of  $+1$  denotes maximum reliability. The  $BP_P$  values at baseline and at the 2-year follow-up were compared using a paired Student's  $t$  test. To compare the differences in variability and ICC in the chosen VOI between inter- and intraobserver processing, between the 2-week and 2-year follow-up, and between different levels of PV correction, Wilcoxon's signed-ranks test was used. To test if correction for the amount of protein binding was sensible, the Pearson correlations comparing

binding potential before correction ( $BP_P = f_P \times B_{max} / K_D$ ) and after correction ( $BP_F = B_{max} / K_D$ ) with the free fraction  $f_P$  were compared. In the large group of healthy subjects, we correlated the scan date and injected amount of unlabelled tracer to the binding potential after linear correction for the observed decline in  $BP_P$  with age ( $-0.08 BP_P$  per decade). Voxel-based analysis of differences during the 2-year period was performed with a threshold of  $p=0.001$  (uncorrected at the voxel level) using SPM2 (paired  $t$  test).

### Results

We found no change in  $BP_P$  during 2-year follow-up in any of the regions (see Table 1). After PV correction using the two-tissue method, test–retest variability (reproducibility) ranged from 12% to 15% in the parietal, temporal, occipital and frontal cortices, while in the orbitofrontal and anterior cingulate cortex the variability ranged from 18% to 23%, and the ICC scores (reliability) ranged from 0.45 to 0.67 in the parietal, temporal, occipital and frontal cortices, and from 0.65 to 0.52 in the orbitofrontal and anterior cingulate cortices. Test–retest within 2 weeks showed higher reproducibility (4.8–12.7%,  $p=0.031$ ) and reliability (0.78–0.94,  $p=0.031$ ) than test–retest within 2 years. Further, the reproducibility and reliability resulting from reprocessing of the same data did not differ significantly from the analysis of two PET scans obtained within 2 weeks. No difference was found between inter- and intraobserver reproducibility ( $p=0.69$ ) and reliability ( $p=0.30$ ), the variability ranging from 3.5% to 8.8% and the ICC scores ranging from 0.90 to 0.98 in the larger regions, while the orbitofrontal cortex had an inter-/intraobserver variability of 19%/19% and ICC scores of 0.58/0.60, and the anterior cingulate cortex had an inter-/intraobserver variability of 4.1%/14% and ICC scores of 0.97/0.83. One- and two-tissue PV corrections increased the  $BP_P$  by a factor of 1.3–2.2 and 2.0–3.7 with the anterior cingulate being the least corrected and the parietal cortex being the most corrected (Table 1).

The baseline nonspecific binding ( $C_{ND}/C_P$ ) increased from 2.39 to 2.89 (factor of 1.2) and 2.96 (factor of 1.2) with one- and two-tissue PV correction, respectively. No significant relative differences were observed between baseline and the 2-year follow-up. Figure 1 shows an increasing reproducibility (on average 18% for the large regions, and 24% and 8% for the orbitofrontal and anterior cingulate cortices) and decreasing reliability (on average 12% for the large regions and 21% and 26% for the orbitofrontal and anterior cingulate cortices) with increasing complexity of PV correction. Correcting for an expected 2-year decline in  $BP_P$  of 1.7% did not diminish the variability. In most regions, reductions in grey matter

**Table 1** Binding potential at increasing complexity of the PV correction

Cortical region	BP <sub>p</sub>			Grey matter volume (cm <sup>3</sup> )								
	No PV correction			Two-tissue PV correction <sup>b</sup>								
	Baseline mean (CV)	Two-year follow-up mean (CV)	Relative difference (SD)	Baseline mean (CV)	Two-year follow-up mean (CV)	Relative difference (SD)						
Orbitofrontal cortex	0.83 (38%)	0.79 (42%)	2.2% (0.38)	1.35 (30%)	1.31 (34%)	1.2% (0.30)	1.85 (27%)	1.84 (27%)	3.8% (0.25)	18.1 (8.4%)	17.7 (10%)	-2.4% (0.06)
Parietal cortex	0.88 (27%)	0.80 (28%)	-6.9% (0.23)	1.86 (23%)	1.76 (20%)	-2.8% (0.21)	3.10 (22%)	2.98 (20%)	-1.6 (0.20)	52.0 (5.7%)	51.0 (4.5%)	-1.8% (0.03)
Temporal cortex	1.02 (27%)	0.97 (26%)	-2.9% (0.18)	1.59 (24%)	1.56 (21%)	0.0% (0.17)	2.25 (22%)	2.23 (17%)	1.3% (0.16)	72.7 (6.9%)	70.6 (7.3%)	-3.0%*** (0.02)
Anterior cingulate cortex	0.93 (36%)	0.81 (36%)	-9.6% (0.25)	1.23 (34%)	1.11 (32%)	-4.6% (0.28)	1.85 (27%)	1.70 (25%)	-3.8% (0.27)	5.02 (6.4%)	4.86 (4.7%)	-3.1%* (0.05)
Occipital cortex	1.04 (28%)	1.04 (24%)	2.2% (0.19)	1.56 (28%)	1.57 (22%)	4.0% (0.19)	2.90 (28%)	2.95 (19%)	5.2% (0.19)	46.7 (5.9%)	45.6 (7.2%)	-2.5%* (0.03)
Frontal cortex	0.81 (30%)	0.76 (28%)	-4.0% (0.21)	1.75 (22%)	1.71 (19%)	0.1% (0.20)	2.72 (21%)	2.67 (15%)	1.1% (0.19)	87.9 (7.6%)	86.1 (6.6%)	-2.0%* (0.03)

CV coefficient of variation (= SD/mean), SD standard deviation; relative difference = (scan2 - scan1)/scan1.

\* $p < 0.05$ , \*\* $p < 0.01$ , \*\*\* $p < 0.001$

<sup>a</sup>One-tissue PV correction: reference 10.

<sup>b</sup>Two-tissue PV correction: reference 11.

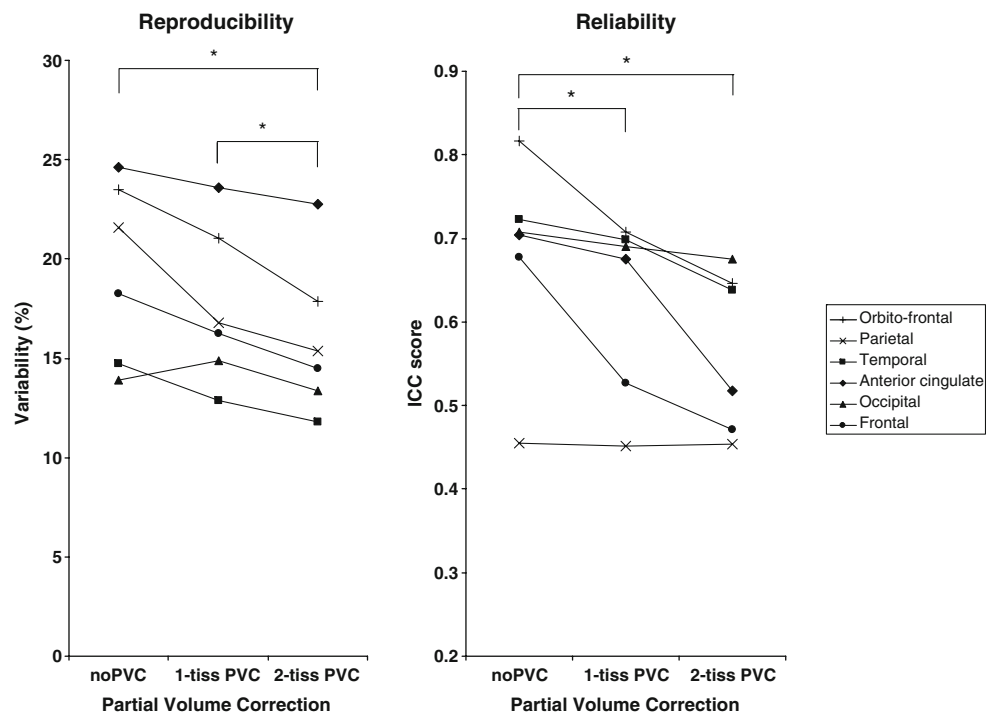
volume were noted (see Table 1). Segmentation of the elderly subjects using SPM2 proved robust by visual inspection and by test–retest reliability with ICC scores ranging from 0.74 to 0.87 in the parietal, temporal, occipital and frontal cortices, but was less reliable in the orbitofrontal and anterior cingulate cortices (ICC 0.72 and 0.48). The free fraction,  $f_p$ , was 0.38% (SD 0.15%) at baseline and 0.41% (SD 0.33%) at 2 years ( $p=0.82$ ). We found no correlation between  $f_p$  and BP<sub>p</sub> in the temporal cortex ( $r=-0.08$ ), but after correction with  $f_p$ , a negative correlation between BP<sub>F</sub> and  $f_p$  was seen ( $r=-0.81$ ).

There was no difference in the injected dose of [<sup>18</sup>F]-altanserin at baseline compared to the 2-year follow-up ( $n=8$ ,  $p=0.99$ , paired  $t$  test). The specific activity was significantly lower at the 2-year follow-up scan ( $n=8$ ,  $p=0.006$ ), and the amount of injected unlabelled tracer was higher ( $n=5$ ,  $p=0.03$ ). However, no correlation was found between the relative change in specific activity and the variability in BP<sub>p</sub> in the temporal cortex (Pearson correlation,  $r=0.26$ ,  $p=0.47$ ), and no correlation was found between the change in the amount of unlabelled tracer and the relative difference between baseline and the 2-year follow-up BP<sub>p</sub> ( $r=0.06$ ,  $p=0.88$ ). The specific activity was always larger than 20 GBq/μmol, thus the occupancy of 5-HT<sub>2A</sub> receptors was less than 5% for VOIs with binding potentials higher than 1 [12]. The fraction of unmetabolized tracer was 0.52 at baseline and 0.54 at the 2-year follow-up (paired  $t$  test,  $p=0.64$ ). No changes in cognitive performance were found and no neuropsychiatric symptoms were observed. The voxel-based analysis revealed no clusters of more than 15 voxels with significant differences with no corrections for multiple comparisons (Fig. 2).  $C_p$  increased from 1.35 kBq/ml to 1.84 kBq/ml during the 2 years (paired  $t$ -test,  $p=0.001$ ), but no correlation was found between the time of scan during 5 years of measurements and the age-corrected binding potential (Pearson correlation,  $n=84$ ), nor was any correlation found between the injected amount of unlabelled tracer and the age-corrected binding potential.

## Discussion

In healthy elderly individuals, we found no change in regional 5-HT<sub>2A</sub> receptor levels at 2-year follow-up regardless of the use of PV correction. The variability was 12–15% and the ICC scores were 0.45–0.67 for larger high binding cortical regions when applying two-tissue PV correction and 14–22% with ICC scores of 0.46–0.72 when no PV correction is applied. The orbitofrontal and anterior cingulate cortices showed higher variability and lower reliability and cannot be recommended as primary VOIs in studies requiring high test–retest performance. The higher variability and lower variability in anterior cingulate

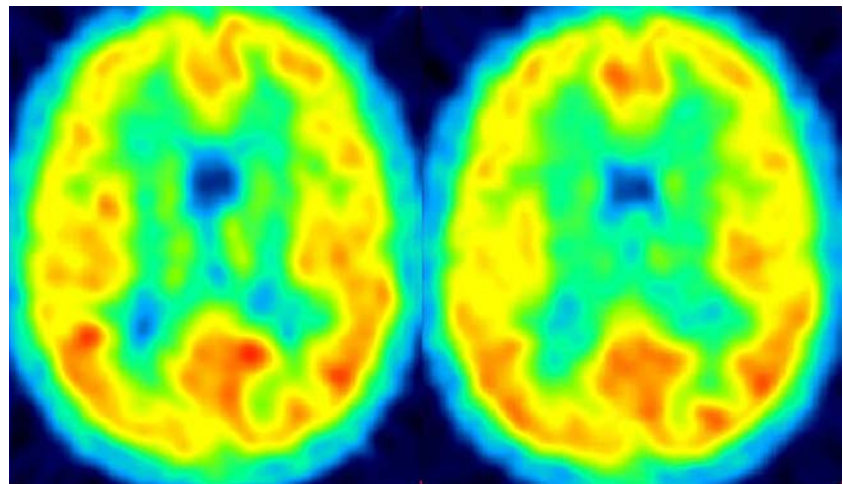
**Fig. 1** Effect of no PV correction, one-tissue PV correction [10] and two-tissue PV correction [11] on 2-year test–retest variability (the lower the better; *left*) and ICC (the higher the better; *right*). Both 2-year test–retest variability ( $p=0.016$ ) and ICC ( $p=0.047$ ) are seen to significantly decline with increasing PV correction (Wilcoxon’s signed-ranks test), thereby contradicting each other (see *Discussion* for further explanation).  $*p<0.05$



cortex is probably due to its small volume while the relatively high variability in the orbitofrontal cortex is caused by the proximity to the air-containing orbita, which makes the region boundaries more prone to coregistration errors. The ICC scores compare well to those found in an earlier [<sup>18</sup>F]-altanserin bolus-injection test–retest study [13] and to those reported for other tracers with bolus injection [14] or bolus/infusion protocols [15]. The reproducibility was, however, lower compared to test–retest over 2 weeks. This could have been due to the higher age of the subjects enrolled in the 2-year follow-up. Correcting for an expected 2-year decline in 5-HT<sub>2A</sub> receptors of 1.7% [3, 4], however, did not seem to diminish variability nor did protein binding or rate of metabolism seem to differ.

The reduction in grey matter volume may be partly explained by an age-related atrophy of grey matter and partly by a lowering of the water content in the grey matter with age [16] resulting in a change in the segmentation into grey and white matter. The use of the MNI template consisting of young subjects with higher contrast compared to elderly subjects could theoretically question the reliability of the segmentation. However, robustness in test–retest was found high with ICC scores of 0.74–0.87 and the segmentation does not seem to have biased our findings, as no change in binding potentials over 2 years were observed regardless of the use of PV correction. Thus, the observed variability in the MR images between baseline and the 2-year follow-up would only account for some of the extra 2-year

**Fig. 2** Parametric images of 5-HT<sub>2A</sub> receptor binding using [<sup>18</sup>F]-altanserin: *left* baseline scan of a 65-year-old woman; *right* 2-year follow-up scan



variability compared to the 2-week variability where the same MR image is used. Increased variability must, however, be expected from the coregistration procedure to different MR images. The influence of the coregistration procedure on variability is seen by the low inter- and intraobserver reproducibility in the orbitofrontal cortex that is susceptible to coregistration errors. We found no difference between inter- and intraobserver variability, and the intraobserver variability for processing the same data sets twice was not different from the 2-week test–retest variability using one MR and two PET images. The lack of difference can partly be accounted for by the low 2-week test–retest variability.

Although perhaps biased, reproducibility in the data processing step is likely to be larger with manual than with automated methods. As the steady-state method does not provide early flow-like tracer uptake images well-suited for automated coregistration, a manual method was chosen for [ $^{18}\text{F}$ ]-altanserin to avoid bias. This increases the amount of coregistration variability compared to dynamic protocols. On the other hand, for dynamic time–activity curves it is likely that there will be a larger variation since modelling and fitting of tracer uptake is a more interactive process than simple ratio measurements. It must be stressed that low variability associated with automated methods does not necessarily imply greater accuracy in the data, and automated methods should always be carefully evaluated for possible biases and a trade-off between bias and variability should be made. We found a higher  $C_p$  and a lower specific activity at the 2-year follow-up. However, no correlations with variability or  $BP_p$  in the temporal cortex were found, and all experiments were conducted at tracer-concentrations with occupancies below 5%. Further, we found no systematic changes in our PET measurements over 5 years and no relation to injected amount of unlabelled tracer. Thus, the higher  $C_p$  at the 2-year follow-up and the higher amount of injected unlabelled tracer do not seem to influence the binding potential. The high variability in the measurements of protein binding and the increased correlation between binding potential and free fraction after correcting for protein binding show that correction increases noise; thus correction was not implemented.

The decrease in variability and decrease in reliability (decreases in ICC) with increasing complexity of PV correction (Fig. 1) is in accordance with earlier findings [6]. The lower variability does not favour applying PV correction as we found that the reliability was diminished as well. The binding potentials with and without PV correction are not comparable as the between-subject variability decreased with PV correction as shown by the decreasing coefficients of variation with increasing complexity of PV correction (Table 1). When applying PV correction, the concentration in a thin cortical region ( $C_T$ ) such as the parietal cortex increased by a factor of 3.7, while the

concentration in the cerebellum ( $C_{ND}$ ), that has little white matter and is large, increased by a factor of only 1.2. Thus, relative differences decreased since the subtraction term,  $C_{ND}$ , remained essentially constant ( $BP_p = (C_T - C_{ND})/C_p$ ). Thus, with increasing complexity of PV correction both within-subject and between-subject variability decreases.

The lower reliability when applying PV correction was most likely partly due to the lower between-subject variability (when  $MSS_{\text{Between}}$  goes down, ICC goes down as well) and partly to more noise due to increased effect of the coregistration of the PET and MR images. However, low between-subject variability and thereby diminished reliability does not by itself decrease the chance of detecting differences between groups, but the expected differences are most likely relatively smaller after PV correction. Thus, when planning future studies, the anticipated relative difference between groups should be dependent on whether PV correction is applied. In studies requiring high test–retest performance, PV correction cannot be recommended, but should on the other hand not be disregarded in studies of degenerative diseases with anticipated differences in volume of grey matter. PV correction is still the only method that allows for a distinction between  $BP_p$  changes due to changes in volume of grey matter and changes in binding of receptors.

To our knowledge no other PET studies on longitudinal brain serotonin receptor binding are available. Evidence indicates that personality, behaviour and cognition are markedly modulated by the serotonin system [17, 18] and show substantial heritability and stability in adulthood [19]. Our findings support a stable 5-HT $_{2A}$  receptor level over 2 years in healthy elderly subjects, which is in accordance with the finding that monozygotic twins show a high degree of covariability of 5-HT $_{2A}$  receptor density compared to dizygotic twins [20].

In conclusion, no change in 5-HT $_{2A}$  receptor binding was found during a 2-year follow-up, and the findings support a stable serotonin system in healthy elderly individuals. The variability was 12–15% in large high binding regions but variability should be interpreted with care when PV correction is applied and cannot be compared to test–retest studies without PV correction. PV correction diminishes the reliability of  $BP_p$  but allows for the distinction between changes in volume of grey matter and binding of receptors. Test–retest reliability with ICC scores of 0.45–0.67 in healthy volunteers is acceptable and provides the basis for longitudinal studies of elderly patients with neuropsychiatric disorders that have presumed changes in their 5-HT $_{2A}$  receptor binding.

**Acknowledgments** We are grateful for financial support from the 1991 Pharmacy Foundation, the Health Insurance Foundation, the Lundbeck Foundation, the Danish Medical Research Council, and

University Hospital Rigshospitalet. The John and Birthe Meyer Foundation is gratefully acknowledged for donation of the cyclotron and PET scanner. The study was funded in part by the EC-FP5 project NCI-MCI, QLK6-CT-2000-00502.

**Conflicts of interest** None.

## References

- Hasselbalch SG, Madsen K, Svarer C, Pinborg LH, Holm S, Paulson OB, et al. Reduced 5-HT(2A) receptor binding in patients with mild cognitive impairment. *Neurobiol Aging* 2007;(in press). DOI 10.1016/j.neurobiolaging.2007.04.011.
- Meltzer CC, Price JC, Mathis CA, Greer PJ, Cantwell MN, Houck PR, et al. PET imaging of serotonin type 2A receptors in late-life neuropsychiatric disorders. *Am J Psychiatry* 1999;156:1871–78.
- Adams KH, Pinborg LH, Svarer C, Hasselbalch SG, Holm S, Haugbol S, et al. A database of [(18)F]-altanserin binding to 5-HT (2A) receptors in normal volunteers: normative data and relationship to physiological and demographic variables. *Neuroimage* 2004;21:1105–13.
- Meltzer CC, Smith G, DeKosky ST, Pollock BG, Mathis CA, Moore RY, et al. Serotonin in aging, late-life depression, and Alzheimer's disease: the emerging role of functional imaging. *Neuropsychopharmacology* 1998;18:407–30.
- Pinborg LH, Adams KH, Svarer C, Holm S, Hasselbalch SG, Haugbol S, et al. Quantification of 5-HT2A receptors in the human brain using [18F]altanserin-PET and the bolus/infusion approach. *J Cereb Blood Flow Metab* 2003;23:985–96.
- Haugbol S, Pinborg LH, Arfan HM, Frokjaer VM, Madsen J, Dyrby TB, et al. Reproducibility of 5-HT(2A) receptor measurements and sample size estimations with [(18)F]altanserin PET using a bolus/infusion approach. *Eur J Nucl Med Mol Imaging* 2007;34:910–15.
- Woods RP, Cherry SR, Mazziotta JC. Rapid automated algorithm for aligning and reslicing PET images. *J Comput Assist Tomogr* 1992;16:620–33.
- Svarer C, Madsen K, Hasselbalch SG, Pinborg LH, Haugbol S, Frokjaer VG, et al. MR-based automatic delineation of volumes of interest in human brain PET images using probability maps. *Neuroimage* 2005;24:969–79.
- Quarantelli M, Berkouk K, Prinster A, Landeau B, Svarer C, Balkay L, et al. Integrated software for the analysis of brain PET/SPECT studies with partial-volume-effect correction. *J Nucl Med* 2004;45:192–201.
- Meltzer CC, Leal JP, Mayberg HS, Wagner HN Jr., Frost JJ. Correction of PET data for partial volume effects in human cerebral cortex by MR imaging. *J Comput Assist Tomogr* 1990;14:561–70.
- Muller-Gartner HW, Links JM, Prince JL, Bryan RN, McVeigh E, Leal JP, et al. Measurement of radiotracer concentration in brain gray matter using positron emission tomography: MRI-based correction for partial volume effects. *J Cereb Blood Flow Metab* 1992;12:571–83.
- Adams KH. The in vivo brain distribution of serotonin 5-HT2A receptors in healthy subjects and in patients with obsessive-compulsive disorder: a positron emission study with [18F]-altanserin. PhD thesis, Copenhagen University, Faculty of Health Sciences; 2004.
- Smith GS, Price JC, Lopresti BJ, Huang Y, Simpson N, Holt D, et al. Test-retest variability of serotonin 5-HT2A receptor binding measured with positron emission tomography and [18F]altanserin in the human brain. *Synapse* 1998;30:380–92.
- Hammers A, Asselin MC, Turkheimer FE, Hinz R, Osman S, Hotton G, et al. Balancing bias, reliability, noise properties and the need for parametric maps in quantitative ligand PET: [(11)C]diprenorphine test-retest data. *Neuroimage* 2007;38:82–94.
- Elmenhorst D, Meyer PT, Matusch A, Winz OH, Zilles K, Bauer A. Test-retest stability of cerebral A(1) adenosine receptor quantification using [(18)F]CPFPX and PET. *Eur J Nucl Med Mol Imaging* 2007;34:1061–70.
- Neeb H, Zilles K, Shah NJ. Fully-automated detection of cerebral water content changes: study of age- and gender-related H2O patterns with quantitative MRI. *Neuroimage* 2006;29:910–22.
- Takano A, Arakawa R, Hayashi M, Takahashi H, Ito H, Suhara T. Relationship between neuroticism personality trait and serotonin transporter binding. *Biol Psychiatry* 2007;62:588–92.
- Frokjaer VG, Mortensen EL, Nielsen FA, Haugbol S, Pinborg LH, Adams KH, et al. Frontolimbic serotonin 2A receptor binding in healthy subjects is associated with personality risk factors for affective disorder. *Biol Psychiatry* 2008;63:569–76.
- Roberts BW, DelVecchio WF. The rank-order consistency of personality traits from childhood to old age: a quantitative review of longitudinal studies. *Psychol Bull* 2000;126:3–25.
- Pinborg LH, Arfan H, Haugbol S, Kyvik KO, Hjelmberg JV, Svarer C, et al. The 5-HT2A receptor binding pattern in the human brain is strongly genetically determined. *Neuroimage* 2008;40:1175–80.

## *Paper 2*

# Kinetic Modeling of [<sup>11</sup>C]SB207145 Binding to 5-HT<sub>4</sub> Receptors in the Human Brain in vivo

Lisbeth Marner<sup>1,3</sup>, Nic Gillings<sup>2,3</sup>, Robert A. Comley<sup>4</sup>, William Baaré<sup>5,3</sup>, Eugenii A. Rabiner<sup>4</sup>, Alan A. Wilson<sup>6</sup>, Sylvain Houle<sup>6</sup>, Steen G. Hasselbalch<sup>1,3</sup>, Claus Svare<sup>1,3</sup>, Roger N. Gunn<sup>4,7</sup>, Marc Laruelle<sup>4,8</sup>, and Gitte M. Knudsen<sup>1,3</sup>

<sup>1</sup>Neurobiology Research Unit, Neuroscience Centre, <sup>2</sup>PET and Cyclotron Unit, Department of Clinical Physiology and Nuclear Medicine, <sup>3</sup>Center for Integrated Molecular Brain Imaging, Copenhagen University Hospital, Rigshospitalet, Copenhagen, Denmark, <sup>4</sup>Clinical Imaging Centre, GlaxoSmithKline, Imperial College London, Hammersmith Hospital, London, UK, <sup>5</sup>Danish Research Center for Magnetic Resonance, Copenhagen University Hospital, Hvidovre Hospital, Copenhagen, Denmark, <sup>6</sup>Vivian M. Rakoff PET Centre, Centre for Addiction and Mental Health, Toronto, Ontario, Canada, <sup>7</sup>Department of Engineering Science, University of Oxford, U.K., <sup>8</sup>Division of Neurosciences and Mental Health, Imperial College, London, UK.

Corresponding author:

Lisbeth Marner, MD, PhD student  
Neurobiology Research Unit N9201  
Copenhagen University Hospital Rigshospitalet  
Blegdamsvej 9  
DK-2100 Copenhagen O  
Denmark  
Tlf.: (+45) 3545 6707  
Fax: (+45) 3545 6713  
E-mail: lisbeth.marner@nru.dk

Supported by The Lundbeck Foundation, Rigshospitalet, and the Danish Medical Research Council. The John and Birthe Meyer Foundation is gratefully acknowledged for the donation of the Cyclotron and PET-scanner.

Running headline: Validation of [<sup>11</sup>C]SB207145 for PET

## Abstract

The 5-HT<sub>4</sub> receptor is known to be involved in learning and memory. We evaluate for the first time the quantification of a novel 5-HT<sub>4</sub>-receptor radioligand, [<sup>11</sup>C]SB207145, for in vivo brain imaging with positron emission tomography (PET) in humans.

**Methods.** For evaluation of reproducibility, six subjects were scanned twice with [<sup>11</sup>C]SB207145 on the same day. A further two subjects were scanned before and after blocking with the selective 5-HT<sub>4</sub>-receptor inverse agonist Piboserod (SB207266). Arterial blood samples were drawn for the calculation of metabolite corrected arterial input functions. Regions of interest were delineated automatically on the individual's magnetic resonance images coregistered to the PET images, and regional time-activity curves were extracted. Quantitative tracer kinetic modeling was investigated with one (1-TC) and two (2-TC) tissue compartment models using plasma input functions and the simplified reference tissue model (SRTM).

**Results.** [<sup>11</sup>C]SB207145 readily entered the brain and showed a distribution consistent with the known localization of the 5-HT<sub>4</sub> receptor (Striatum > Hippocampus > Cortex > Cerebellum). Using plasma input models, the time activity data was well described by the two-tissue compartment model in all regions and allowed for the estimate of binding potentials (BP<sub>ND</sub>: Striatum 3.38±0.72, Hippocampus 0.82±0.19, Parietal Cortex 0.30±0.08). Quantification with the 1-TC model, 2-TC model, and SRTM were associated with good test-retest reproducibility, reliability and good time-stability. However, the SRTM generated binding potentials (BP<sub>ND</sub>) in the striatum were underestimated by 20-43% in comparison to the 2-TC model. The blocking study with Piboserod confirmed the selectivity of the radioligand for the 5-HT<sub>4</sub> receptor, that the cerebellum was a suitable reference region devoid of specific binding, and that non-specific binding was constant across different brain regions. Simulated changes in local or global blood flow did not affect the 2-

TC modeling outcomes, whereas with the SRTM, a bias was introduced for the highest binding regions.

**Conclusion.** In vivo imaging of cerebral 5-HT<sub>4</sub> receptors can be reliably determined with [<sup>11</sup>C]207145 PET in the humans with arterial input. SRTM showed high reproducibility and reliability but bias in striatum and sensitivity to blood flow changes, and therefore the use of SRTM should be considered carefully for individual applications.

Keywords: Positron emission tomography (PET), test-retest, blocking, kinetic modeling, quantification

## ***Introduction***

The 5-HT<sub>4</sub> receptor is a G-protein coupled serotonin receptor with its' highest cerebral density in the basal ganglia and medium density in hippocampus (1). Animal studies have found procognitive and memory enhancing effects of 5-HT<sub>4</sub> partial agonists (2) (3) (4) possibly mediated by a modulation of other neurotransmitter systems (5) such as the dopaminergic(6), GABAergic (7) and acetylcholinergic systems. Thus, 5-HT<sub>4</sub> agonists are shown to facilitate at least in part the release of the neurotransmitter acetylcholine in frontal cortex (8) and hippocampus (2). Moreover, 5-HT<sub>4</sub> receptor stimulation in a transgenic mouse model (9) increases the cerebral levels of the soluble amyloid precursor protein (sAPP $\alpha$ ) that is believed to be neuroprotective and enhance memory consolidation, for a review, see (10).

Recently, a new radioligand, [<sup>11</sup>C]SB207145, was introduced for PET-imaging of the 5-HT<sub>4</sub> receptor (11). PET studies in pigs showed that the radiotracer readily entered the brain and gave a heterogenous distribution consistent with known 5-HT<sub>4</sub> density (striatum > thalamus > cortical regions > cerebellum). In the minipig, [<sup>11</sup>C]SB207145 time activity curves are described equally well by one-tissue compartment (1-TC) and two-tissue compartment (2-TC) kinetics, and in all brain regions the simplified reference tissue model (SRTM2) with fixed k<sub>2</sub>' provides stable and precise estimates of the binding potential, which are highly correlated to in vitro binding, as measured in the same pigs' brains (12). Preliminary data in six human subjects showed the same rank order of binding as reported in-vitro (11) and slower tissue kinetics compared to the in vivo pig data. The radioligand metabolism was, however, not reliably assessed in this initial study in humans due to a continuing metabolism of tracer in plasma samples, which limited the quantification of the human data.

This study provides the first comprehensive quantification of the binding of [<sup>11</sup>C]SB207145 to cerebral 5-HT<sub>4</sub> receptors in the human brain in vivo. Tracer quantification was investigated with

one- and two-tissue compartment models and SRTM on test-retest and blocking data sets. The outcome measures of interest were the binding potential relative to the reference region ( $BP_{ND}$ ), relative to plasma ( $BP_P$ ), and the total distribution volume ( $V_T$ ). The models were assessed in terms of their goodness of fit, reproducibility and reliability on test-retest data and parameter estimation stability over different scan durations.

## Materials and Methods

### *Test-retest study*

Six healthy subjects were included in the test-retest part of the study (age-range 21-44 years, 3 males) that was performed at Copenhagen University Hospital, Rigshospitalet, Copenhagen, Denmark. Subjects were recruited by newspaper advertisements and the study was approved by the Ethics Committee for Copenhagen and Frederiksberg ((KF)01-274821). Exclusion criteria included pregnancy, a history of or present neurological or psychiatric disease, abuse of alcohol or drugs (including sedatives), head trauma, family history of mental illness in first-degree relatives, use of a drug within the last three months known to act on the serotonergic/noradrenergic system, or neurological signs suggesting a neurological disorder. [ $^{11}\text{C}$ ]SB207145 was synthesized with a modification of the method described earlier (11) using a fully automated radiosynthesis system (13). Briefly, [ $^{11}\text{C}$ ]methyl iodide, made from in-target produced [ $^{11}\text{C}$ ]methane using a gas phase methylation system, was reacted with the labeling precursor SB206453A in the presence of base. Following preparative high performance liquid chromatography (HPLC) and formulation, 2-4 GBq of [ $^{11}\text{C}$ ]SB207145 was produced. Arterial cannulation was performed after applying local anesthesia, and subjects received via a venous catheter a 20s-bolus injection of [ $^{11}\text{C}$ ]SB207145 (mean 572 Mbq range 512-601), with good specific radioactivity (mean 48.4 GBq/ $\mu\text{mol}$ , range 34.2-71.0) and radiochemical purity (>99%), (see table 1 for more details). A two-hour dynamic

emission scan (6x5s, 10x15s, 4x30s, 5x2min, 5x5min, 8x10min) was acquired with an eighteen-ring GE-Advance scanner (GE, Milwaukee, Wisconsin, USA) operating in 3D-acquisition mode with an approximate in-plane resolution of 6 mm. The frames were reconstructed using 2D filtered back projection (6 mm Hann filter and 8.5 mm axial ramp filter) into a sequence of 128 x 128 x 35 volumes with a voxel size of 2.0 mm x 2.0 mm x 4.25 mm. Corrections for randoms, deadtime and scatter were performed and a transmission scan allowed for the correction of attenuation (14).

#### *Esterase Inhibition in Plasma*

An earlier study had described a continuing metabolism of [<sup>11</sup>C]SB207145 ex vivo in plasma samples (11). Initial experiments of the effect of immediate cooling of arterial samples on ice was tested by adding [<sup>11</sup>C]SB207145 to whole blood stored at 37°C. The samples were immediately cooled on ice for 7 min, centrifuged at 4°C for 8 min, and placed on ice until analyzed by HPLC (set-up described below). Adding ascorbic acid to the samples resulted in a redistribution of radioactivity from red blood cells into plasma even at pH=7 (ascorbate) and was given up (data not shown). [<sup>11</sup>C]SB207145 is an ester, and thus the main metabolism is likely to be caused by plasma esterases. We investigated the stability of [<sup>11</sup>C]SB207145 in human plasma by spiking plasma samples with the tracer in the presence or absence of Dichlorvos®, a pesticide that is known to inhibit plasma esterases. Samples were incubated at 37°C or 22°C, withdrawn after 20, 40 or 60 min, and placed on ice until analyzed by HPLC.

#### *Input Function Measurement*

Blood samples for measurement of the radioactivity concentration were drawn at 5-10 s intervals during the first 2 min and subsequently at the mid frame times. In addition 7 samples (3.5, 10, 17.5, 32.5, 55, 85, 115 min) were acquired for metabolite measurements. Following withdrawal, the blood samples were immediately heparinized and Dichlorvos® (1 µg/mL blood) added to avoid further decomposition of the radiotracer in plasma. Since dichlorvos is slowly hydrolyzed in

aqueous solution and most organic solvents haemolyse blood, a concentrated solution in acetonitrile (20 mg/mL stored at -20 °C) was diluted 100-fold with water on the morning of the study.

Heparinized blood tubes were spiked with this solution (5 µl/mL blood), and blood samples mixed thoroughly as soon as possible after collection, to give a dichlorvos concentration of 1 µl/mL blood.

Whole blood and plasma radioactivity concentration were measured in a well counter (COBRA 5003, Packard Instruments, Meriden, CT, USA).

The fraction of unmetabolized tracer in arterial plasma was determined using a column-switching HPLC method (15). Briefly, plasma samples (4 mL) were filtered through a 0.45 µm filter and injected into a small capture column eluted with 2% 2-propanol in phosphate buffer (pH 10) at a flow rate of 5 mL/min followed by on-line measurement of the polar fraction in the plasma using a radio detector (Packard flow scintillation analyzer). The capture column was then back-flushed with 50% aqueous acetonitrile also at a flow rate of 5 mL/min to elute the trapped parent compound, which was subsequently measured by the online radio detector. All radioactivity data were automatically corrected for physical decay and integrated using Chromeleon software (Dionex). For late plasma samples, HPLC fractions were collected and the radioactivity was measured in a well counter (Cobra, Packard).

#### *Protein Binding Measurements*

The degree of protein binding was estimated by measurement of the free fraction,  $f_p$ , of [<sup>11</sup>C]SB207145 using equilibrium dialysis, as preliminary experiments suggested that the tracer was too sticky for ultra filtration. First, the necessary length of incubation was assessed in a temporal study (n=2; Subjects 1 and 2). Five hundred µl of plasma with 0.5 mg dichlorvos and about 500 kBq [<sup>11</sup>C]SB207145 was dialyzed against 500 µl of buffer with a semi-permeable cellulose membrane retaining proteins >10kDa in Teflon-coated dialysis chambers (Harvard Bioscience, Amika, Holliston, MA) at 37°C for 20, 40, 60, 80, 100, 120, 140, 160, and 180 min to evaluate how

long incubation time was necessary to obtain stable measurements. After incubation, 400  $\mu$ l of both plasma and buffer were measured in a well counter and the free fraction was determined as  $f_p = C_{\text{buffer}}/C_p = \text{free}/(\text{free} + \text{protein bound})$ ,  $C_{\text{Buffer}}$  being the radioactive concentration in buffer,  $C_p$  in plasma. The buffer consisted of 135 mM NaCl, 3.0 mM KCl, 1.2 mM CaCl<sub>2</sub>, 1.0 mM MgCl<sub>2</sub>, and 2.0 mM phosphate (pH 7.4). For the four remaining test-retest subjects, the  $f_p$  was measured in triple solely from data acquired following an incubation of 140 min.

### *Magnetic Resonance Imaging*

Structural magnetic resonance imaging (MRI) was conducted on a 3 T Trio scanner (Siemens, Erlangen, Germany). A high resolution 3D T1-weighted sagittal, magnetization prepared rapid gradient echo (MPRAGE) scan of the whole head was acquired for each subject. Scans were corrected for gradient non-linearity distortions and intensity inhomogeneities (16) (17).

### ***Blocking study***

Two healthy male subjects (aged 37 and 29) were included in the blocking part of the study that was performed at the Vivian M. Rakoff PET Centre, Centre for Addiction and Mental Health, Toronto, Canada. [<sup>11</sup>C]SB207145 PET scans were acquired pre-and post administration of the selective 5-HT<sub>4</sub> inverse agonist, Piboserod (SB207266) (18). This part of the study was approved by the Research Ethics Board for human subjects at the Centre for Addiction and Mental Health, Toronto, Canada and the same exclusion criteria as above applied. Subjects received a baseline PET scan followed by a second scan approximately 4 hours after receiving an oral dose of 150 mg of Piboserod (SB207266). The methods for synthesis, scanning, and input function measurements were almost similar to the above mentioned.

[<sup>11</sup>C]SB207145 was synthesized according to the following method: [<sup>11</sup>C]methylation of SB206453 (hydrochloride salt) with [<sup>11</sup>C]iodomethane was carried out inside an HPLC sample loop using our previously described “Loop” method (19). Following purification and formulation

[<sup>11</sup>C]SB207145 was obtained in 20-25% radiochemical yield (uncorrected for decay, from [<sup>11</sup>C]CO<sub>2</sub>) in 25 min post end-of-bombardment. The PET scans were performed as described above. Subjects were injected with [<sup>11</sup>C]SB207145 (mean 359 MBq, range 329-389 MBq) with a good specific activity (mean 26 GBq/μmol, range 20-32 GBq/μmol) and high radiochemical purity (>95%) (see table 1). The PET scans were performed using a Siemens-Biograph HiRez XVI PET tomograph (Siemens Molecular Imaging, Knoxville, TN, U.S.A.) and the two-hour dynamic emission scans (30 s background, 8x15s, 3x60s, 5x2min, 5x5min, 8x10min) were acquired in 32-bit list mode. The images were reconstructed using 2D filtered back projection (5 mm Gaussian filter and a ramp filter at Nyquist cut-off frequency).

#### *Input Function Measurement*

Initial blood sampling was done using an on-line automatic sampler (PBS-101 Programmable Blood Sampler, Veenstra Instruments, Joure, The Netherlands) during the first 15 min and thereafter manually at mid-frame times. HPLC analysis of plasma samples (2.5, 4, 7, 10, 15, 30, 45, 60, 75 min) were performed by minor modifications of the method of Hilton (20) using a small capture column (4.6 x 20 mm) packed in house with OASISTM HLB 30μm, (Waters, NJ), back-flushed with 25% acetonitrile, 75% H<sub>2</sub>O, 0.1N ammonium formate and pH 4, and measured with a Phenomenex 10μ Luna C18 column (250 x 4.6 mm). Column effluents were monitored through a flow detector (Bioscan Flow-Count) operated in coincidence mode.

#### *Magnetic Resonance Imaging*

MR scans were performed using a GE medical system Signa Excite HD 1.5T scanner system (GE Healthcare, U.S.A.) with 3D volumetric T1-weighted MRI and using a fast spoiled gradient-recalled (FSPGR) sequence acquired in the axial plane.

### ***Image Processing***

Scans from all eight subjects were processed the same way. The temporal frames of the PET emission scans were aligned to correct for motion artifacts using an automated image registration software(21). PET- and MR-images were co-registered to a 5 min frame (15-20 min after injection) with flow-like tracer distribution using a program with manual translation and rotation of the PET image (in-house software) (22). The MR images were segmented into gray matter, white matter, and cerebrospinal fluid by means of Statistical Parametric Mapping (SPM2; Wellcome Department of Cognitive Neurology, London, UK). A total of 19 regions in both hemispheres were automatically delineated (23) on each subject's MR image in a user-independent fashion with the Pvelab software package ([www.nru.dk/downloads](http://www.nru.dk/downloads)) (24). Striatum was constructed as a volume-weighted average of the caudate nuclei and the putamen. The regions of interest were applied to the motion corrected PET data and decay-corrected time-activity curves were derived. The superior frontal and parietal cortici, hippocampus and striatum were chosen as regions of interest to reflect both low-, moderate- and high-binding regions.

### ***Plasma Input Function***

We compared several models for fitting the fraction of measured parent compound as a function of time<sup>1</sup>. The two most optimal models based on visual inspection of the fit were the Hill function  $M_p(t)=\alpha*t^\beta/(t^\beta+\gamma)$  (25) and a bi-exponential function with the slowest exponential constrained to the difference in washout in plasma and the reference region (cerebellum) (26). The

---

<sup>1</sup> For test-retest subject five, metabolite measurements were only available only for the first 30 min for the test scan the first measurement for the retest scan was missing. As no systematic differences in the metabolite profiles was evident for the available data between test and retest (data not shown), a common parent fraction derived from the pooled data was used for subject five. For blocking subject 2, the 75 min metabolite points failed and the 60 min points were excluded as they were deemed outliers.

parent arterial plasma input function was calculated as the total measured plasma activity multiplied by the fitted parent fraction and constrained to be equal to a sum of exponentials following the peak.

### ***Kinetic Modeling***

Three kinetic models were investigated using the test-retest data (1-TC, 2-TC and SRTM). We estimated two different binding potentials ( $BP_{ND}$  and  $BP_P$ ) (27) using the 1-TC and 2-TC models with blood volume fixed at  $0.05 \text{ mL/cm}^3$ . As a non-invasive reference tissue method, we explored the simplified reference tissue model (SRTM) (28) to derive estimates of  $BP_{ND}$ . All modeling was performed using in-house software at GSK implemented within Matlab (version 7.5, MathWorks, Natick, Massachusetts, US); the plasma input models used a Levenberg-Marquadt optimizer and SRTM used a basis function implementation (29). The outcome parameters from right and left hemisphere were averaged and the different models were compared using the Akaike Information Criteria, test-retest reproducibility and reliability, and time stability.

A time stability analysis was performed to determine the minimal scanning duration for reliable estimation of the outcome measures of interest. The distribution volumes ( $V_T$ ) or  $BP_{ND}$  were calculated for a range of truncated data sets using 1-TC, 2-TC, and SRTM. Estimation was performed on data sets corresponding to durations of 120, 110, 100, 90, 80, 70, 60 and 50 min. Hippocampus and striatum were used for the analysis as they were deemed representative of moderate- and high-binding regions respectively. The outcome parameters were normalized to the value obtained from the full 120 min scan analysis and the mean and standard deviations for all test-retest scans were plotted as a function of the scan length.

A significance level of 0.05 was adopted throughout. The Akaike Information Criteria were used to assess the goodness of fit with a penalty for increasing number of parameters in the model. For the descriptive analysis of the test-retest data, a relative test-retest difference was calculated per region as

$$\Delta\% = \frac{2 \cdot (\text{retest\_value} - \text{test\_value})}{\text{test\_value} + \text{retest\_value}} \cdot 100\%$$

the mean of  $\Delta\%$  across subjects is a measure of systematic differences (bias) and the standard deviation of  $\Delta\%$  is referred to as the average test-retest difference and characterizes the reproducibility (30).

Reliability was assessed using the intraclass correlation coefficient (ICC), determined as:

$$ICC = \frac{MSS_{\text{Between}} - MSS_{\text{Within}}}{MSS_{\text{Between}} + MSS_{\text{Within}}}$$

$MSS_{\text{Between}}$  is the mean sum of squares between subjects and  $MSS_{\text{Within}}$  is the mean sum of squares within subjects. An ICC score of  $-1$  denotes no reliability and  $+1$  denotes maximum reliability. The reproducibility is characterized by the relative test-retest differences ( $2 \cdot (\text{scan2} - \text{scan1}) / (\text{scan1} + \text{scan2}) \cdot 100\%$ ) as well as the standard deviation (SD) of this metric, which is the average test-retest difference.

### ***Simulations of Cerebral Blood Flow Changes***

In order to assess the potential impact of cerebral blood flow alterations on the outcome parameters,  $V_T$  or  $BP_{ND}$ , simulations of flow changes were performed by taking the population average from the test-retest data for  $K_1$ ,  $k_2$ ,  $k_3$ ,  $k_4$  and the parent plasma input function to construct noise-free population time-activity curves for cerebellum, striatum and hippocampus. To simulate stationary changes in blood flow lasting for the entire duration of the scan, we multiplied  $K_1$  and  $k_2$  by 1.3 (30% increase) or 0.7 (30% decrease) in cerebellum, striatum and hippocampus, and constructed new time-activity curves based on the common input function. Gaussian noise was added using the standard deviations derived from the residuals of the associated 2-TC modeling of the measured data. Kinetic modeling of the resulting noisy time-activity curves was performed with 2-TC and SRTM modeling to investigate whether there was any bias in the estimation of  $BP_{ND}$ 's in the striatum and hippocampus.

## Results

The initial experiments showed significant metabolism of [ $^{11}\text{C}$ ]SB207145 when adding the radiotracer directly to whole blood and immediately placing the samples on ice for 7 min (79% parent compound remaining). At 37°C, [ $^{11}\text{C}$ ]SB207145 was rapidly degraded in human plasma with a half life of 18 min, and at 22°C the half life was 44 min (figure 1). Addition of as little as 0.25  $\mu\text{g}$  Dichlorvos® per millilitre of plasma fully inhibited any further radiotracer degradation, even at 37°C (figure 1). The metabolism of [ $^{11}\text{C}$ ]SB207145 in vivo was even faster and fairly constant across subjects with the coefficients of variation ( $\text{CV}=\text{SD}/\text{mean}*100\%$ ) of around 11% for the early HPLC samples increasing to around 24% at the late samples (>45 min) (figure 2). The constrained bi-exponential and Hill metabolite models were reasonably good descriptors of the parent fraction with the Hill function typically yielding slightly better goodness of fit. However, for some scans the Hill function derived input function led to infinite distribution volume estimates and so the constrained bi-exponential model was used for all scans (figure 2B).

Equilibrium dialysis was able to measure a stable free fraction estimate by 140 min (data not shown). The average free fraction of unbound tracer in plasma,  $f_p$ , was 0.25 (range 0.08 to 0.43) ( $n=7$ , we failed to obtain measurements in subject 3 and retest measurements in subject 1, 2 and 5). The  $f_p$  correction was not applied to  $\text{BP}_p$  in order to derive  $\text{BP}_f$ , because we found no correlation between  $f_p$  and the uncorrected binding potential in hippocampus ( $r = -0.41$ ,  $p = 0.36$ ) and a strong negative correlation between  $f_p$  and the corrected binding potential ( $r = -0.87$ ,  $p=0.01$ ). No correlation was observed between the free fraction and the distribution volume of cerebellum, age, sex, time of the day, or amount of injected cold tracer.

### ***Modeling of [<sup>11</sup>C]SB207145 Binding in the Brain***

An example of the [<sup>11</sup>C]SB207145 tissue time-activity curves from a representative subject are shown in figure 3. Slower kinetics was observed in the highest binding region of the striatum, which displayed a later peak and slower wash-out than all other regions.

The results of the kinetic modeling are shown in table 2. The 2-TC model was superior to the 1-TC model, as judged by the Akaike Information criteria in all regions. There were systematic higher binding potentials relative to plasma at second scan compared to first for both 1-TC and 2-TC modeling, i.e. relative % test-retest differences (table 2) were significantly different from zero (paired t-test). We found no significant differences between test and retest scans with regard to the area under curve for cerebellum normalized to injected dose (paired t-test,  $p=0.24$ ), injected activity ( $p=0.67$ ), injected mass ( $p=0.56$ ),  $V_{ND}$  ( $p=0.57$ ), or parent plasma clearance ( $p=0.19$ ).

We observed a slight overestimation of  $BP_{ND}$  in the cortical regions and an underestimation of 20-43% in striatum when using the SRTM as compared to 2-TC modeling (figure 4). Applying SRTM2 by fixing  $k_2'$  did not change the results significantly (31).

The time-stability analyses revealed no major bias or variance after 100 min in both hippocampus and striatum with any of the three models (figure 5). Using SRTM, a slight bias was present with a scan length of 100 min in hippocampus.

Blocking by Piboserod (SB207266) reduced time activity curves and resultant binding outcome measures in all regions studied to the level of the cerebellum and cerebellar distribution volumes were not changed (figure 6 and 7). We compared the  $V_T$  and  $BP_{ND}$  from the blocking part and test-retest part (table 3) for differences across sites and found slightly higher values in cortical regions and striatum favoring the blocking part.

Simulated flow-changes locally and globally did not induce changes in  $BP_{ND}$  when using 2-TC modeling with arterial input. No changes of  $BP_{ND}$  above 4% were observed with simulated global

or local blood flow changes ( $\pm 30\%$ ). However, a clear positive correlation between SRTM generated  $BP_{ND}$  and local changes in blood flow was seen (figure 8) with +12% bias with 30% increased and -19% bias with 30% decreased cerebral blood flow. However, if the changes in blood flow in the target region were followed by a similar change in cerebellar blood flow ( $\pm 30\%$ ), i.e. global changes, the bias was diminished to +6.9% and -11% with slightly less bias in hippocampus as compared to striatum.

## Discussion

As described previously (11) [ $^{11}C$ ]SB207145 readily crosses the blood brain barrier in humans and yields a heterogeneous distribution consistent with the known 5-HT<sub>4</sub> receptor localization. The kinetics of the radioligand is reversible and well described by a two tissue compartment plasma input model. In addition, the SRTM with cerebellum input was able to successfully quantify the binding of the radiotracer, although with a bias in the slowest kinetic regions of the striatum. We observed a bias of 20-43% in the striatum (figure 4) as a result of violations of SRTM assumptions, likely due to the required two-tissue kinetics in cerebellum (32). Given this, care should be exercised in the choice between 2-TC (blood sampling) and SRTM (no blood sampling) approaches depending on the particular application in question. The SRTM yielded low test-retest differences (6-10% in moderate- to high-binding regions and 12-14% in low-binding regions), reliability (ICC: 0.76-0.88), and good time stability. The low-binding cortical regions have small binding potentials in the range of 0.3-0.4, however, the observed reproducibility and reliability support the use of cortical binding potentials in future clinical studies.

We observed an increase in  $BP_P$  from first to second scan of 10-20% (table 2). Nonspecific binding, parent plasma clearance, injected mass, and injected dose were not significantly different

between first and second scan, and as  $BP_{ND}$  did not show the same significant differences, we believe the most likely explanation is a type II error.

No major differences between the blocking experiment and the test-retest experiment (table 3) was found and supports the use of [ $^{11}C$ ]SB207145 across sites. The slightly higher values for the cortical regions and striatum is most likely due to a higher resolution and thereby less partial volume effect with the Siemens-Biograph HiRez XVI PET tomograph at the Vivian M. Rakoff PET Centre in Toronto as compared to the eighteen-ring GE-Advance scanner used at the Neurobiology Research Unit in Copenhagen. Subject two in the blocking part show very high distribution volumes, which are sensitive to noise in the blood measurements, however, the difference cancels out when calculating the binding potential.

### ***Time Stability***

The time stability analysis allows for an assessment of the stability of the model and selection of optimal scan duration. For acquisitions of 100 min or longer, all three models yielded relatively stable outcome parameters in terms of bias and variance, although there was a slight bias present at 100 min for hippocampus when using SRTM. Thus, 100 min of dynamic data is suitable for quantitative assessment of 5-HT<sub>4</sub> receptors when using arterial input, however, 120 min is recommended when SRTM is to be employed.

### ***Blocking***

Following blocking with a structurally dissimilar selective 5-HT<sub>4</sub> inverse agonist (Piboserod), the distribution volumes in all regions were reduced to the level of the cerebellum in the baseline scan with the cerebellum remaining unchanged. These data support the use of the cerebellum as a reference region and the assumption of homogeneous non-specific binding. In addition, they confirm the selectivity of the specific signal for the 5-HT<sub>4</sub> receptor.

### ***Metabolite Measurements***

We chose to use a constrained bi-exponential model for the parent fraction in plasma even though the goodness of fit was not quite as good as that achieved with the Hill function and the measured rate of metabolism was slightly underestimated. Use of the Hill function derived input had led to problems in estimating finite  $V_T$  in the cerebellum for several scans. One explanation for this observation could be the accumulation of radioactive metabolites in the brain; but previous rat experiments have revealed that at 180 min post-injection, the major radioactive component in rat brain is SB207145, making it unlikely that accumulation of radiolabeled metabolites takes place (11). We find that a more likely explanation is a bias in the late metabolite measurements, which suffer from high noise and potential bias, due to subtraction of background radioactivity. Applying the constrained bi-exponential parent fraction model significantly increased the robustness of the outcome measures and is acceptable as a secular equilibrium should be reached between the cerebellum and the parent plasma concentration late in the scan.

### ***Cerebral Blood Flow Simulations***

When we simulated flow-changes by scaling  $K_1$  and  $k_2$ , we saw no significant bias with 2-TC modeling. By contrast, for the SRTM we found a bias in  $BP_{ND}$  of up to 19% with a decrease in blood flow of 30% when cerebellar blood flow remained constant. The finding was less marked for global cerebral blood flow changes. Thus, blood flow changes as seen in e.g., Alzheimer's disease with hypoperfusion of cerebral cortex and stable cerebellar perfusion will result in increased bias and care should be taken when applying the SRTM to scans of subjects with expected local flow-changes. Medication-induced blood flow changes are more likely to be global and will result in less bias. The simulated change of 30% was chosen to evaluate the worst case scenario and physiological blood flow changes are mostly less pronounced.

## Conclusions

[<sup>11</sup>C]SB207145 can be used for quantitative PET measurements of 5-HT<sub>4</sub> receptors in the human brain. The distribution volumes and binding potentials can be reliably estimated using 2-TC modeling with arterial input measurements. Use of the SRTM to avoid invasive arterial cannulation gives high reproducibility and reliability at scan times of 120 min but bias with lower values in high binding regions and associated sensitivity to non-global blood flow changes. Thus, the use of SRTM should be considered for individual applications.

## Acknowledgements

Karin Stahr, Bente Høy, Anita Dole, and Kirsten Honsyld are thanked for invaluable technical assistance and the valuable contributions from the employees and students at Neurobiology Research Unit are highly appreciated. We are grateful for the support by The Lundbeck Foundation, Rigshospitalet, and the Danish Medical Research Council. The John and Birthe Meyer Foundation is gratefully acknowledged for the donation of the Cyclotron and PET-scanner. Drs. Comley, Laruelle, Rabiner, and Gunn are GlaxoSmithKline employees and report owning shares in GSK but declare that they have no financial interest in or financial conflict with the subject matter or materials discussed in this article.

## References

- (1) Varnas K, Halldin C, Pike VW, Hall H. Distribution of 5-HT<sub>4</sub> receptors in the postmortem human brain--an autoradiographic study using [<sup>125</sup>I]SB 207710. *Eur Neuropsychopharmacol.* 2003;13(4):228-234.
- (2) Mohler EG, Shacham S, Noiman S et al. VRX-03011, a novel 5-HT<sub>4</sub> agonist, enhances memory and hippocampal acetylcholine efflux. *Neuropharmacology.* 2007;53(4):563-573.
- (3) Orsetti M, Dellarole A, Ferri S, Ghi P. Acquisition, retention, and recall of memory after injection of RS67333, a 5-HT<sub>4</sub> receptor agonist, into the nucleus basalis magnocellularis of the rat. *Learn Mem.* 2003;10(5):420-426.
- (4) Terry AV, Jr., Buccafusco JJ, Jackson WJ et al. Enhanced delayed matching performance in younger and older macaques administered the 5-HT<sub>4</sub> receptor agonist, RS 17017. *Psychopharmacology (Berl).* 1998;135(4):407-415.
- (5) Bockaert J, Claeysen S, Compan V, Dumuis A. 5-HT<sub>4</sub> receptors. *Curr Drug Targets CNS Neurol Disord.* 2004;3(1):39-51.
- (6) Porras G, Di Matteo V, De Deurwaerdere P, Esposito E, Spampinato U. Central serotonin<sub>4</sub> receptors selectively regulate the impulse-dependent exocytosis of dopamine in the rat striatum: in vivo studies with morphine, amphetamine and cocaine. *Neuropharmacology.* 2002;43(7):1099-1109.
- (7) Cai X, Flores-Hernandez J, Feng J, Yan Z. Activity-dependent bidirectional regulation of GABA(A) receptor channels by the 5-HT<sub>4</sub> receptor-mediated signalling in rat prefrontal cortical pyramidal neurons. *J Physiol.* 2002;540(Pt 3):743-759.
- (8) Yamaguchi T, Suzuki M, Yamamoto M. Evidence for 5-HT<sub>4</sub> receptor involvement in the enhancement of acetylcholine release by p-chloroamphetamine in rat frontal cortex. *Brain Res.* 1997;772(1-2):95-101.
- (9) Cachard-Chastel M, Lezoualc'h F, Dewachter I et al. 5-HT<sub>4</sub> receptor agonists increase sAPP $\alpha$  levels in the cortex and hippocampus of male C57BL/6j mice. *Br J Pharmacol.* 2007;150(7):883-892.
- (10) Turner PR, O'Connor K, Tate WP, Abraham WC. Roles of amyloid precursor protein and its fragments in regulating neural activity, plasticity and memory. *Prog Neurobiol.* 2003;70(1):1-32.
- (11) Gee AD, Martarello L, Passchier M et al. Synthesis and Evaluation of [<sup>11</sup>C]SB207145 as the First *In Vivo* Serotonin 5-HT<sub>4</sub> Receptor Radioligand for PET Imaging in Man. *Current Radiopharmaceuticals.* 2008;1.

- (12) Kornum BR, Lind NM, Gillings N, Marner L, Andersen F, Knudsen GM. Evaluation of the novel 5-HT<sub>4</sub> Receptor PET ligand [<sup>11</sup>C]SB207145 in the Göttingen minipig. *J Cereb Blood Flow Metab.* 2008.
- (13) Gillings N, Larsen P. A Highly Flexible Modular Radiochemistry System [abstract]. *J Label Compd Radiopharm.* 2005;48:S338.
- (14) Pinborg LH, Adams KH, Svarer C et al. Quantification of 5-HT<sub>2A</sub> receptors in the human brain using [<sup>18</sup>F]altanserin-PET and the bolus/infusion approach. *J Cereb Blood Flow Metab.* 2003;23(8):985-996.
- (15) Gillings N, Marner L, Knudsen GM. A Rapid, Robust and Fully Automated Method for Analysis of Radioactive Metabolites in Plasma Samples from PET Studies [abstract]. *J Label Compd Radiopharm.* 2007;50:S503.
- (16) Jovicich J, Czanner S, Greve D et al. Reliability in multi-site structural MRI studies: effects of gradient non-linearity correction on phantom and human data. *Neuroimage.* 2006;30(2):436-443.
- (17) Sled JG, Zijdenbos AP, Evans AC. A nonparametric method for automatic correction of intensity nonuniformity in MRI data. *IEEE Trans Med Imaging.* 1998;17(1):87-97.
- (18) Claeysen S, Sebben M, Becamel C et al. Pharmacological properties of 5-Hydroxytryptamine(4) receptor antagonists on constitutively active wild-type and mutated receptors. *Mol Pharmacol.* 2000;58(1):136-144.
- (19) Wilson AA, Garcia A, Jin L, Houle S. Radiotracer synthesis from [(<sup>11</sup>C)]iodomethane: a remarkably simple captive solvent method. *Nucl Med Biol.* 2000;27(6):529-532.
- (20) Hilton J, Yokoi F, Dannals RF, Ravert HT, Szabo Z, Wong DF. Column-switching HPLC for the analysis of plasma in PET imaging studies. *Nucl Med Biol.* 2000;27(6):627-630.
- (21) Woods RP, Cherry SR, Mazziotta JC. Rapid automated algorithm for aligning and reslicing PET images. *J Comput Assist Tomogr.* 1992;16(4):620-633.
- (22) Willendrup P. Assessment of the Precision in Co-Registration of Structural MR-Images and PET-Images With Localized Binding [abstract]. *International Congress Series.* 2004;V:275-280.
- (23) Svarer C, Madsen K, Hasselbalch SG et al. MR-based automatic delineation of volumes of interest in human brain PET images using probability maps. *Neuroimage.* 2005;24(4):969-979.
- (24) Quarantelli M, Berkouk K, Prinster A et al. Integrated software for the analysis of brain PET/SPECT studies with partial-volume-effect correction. *J Nucl Med.* 2004;45(2):192-201.
- (25) Gunn RN, Sargent PA, Bench CJ et al. Tracer kinetic modeling of the 5-HT<sub>1A</sub> receptor ligand [carbonyl-<sup>11</sup>C]WAY-100635 for PET. *Neuroimage.* 1998;8(4):426-440.

- (26) Abi-Dargham A, Simpson N, Kegeles L et al. PET studies of binding competition between endogenous dopamine and the D1 radiotracer [11C]NNC 756. *Synapse*. 1999;32(2):93-109.
- (27) Innis RB, Cunningham VJ, Delforge J et al. Consensus nomenclature for in vivo imaging of reversibly binding radioligands. *J Cereb Blood Flow Metab*. 2007;27(9):1533-1539.
- (28) Lammertsma AA, Hume SP. Simplified reference tissue model for PET receptor studies. *Neuroimage*. 1996;4(3 Pt 1):153-158.
- (29) Gunn RN, Lammertsma AA, Hume SP, Cunningham VJ. Parametric imaging of ligand-receptor binding in PET using a simplified reference region model. *Neuroimage*. 1997;6(4):279-287.
- (30) Hammers A, Asselin MC, Turkheimer FE et al. Balancing bias, reliability, noise properties and the need for parametric maps in quantitative ligand PET: [(11)C]diprenorphine test-retest data. *Neuroimage*. 2007;38(1):82-94.
- (31) Wu Y, Carson RE. Noise reduction in the simplified reference tissue model for neuroreceptor functional imaging. *J Cereb Blood Flow Metab*. 2002;22(12):1440-1452.
- (32) Slifstein M, Parsey RV, Laruelle M. Derivation of [(11)C]WAY-100635 binding parameters with reference tissue models: effect of violations of model assumptions. *Nucl Med Biol*. 2000;27(5):487-492.

	Test-retest		Block	
	Test (n=6)	Retest (n=6)	Baseline (n=2)	Block (n=2)
Age (years)	34.6±7.0		[37, 29]	
Body weight (kg)	75.0±17		[67.2, 75.8]	
Injected dose (MBq)	566±41	577±26	[329, 370]	[389, 335]
Injected mass (µg)	4.09±1.2	4.47±0.92	[4.31, 4.39]	[4.16, 5.87]
Parent plasma clearance (L/h)	191±28	214±55	[164, 324]	[178, 236]

Table 1. Subject information for the test-retest and blocking parts of the study (either mean ±SD or individual values).

	Regions	K <sub>1</sub> (mL cm <sup>-3</sup> min <sup>-1</sup> )	k <sub>2</sub> (min <sup>-1</sup> )	k <sub>4</sub> (min <sup>-1</sup> )	V <sub>T</sub> (mL/cm <sup>3</sup> )	BP <sub>ND</sub>	BP <sub>P</sub> (mL/cm <sup>3</sup> )	Akaike Inf. Criteria	Relative diff BP <sub>ND</sub> (%)	Average diff BP <sub>ND</sub> (%)	ICC BP <sub>ND</sub>	Relative diff BP <sub>P</sub> (%)	Average diff BP <sub>P</sub> (%)	ICC BP <sub>P</sub>
<b>1-TC model</b>	Cerebellum	0.19 ±0.07	0.023 ±0.003	-	7.86 ±2.23	-	-	586 ±20	-	-	-	-	-	-
	Parietal ctx	0.19 ±0.07	0.016 ±0.003	-	11.8 ±3.26	0.51 ±0.10	3.97 ±1.22	542 ±26	7.50	13.2	0.82	11.6*	10.7	0.88
	Sup. fr. ctx	0.19 ±0.07	0.016 ±0.003	-	11.3 ±3.17	0.43 ±0.10	3.39 ±1.16	541 ±23	8.08	12.5	0.87	12.2*	9.70	0.89
	Hippocampus	0.17 ±0.06	0.010 ±0.002	-	16.2 ±4.59	1.07 ±0.21	8.38 ±2.63	569 ±13	6.27	13.0	0.80	10.4*	7.53	0.91
	Striatum	0.23 ±0.08	0.006 ±0.002	-	40.4 ±11.7	4.20 ±0.93	32.5 ±10.1	536 ±27	11.4**	8.2	0.84	15.5*	8.69	0.80
<b>2-TC model</b>	Cerebellum	0.24 ±0.08	0.056 ±0.009	0.018 ±0.003	9.50 ±2.58	-	-	510 ±28	-	-	-	-	-	-
	Parietal ctx	0.23 ±0.08	0.054 ±0.019	0.050 ±0.023	12.3 ±3.42	0.30 ±0.08	2.83 ±1.02	506 ±30	11.9	13.6	0.80	13.8*	10.7	0.87
	Sup. fr. ctx	0.22 ±0.08	0.057 ±0.021	0.050 ±0.023	11.7 ±3.32	0.23 ±0.08	2.22 ±0.95	504 ±26	17.7	19.4	0.79	19.7*	11.8	0.84
	Hippocampus	0.23 ±0.07	0.110 ±0.032	0.026 ±0.008	17.3 ±5.01	0.82 ±0.19	7.81 ±2.73	517 ±21	10.9	12.9	0.82	12.8*	5.95	0.90
	Striatum	0.27 ±0.09	0.066 ±0.032	0.060 ±0.063	41.4 ±12.0	3.38 ±0.72	31.9 ±10.0	519 ±31	13.9*	7.9	0.68	15.8**	7.82	0.81
<b>SRTM</b>	Cerebellum	-	0.016 ±0.012	-	-	-	-	-	-	-	-	-	-	-
	Parietal ctx	-	0.069 ±0.011	-	-	0.36 ±0.06	-	449 ±25	5.73	13.6	0.77	-	-	-
	Sup. fr. ctx	-	0.067 ±0.008	-	-	0.30 ±0.07	-	467 ±20	6.60	12.6	0.84	-	-	-
	Hippocampus	-	0.037 ±0.005	-	-	0.70 ±0.13	-	517 ±14	4.00	9.92	0.88	-	-	-
	Striatum	-	0.054 ±0.004	-	-	2.21 ±0.21	-	496 ±28	3.74	6.06	0.76	-	-	-

Table 2. Summary of parameter estimation for the test-retest part (n=6) for five selected regions using 1-TC model, 2-TCM, and SRTM

kinetic models. K<sub>1</sub>, k<sub>2</sub>, and k<sub>4</sub> are the rate constants, V<sub>T</sub> is the total volume of distribution, BP<sub>ND</sub>=V<sub>T</sub>/V<sub>ND</sub> - 1 is the binding potential

relative to non-displaceable binding, BP<sub>P</sub>=V<sub>T</sub>-V<sub>ND</sub> is the binding potential relative to plasma, the (minimum) Akaike Information

Criterion indicates a more statistically appropriate model. For BP<sub>ND</sub> and BP<sub>P</sub> are given the mean of the relative test-retest

differences (Δ%=2\*(scan2-scan1)/(scan1+scan2)\*100%) and the average test-retest difference, which is the standard deviation (SD)

of Δ%. The intraclass correlation coefficient (ICC) indicates the reliability. The outcome parameters and Akaike Information

Criteria are given as mean ± SD. A paired Student's t-test was performed to evaluate for systematic differences between first and

second scan.

\* p<0.05, \*\*p<0.01.

Region	Test-retest		Blocking	
	$V_T$ (mL/cm <sup>3</sup> )	BP <sub>ND</sub>	$V_T$ (mL/cm <sup>3</sup> )	BP <sub>ND</sub>
Cerebellum	9.50 ±2.58	-	[9.14, 15.3]	-
Parietal ctx	12.3 ±3.42	0.30 ±0.08	[12.6, 22.1]	[0.38, 0.45]
Sup. fr. ctx	11.7 ±3.32	0.23 ±0.08	[12.8, 21.0]	[0.40, 0.38]
Hippocampus	17.3 ±5.01	0.82 ±0.19	[16.6, 26.0]	[0.82, 0.70]
Striatum	41.4 ±12.0	3.38 ±0.72	[48.5, 69.5]	[4.30, 3.55]

Table 3. Comparison of distribution volumes,  $V_T$ , and binding potential relative to plasma, BP<sub>P</sub>, between centers (either mean ±SD or individual values).

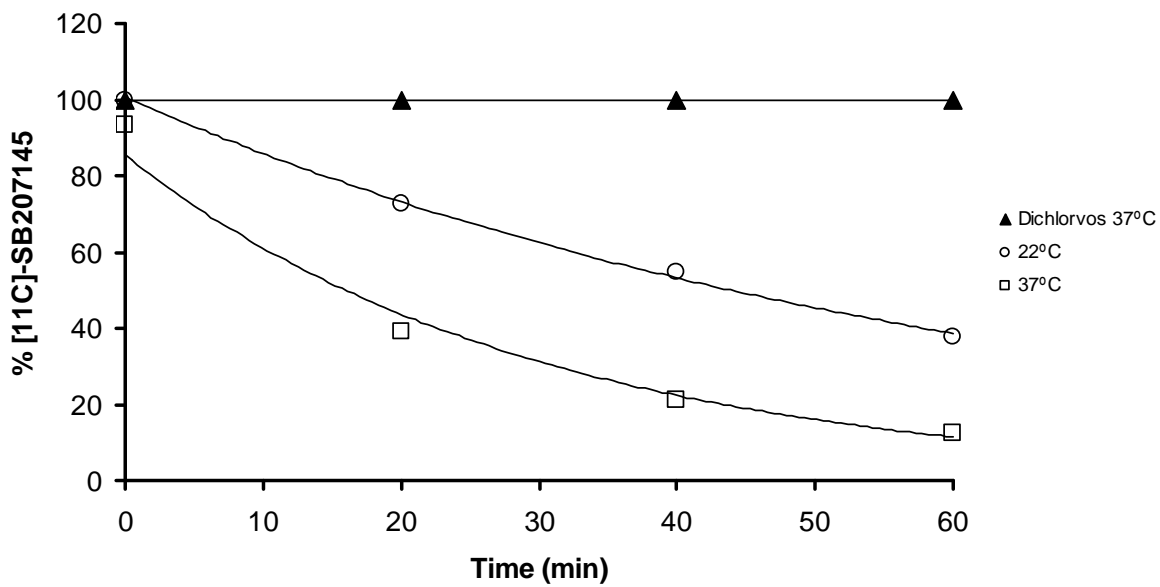


Figure 1. Time dependent metabolism of [<sup>11</sup>C]SB207145 in plasma at 22°C and 37°C. The metabolism is prevented when Dichlorvos® is added. The exponential fits correspond to half lives of 18 min at 22°C, and 44 min at 37°C.

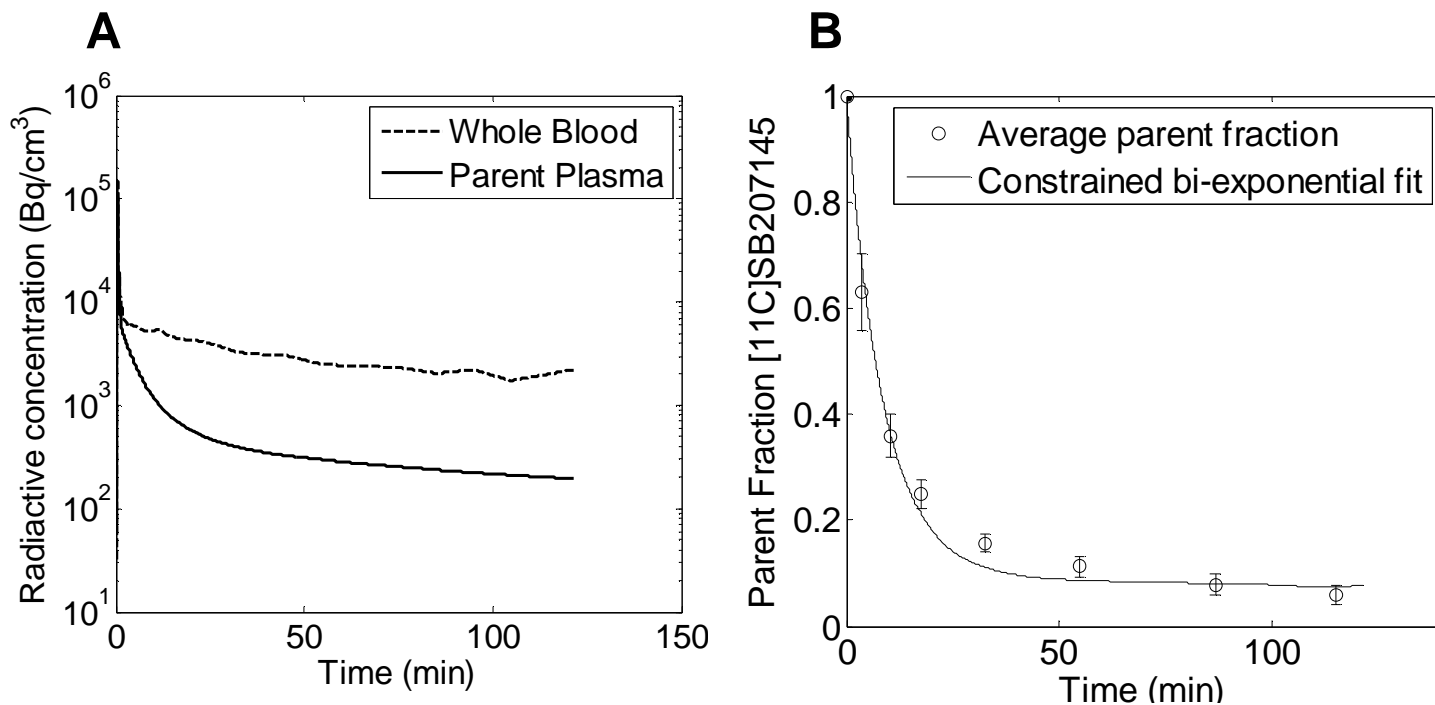


Figure 2. A. The radioactive concentrations in whole blood and plasma from a representative subject. The plasma curve is corrected for radioactive metabolites and fitted to a bi-exponential function after the peak.

B. Fitting of the measured metabolite data with a constrained bi-exponential function. The mean and standard deviation (error bars) across subjects of the measured metabolite fraction are shown with the average fit using a constrained bi-exponential function (26).

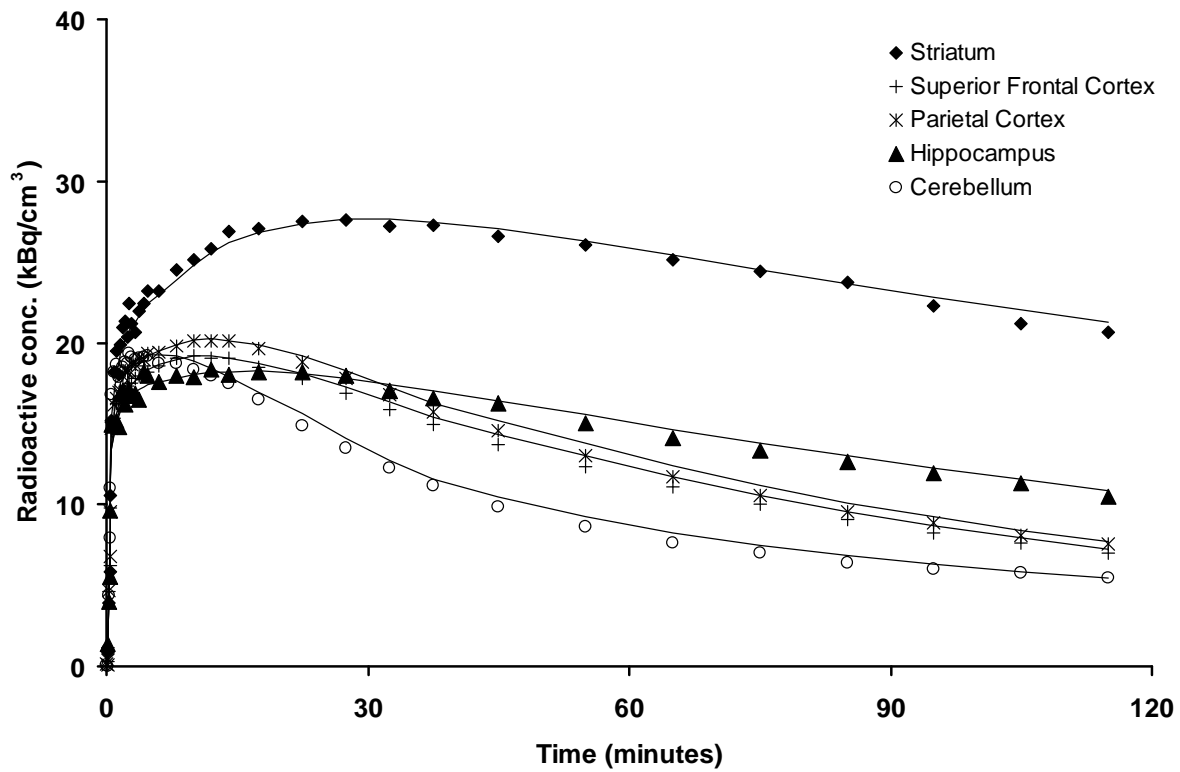


Figure 3. Time-activity curves for five brain regions. The striatum shows the highest and latest peak and the slowest wash-out due to the high density of receptors while superior frontal and parietal cortices show a faster wash-out as there are fewer receptors in these regions. Cerebellum has the fastest wash-out since there is no specific binding in this region. The fits with 2-TC modeling are shown as solid lines.

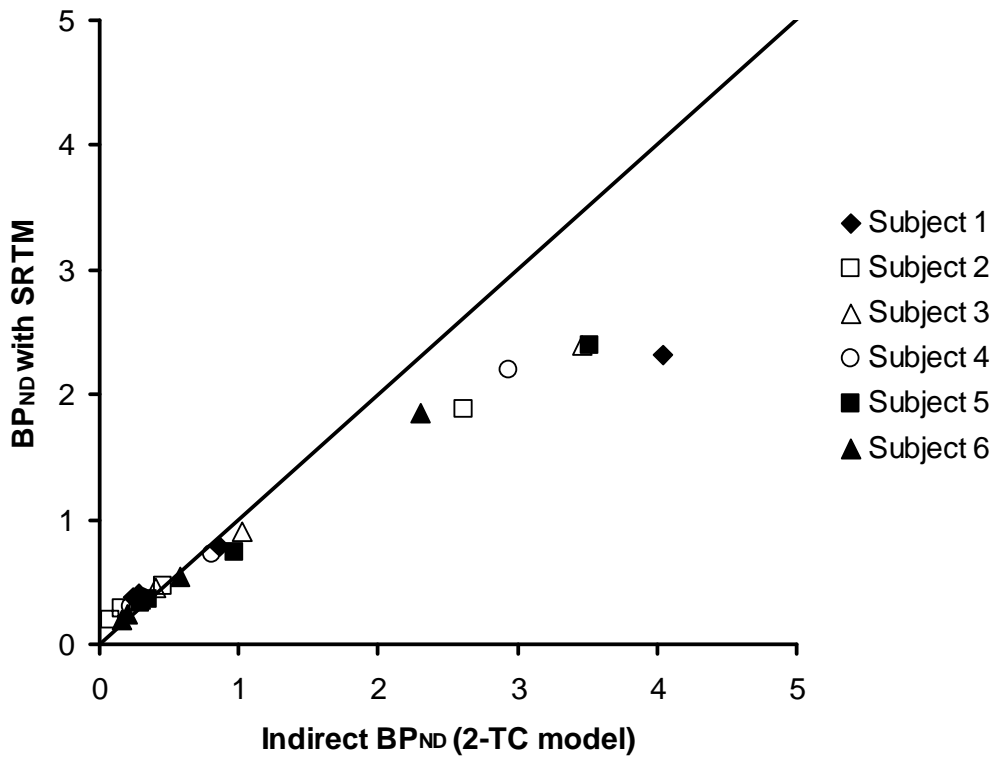


Figure 4. BP<sub>ND</sub> estimated with the SRTM compared to BP<sub>ND</sub> determined by arterial input (2-TC model) from the test scans of the test-retest data set. The graph shows that a bias is introduced in areas of high binding with SRTM (on average 30%, range 20-43%). The solid line is the line of identity.

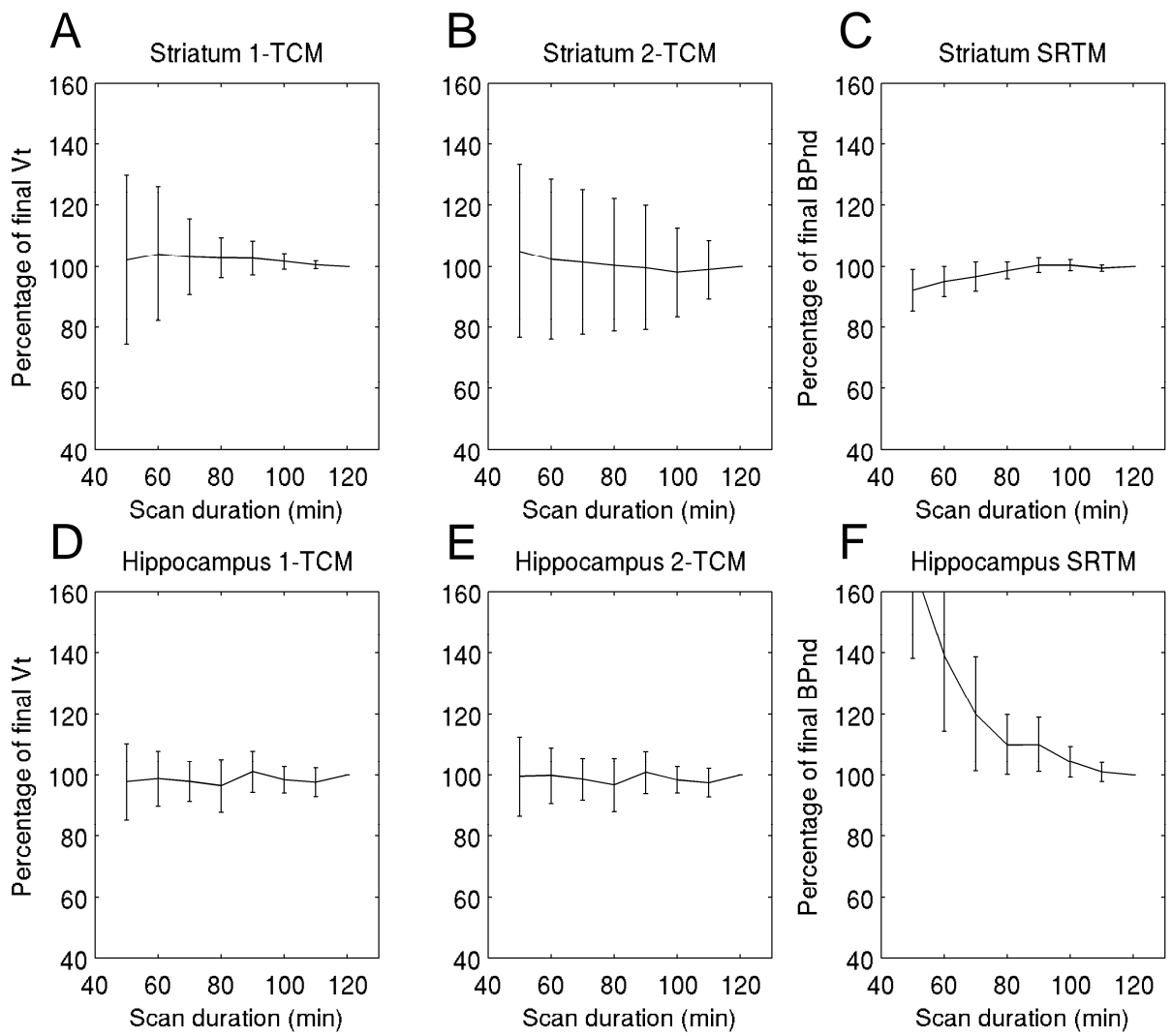


Figure 5. Time stability using the 1-TC model (A), 2-TC model (B), and SRTM (C) for striatum and for hippocampus (D, E, F) for the six test and retest scans. Error bars represent one standard deviation.

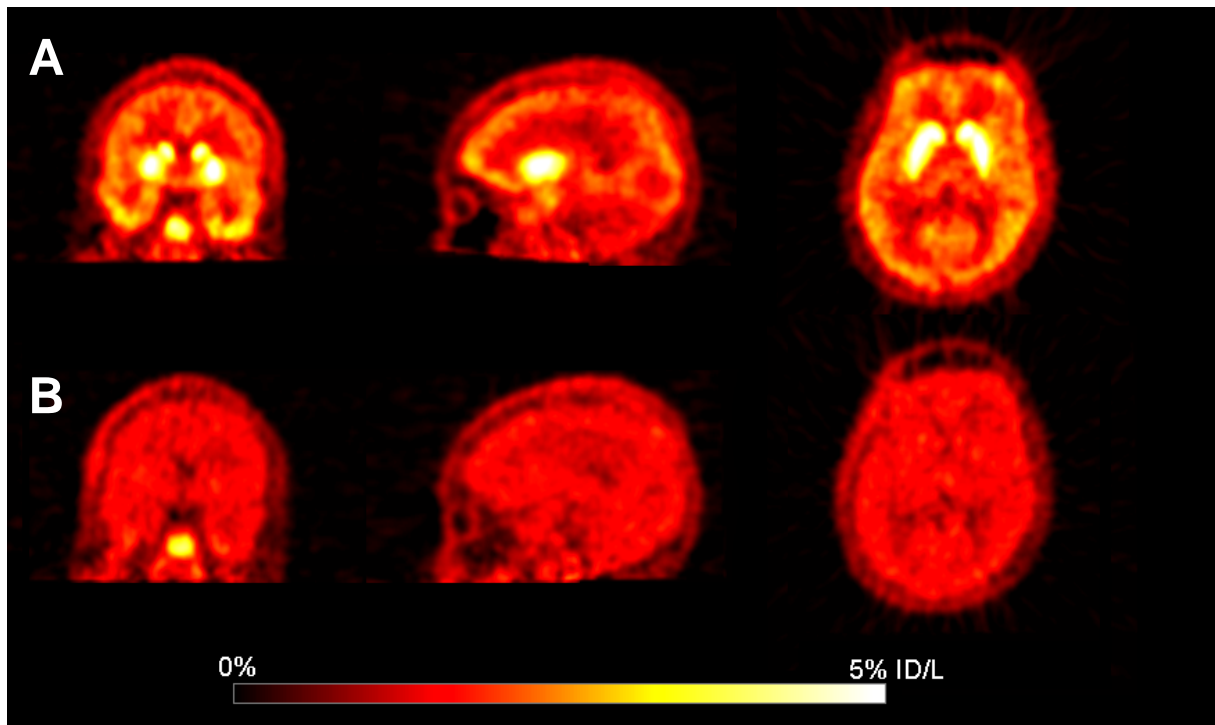


Figure 6. Baseline (A) and a blocked (B)  $[^{11}\text{C}]$ SB207145 scan (male, 29 years) before and after oral administration of Piboserod (SB207266). The mean images from 30 to 120 min after injection are normalized to injected dose to obtain a standard uptake value (% ID/L= percentage of injected dose per liter). The chosen orthogonal sections pass through the highest binding region of the striatum.

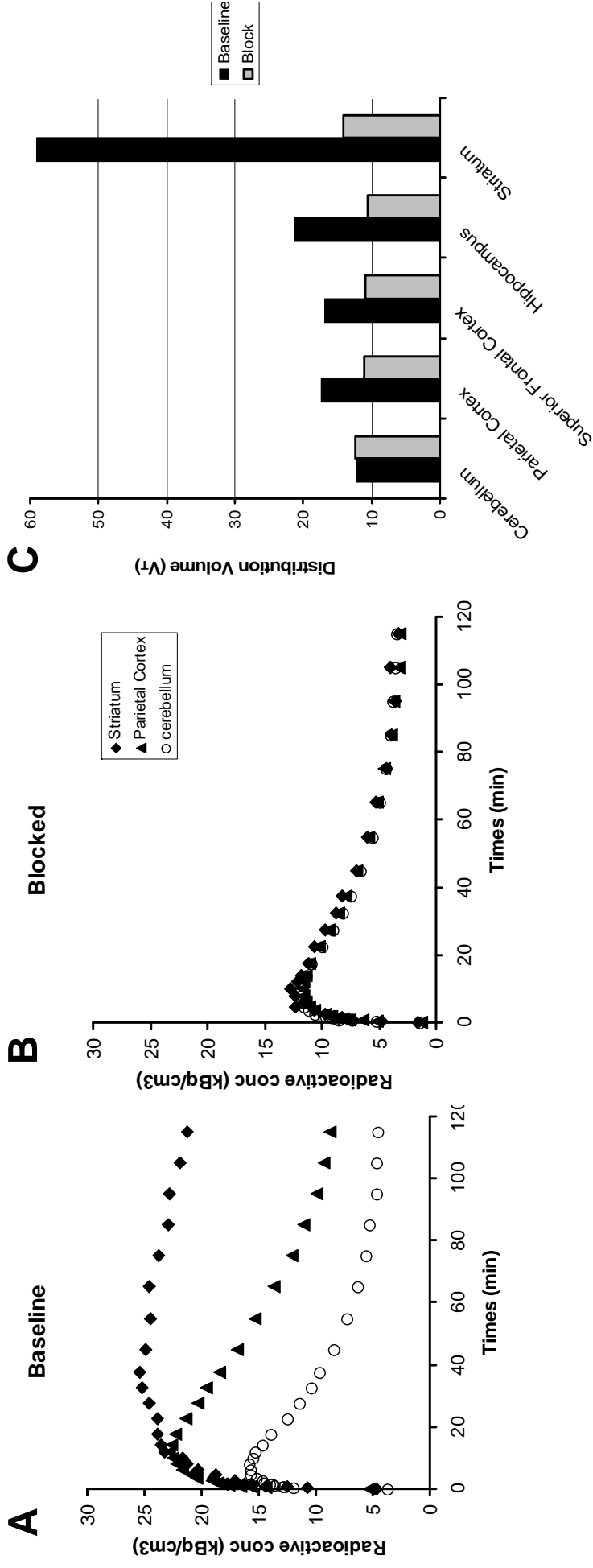


Figure 7. Time activity curves for the baseline (A) and the blocked (B) scans (male, 29 years). After 150 mg oral administration of a structural dissimilar compound Piboserod (SB207266), the [<sup>11</sup>C]SB207145 distribution volumes (C) are reduced to a homogenous level that is in agreement with the baseline cerebellum value (n=2). This supports the use of the cerebellum as a reference region and the specificity of the 5-HT<sub>4</sub> binding signal.

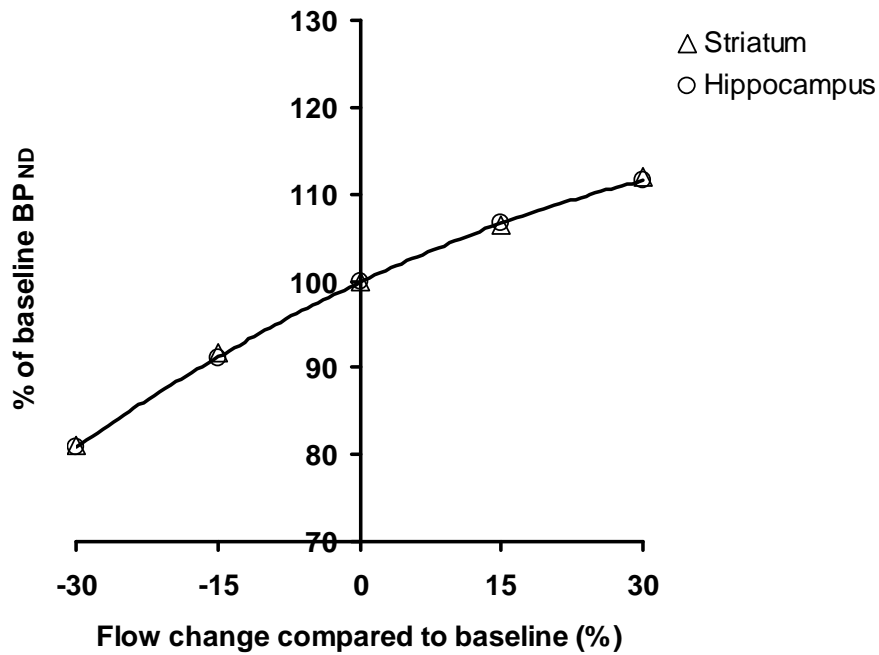


Figure 8. Relative change in SRTM BP<sub>ND</sub> (baseline =100%) with changes in blood flow for striatum and hippocampus. The effects of blood flow changes are simulated using noise-free time-activity curves to be able to estimate the bias. A second order polynomial had a better fit ( $p=0.0003$ ) compared to a linear fit ( $p=0.001$ ). A positive bias of 12% is commensurate with flow increase of 30% and a negative bias of 19% is commensurate with flow decrease of 30%. When the blood flow change is global, i.e. cerebellar flow changes accordingly, the bias is smaller.

*Paper 3*

# Brain Imaging of Serotonin 5-HT<sub>4</sub> Receptors in Humans with [<sup>11</sup>C]SB207145-PET

Lisbeth Marner<sup>1,3</sup>, Nic Gillings<sup>2,3</sup>, Karine Madsen<sup>1,3</sup>, David Erritzoe<sup>1,3</sup>, William Baaré<sup>3,4</sup>, Steen G. Hasselbalch<sup>1,3</sup> and Gitte M. Knudsen<sup>1,3</sup>

*<sup>1</sup>Neurobiology Research Unit, The Neuroscience Centre, <sup>2</sup>PET and Cyclotron Unit, <sup>3</sup>Center for Integrated Molecular Brain Imaging, Rigshospitalet and University of Copenhagen, Copenhagen, Denmark, <sup>4</sup>Danish Research Center for Magnetic Resonance, Hvidovre Hospital, Copenhagen, Denmark*

Corresponding author:

Lisbeth Marner, MD,  
Neurobiology Research Unit N9201  
Rigshospitalet and University of Copenhagen  
Blegdamsvej 9  
DK-2100 Copenhagen O  
Denmark  
Tlf.: (+45) 3545 6707  
Fax: (+45) 3545 6713  
E-mail: lisbeth.marner@nru.dk

Supported by The Lundbeck Foundation, Rigshospitalet, and the Danish Medical Research Council. The John and Birthe Meyer Foundation is gratefully acknowledged for the donation of the Cyclotron and PET-scanner.

Running headline: 5-HT<sub>4</sub> receptors measured with [<sup>11</sup>C]SB207145-PET

## Abstract

The serotonin 4 (5-HT<sub>4</sub>) receptor is a postsynaptic G<sub>s</sub> protein-coupled 5-HT receptor; it is abundantly represented in the brain, where its neurobiological functions include memory and learning, control of food intake, and pain response. Pharmacological stimulation of the 5-HT<sub>4</sub> receptor has shown promise for treatment of Alzheimer's disease and major depression. In this study, we present the first radioligand that enables quantitative *in vivo* imaging in humans of the cerebral 5-HT<sub>4</sub> receptor binding.

Positron emission tomography (PET) scanning was done in sixteen healthy subjects after administration of the novel and selective 5-HT<sub>4</sub> receptor antagonist radioligand [<sup>11</sup>C]SB207145. A quantitative measure of the regional density of 5-HT<sub>4</sub> receptors divided by the equilibrium dissociation constant for [<sup>11</sup>C]SB207145, relative to its non-displaceable binding ( $BP_{ND}$ ), was calculated. The 5-HT<sub>4</sub> receptor radiotracer's sensitivity to acute fluctuations in cerebral 5-HT levels was assessed in seven subjects before and after blockade of 5-HT<sub>1A</sub> and the serotonin transporter.

The regional cerebral distribution of 5-HT<sub>4</sub> receptor, as measured *in vivo* with [<sup>11</sup>C]SB207145 PET, was in high accordance with the distribution found in *post mortem* human brain materials. Based on the intra- and interindividual variability measures, we found that in order to detect a 15% difference in striatal  $BP_{ND}$  with a power of 0.8, a group size of 11-18 subjects is required. Similarly, detection of a 15% difference in the same subject, e.g., before and after a drug treatment, requires inclusion of 4 subjects only. Induction of increased cerebral 5-HT levels did not affect the [<sup>11</sup>C]SB207145 estimate of 5-HT<sub>4</sub> receptor binding.

In conclusion, we here present a validation of the first radiotracer that can reliably be used for quantitative *in vivo* assessment of 5-HT<sub>4</sub> receptor binding in the human brain. The methodology allows

for *in vivo* investigation of cerebral 5-HT<sub>4</sub> receptor binding in studies of its pharmacology, such as in drug occupancy studies, as well as in neuropsychiatric disorders.

## **Introduction**

The brain serotonin 4 (5-HT<sub>4</sub>) receptor is a post-synaptic G<sub>s</sub> protein-coupled 5-HT receptor; stimulation of the receptor inhibits neuronal K<sup>+</sup> currents, resulting in increased neuronal excitability (Fagni et al., 1992).

Judged from *post mortem* human brain studies, the 5-HT<sub>4</sub> receptor is found at high density in striatum, globus pallidus, nucleus accumbens, and substantia nigra, at intermediate density in the hippocampal formation and the superficial layers of the neocortex, whereas cerebellum is practically devoid of receptors (Bonaventure et al., 2000; Reynolds et al., 1995; Varnas et al., 2003). This distribution is consistent with its role in learning and memory processes: Animal studies support a memory-enhancing effect of 5-HT<sub>4</sub> receptor agonists (Orsetti et al., 2003; Terry, Jr. et al., 1998) possibly mediated through enhanced hippocampal release of acetylcholine (Mohler et al., 2007). Administration of selective 5-HT<sub>4</sub> receptor partial agonists such as RS67333 and RS17017 to rodents also improves performance in tests of social, olfactory associative learning, and spatial memory (King et al., 2008) and treatment with the 5-HT<sub>4</sub> receptor agonist, VRX-03011 improved scores in the spontaneous alternation test in rats, in a synergistic action with the acetylcholinesterase (AChE) inhibitor, galantamine (Mohler et al., 2007). In addition, the partial agonist RS67333 has in rats been shown to exert a neuroprotective effect on the processing of amyloid precursor protein (Turner et al., 2003), resulting in less intracellular accumulation of the pathologic  $\beta$ -amyloid peptide (A $\beta$ ) (Cho and Hu, 2007; Robert et al., 2001). In line with this observation, 5-HT<sub>4</sub>-stimulation increases levels of the non-amyloidogenic soluble form, sAPP $\alpha$ , in wild-type mice (Cachard-Chastel et al., 2007). In summary, 5-HT<sub>4</sub> receptors are an exciting potential target for the treatment of Alzheimer's disease, both for symptomatic and neuroprotective treatment strategies. Accordingly, several clinical trials have

now been instituted to evaluate the effectiveness of 5-HT<sub>4</sub> receptor compounds in the treatment of Alzheimer's disease (King et al., 2008).

Preclinical studies also point at 5-HT<sub>4</sub> receptors as a potential target for treatment of depression: The 5-HT<sub>4</sub> receptor is implicated in normal reactions to stress and novelty (Compan et al. 2004), and the partial agonist RS 67333 improved scores in the forced swim test (Lucas et al., 2007). This behavioral change was obtained after only three days of treatment, in contrast to the usual finding of delayed response to serotonin uptake inhibitors and tricyclic antidepressants (Blier, 2003).

*In vivo* imaging has emerged as an important tool for assessment of new drugs, particularly in phase I trials but until now, quantitative *in vivo* brain imaging of the 5-HT<sub>4</sub> receptor in humans has not been possible. The compound SB207145 (figure 1) is a novel 5-HT<sub>4</sub> receptor antagonist with high selectivity and affinity for the 5-HT<sub>4</sub> receptor with a  $K_D$  value of about 0.40 nM (Kornum et al., 2008). The <sup>11</sup>C-labeled ligand has recently proven valuable for *in vivo* quantification of cerebral 5-HT<sub>4</sub> receptor binding in Göttingen minipigs (Kornum et al., 2008). The human 5-HT<sub>4d</sub> receptor has two binding sites, a high-affinity and a low-affinity site (Mikami et al., 2008), suggesting that [<sup>11</sup>C]SB207145 binding may be sensitive to acutely induced endogenous 5-HT competition.

In this study we quantified regional cerebral 5-HT<sub>4</sub> receptor binding a group of healthy subjects with [<sup>11</sup>C]SB207145 PET. The effect of age, sex, and gray matter volume on *in vivo* cerebral 5-HT<sub>4</sub> receptor binding was determined. Based on the intra- and interindividual variability of the outcome parameter,  $BP_{ND}$ , we estimated the required population size for future clinical studies. Finally, we examined the susceptibility of [<sup>11</sup>C]SB207145 binding to acute changes in endogenous serotonin levels, by a combined pharmacological intervention with oral treatment of pindolol that blocks the autoregulation via the 5-HT<sub>1A</sub> receptors in nucleus raphe and infusion of citalopram that increases the extracellular concentration of serotonin.

## ***Material and Methods***

### **Subjects**

Sixteen healthy subjects (mean age: 28.5 years  $\pm$  7.92, range 20-45 years, 8 males) were recruited by newspaper advertisements and gave a written informed consent for participation. Sex-specific values for age, body weight, body-mass index, and years of education are given in table 1. Thirteen of the subjects had two PET recordings on the same day and seven of these subjects received pharmacological challenges (described below) to increase cerebral 5-HT levels. The study was approved by the Capital Regions Ethics Committee ((KF)01-274821 and (KF)01 2006-2). Exclusion criteria were pregnancy, a history of or present neurological or psychiatric disease, abuse of alcohol or drugs (including sedatives), head trauma, family history of mental illness in first-degree relatives, use of a drug known to act on the serotonergic/noradrenergic system within the preceding three months, or abnormal neurological signs. In all subjects, structural brain imaging (T1- and T2-weighted) with magnetic resonance imaging (MRI) was done with a 3.0 T Trio scanner (Siemens, Erlangen, Germany); all subjects had unremarkable brain MRI scans.

### **Imaging**

In a modification of a published method (Gee et al., 2008), [ $^{11}\text{C}$ ]SB207145 was synthesized with [ $^{11}\text{C}$ ]methyl-iodine using a fully automated radiosynthesis system (Gillings and Larsen, 2005) resulting in a >99% radiochemical purity of [ $^{11}\text{C}$ ]SB207145. An intravenous bolus injection of [ $^{11}\text{C}$ ]SB207145 was given over 20 seconds, the mean injected dose and injected mass are given in table 1. After injection, acquisition of a two-hour dynamic emission scan (6x5 s, 10x15 s, 4x30 s, 5x120 s, 5x300 s, and 8x600 s) was initiated, using an eighteen-ring GE-Advance scanner (GE, Milwaukee, WI)

operating in 3D-acquisition mode with an approximate in-plane resolution of 6 mm. The images were reconstructed with 2D filtered back projection and corrected for attenuation, dead-time and scatter. Venous blood samples were drawn 32 and 55 min after injection, and total plasma radioactivity concentration was determined. Plasma parent [ $^{11}\text{C}$ ]SB207145 and its radiolabeled metabolites were measured with HPLC and plasma free fraction,  $f_p$ , measured, as described previously (Kornum et al., 2008).

## Pharmacological Challenge

For pharmacological induction of acutely increased cerebral 5-HT, we used a set-up similar to what is previously reported (Pinborg et al., 2004). The experimental design consisted of a baseline and a pharmacologically-stimulated PET recording with high concentrations of serotonin in the extracellular space during the initial part of the second scan. The subjects were blinded to active versus placebo (saline) treatment and citalopram dose and infusion time were based upon earlier reports that prolactin levels, a well-known biomarker of hypothalamic serotonin release, could be increased for up to three hours (Goldberg et al., 2004; Smith et al., 2002). Nucleus raphe 5-HT autoreceptors were blocked by the 5-HT<sub>1A</sub> partial agonist/ $\beta$ -adrenoceptor antagonist pindolol (Hexapindol, Sandoz) with increasing doses of 2.5 mg x 3 per day to 7.5 mg x3 per day the last three days before the PET session, and on the day of the PET recording. As pindolol is a partial agonist, its actions depend on the system investigated, i.e. pindolol reduces serotonergic release at low serotonin levels and increases at high serotonin levels. Thus, pretreatment of test persons with pindolol is unlikely to increase serotonergic levels by itself but will merely enlarge the difference between conditions with and without citalopram. About 30 min prior to injection of [ $^{11}\text{C}$ ]SB207145, a 60-min infusion of the selective serotonin reuptake inhibitor citalopram (Seropram®, Lundbeck Pharma A/S, Denmark), 40 mg/h, was initiated. This combined treatment has earlier been studied in rats using microdialysis and increased levels of

serotonin up to a factor of 4-5 has been reported (Hjorth et al., 1997) using citalopram and the 5-HT<sub>1A</sub> antagonist, WAY100635.

## Data Processing

To correct for head-motion artifacts, the frames of the dynamic PET scan were aligned using the AIR routines (alignlinear combined reconcile, Air version 5.2.5). A (flow-weighted) mean emission image of the first 20 min was automatically aligned to same individuals T1-weighted brain MR image, segmented into gray matter, white matter, and cerebrospinal fluid using Statistical Parametric Mapping (SPM2; Wellcome Department of Cognitive Neurology, London, UK). The T2 weighted images served for brain masking purposes. In the segmented MR image, each voxel was assigned to the tissue class with the highest probability and this segmentation was subsequently used for partial volume (PV) correction (Muller-Gartner et al., 1992). The PV effect is caused by the low resolution that makes the radioactivity from the brain tissues appear merged and averaged in the final PET image. A total of 24 bilateral regions were automatically delineated on each subject's MR image in a user-independent fashion with the Pvelab software package (freely available on [www.nru.dk/downloads](http://www.nru.dk/downloads)) (Svarer et al., 2005).

Regional time radioactivity curves (TAC's) were extracted, both with and without PV correction. Volume weighted averaged TAC's from both hemispheres were constructed and kinetic modeling was performed with the simplified reference tissue model (SRTM) using cerebellum as reference region. The outcome parameter of the SRTM was  $BP_{ND}$ . We have validated the SRTM in humans and found that it is a reliable and reproducible method for quantification of [<sup>11</sup>C]SB207145 and confirmed that cerebellum is a suitable reference region by blocking with the selective 5-HT<sub>4</sub> receptor compound prior to radiotracer administration (Marnier et al., 2008a). For modeling purposes, we used the commercially available software PMOD (version 2.95, PMOD Inc, Zürich, Switzerland).

## Statistics

Spearman's rank correlation test was used to evaluate the correlation between 5-HT<sub>4</sub> receptor *in vivo* binding and literature based *post mortem* specific binding across brain regions. In order to enable comparison between reported human *post mortem* brain data (Bonaventure et al., 2000; Reynolds et al., 1995; Varnas et al., 2004), the binding measures were normalized to hippocampal values. For the remaining correlations, Pearson product-moment correlations were used. The required sample size to detect group differences of 15% with a power of 0.8 were calculated using the regional mean and standard deviation of  $BP_{ND}$  across and within subjects. Sex differences were evaluated using a linear mixed effect model. To include repeated measures from several regions for each subject, region and subject were used as a within-subject factors and sex and age as between-subject factors. Here, we used logarithmic transformation of  $BP_{ND}$  to improve the normal distribution, since  $BP_{ND}$  varied over a large range, according to region; from 0.4 in prefrontal cortex to 2.3 in the caudate nucleus. In order to include brain regions representative of various functional brain areas and with range of receptor densities, eight bilateral regions were selected for the analysis: cingulate cortex (average of anterior and posterior), insula, caudate nucleus, putamen (average of putamen and globus pallidum), temporal cortex (average of superior and medial inferior temporal gyri), prefrontal cortex (average of dorsolateral and ventrolateral), hippocampus and amygdala. Student's t-test was used to compare the non-displaceable binding as assessed by the area under curve (AUC) for the cerebellum time activity normalized to the dose per kg bodyweight. For statistical analysis SAS (version 9.1.3, SAS inc. Cary, NC) was used and throughout, we adopted a significance level of 0.05.

## Results

An example of a 3D image of the distribution of cerebral [<sup>11</sup>C]SB207145 binding is given in figure 2; the binding was generally 3-4 fold higher in striatum than in neocortex. The specific 5-HT<sub>4</sub>

receptor binding as determined from *post mortem* brain data (Bonaventure et al., 2000; Reynolds et al., 1995; Varnas et al., 2004), significantly correlated to PV corrected average  $BP_{ND}$  in males ( $p=0.0003$ ) and a tendency for a correlation was seen for non-PV corrected  $BP_{ND}$  ( $p=0.10$ ) (figure 3).

A tendency to an inverse correlation between age and non-PV corrected  $BP_{ND}$  was found with the mixed model ( $t=-2.15$ ,  $df=13$ ,  $p=0.051$ ) and we found an overall significant sex effect both when age was included ( $t=-2.49$ ,  $df=13$ ,  $p=0.027$ ) and without age ( $t=-2.57$ ,  $df=14$ ,  $p=0.022$ ) but no significant sex  $\times$  region effects (figure 4). The found sex effect was on average 15% in favor of the males, whereas no significant sex differences were found in the estimate for the non-displaceable binding, the normalized cerebellum AUC ( $p=0.17$ ) (table 1) and no correlations between this measure and  $BP_{ND}$  was found in a representative region (hippocampus) in males ( $p=0.54$ ) or females ( $p=0.23$ ). We found no sex differences in tracer metabolism as measured in venous blood samples during the scan (table 1) and in total plasma radioactivity when correcting for injected dose per kg body weight ( $n=16$ ).

Table 2 shows the regional  $BP_{ND}$  with [ $^{11}C$ ]SB207145, with and without PV correction, and it reports the necessary sample size to detect group or paired differences. The calculations are based on non-PV corrected  $BP_{ND}$ 's as PV correction lowers the inter-subject variation and lead to erroneously small sample sizes (Marner et al., 2008b). Males had larger brains compared to females (results not shown) but we found no correlations between hippocampal size and  $BP_{ND}$  (males  $p=0.46$ , females  $p=0.65$ ) and no positive correlations between total brain volume and  $BP_{ND}$  (non-PV corrected) in any region (results not shown).

The subjects tolerated the combined treatment with pindolol well, without significant changes in cardiovascular measures and without any noticeable side effects. Three subjects experienced nausea after half an hour of citalopram infusion and one subject also experienced hot flushes, but none of the subjects on active treatment had to be discontinued from treatment during the scanning session. One

subject experienced nausea starting after the infusion and lasting for two days. We deduced a significant release of hypothalamic serotonin, as revealed by increased plasma prolactin and cortisol levels during the entire PET recording (figure 5). The neuroendocrine response was highly variable with prolactin increases of on average 3.9 (range 1.2 - 8.9) times baseline levels (77-373 mIU/L), and a plasma cortisol increase of 1.8 (range 1.2 - 4.0) times (baseline 227-1129 nmol/L). Prolactin levels remained stable throughout the untreated scanning session. In spite of the profound increase in plasma prolactin level as proxy for increased cerebral 5-HT levels,  $BP_{ND}$  was unaltered in all tested regions (caudate nucleus, putamen, insula, and hippocampus). Further, the group receiving citalopram treatment during second PET recording did not show larger  $BP_{ND}$  changes compared to the test-retest subjects not receiving any treatment (figure 6). No correlations between change in  $BP_{ND}$  and change (relative to baseline or absolute values) in plasma prolactin levels were identified. The injected dose, non-displaceable binding, and  $f_P$  did not differ between baseline and citalopram conditions (results not shown).

## **Discussion**

We here report the first *in vivo* imaging study with quantitative assessment of cerebral 5-HT<sub>4</sub> receptor binding in a group of healthy human subjects. When compared to postmortem human data, averaged from three different studies, a clear rank order correlation was found to our regional  $BP_{ND}$  values for [<sup>11</sup>C]SB207145 binding. This is also in line with a study involving a direct comparison of [<sup>11</sup>C]SB207145 PET binding determined in the minipig, with subsequent [<sup>3</sup>H]SB207145 postmortem autoradiography and binding assay measurements in the same pigs (Kornum et al., 2008). The 5-HT<sub>4</sub> receptor consists of several splice variants that are expressed differentially in the human brain. The divergence in the sequence of these splice variants, however, usually starts after amino acid Leu358, resulting in COOH-terminal splice variants (De Maeyer et al., 2008), and therefore, antagonists are

considered to bind equally well to all the variants. In support of this notion, no regional differences in [<sup>3</sup>H]SB207145 affinities was found across brain regions (Kornum et al., 2008).

We found a trend for 5-HT<sub>4</sub> receptor binding to decrease with age, even within the limited age span of our sample (20-45 years). Other receptors within the serotonin system are known to decline with age, including the 5-HT<sub>2A</sub> (Adams et al., 2004) and 5-HT<sub>1A</sub> (Tauscher et al., 2001) receptors, although the latter has been disputed (Rabiner et al., 2002). It is also debatable if an age-related reduction constitute a real decline in the receptor density, or if such a relationship could be partly explained by age-related changes in brain structure.

In the eight selected regions, males had about 15% higher binding than females (figure 4); this seemed to be a global phenomenon since no sex × region effects were found. The sex difference could not readily be ascribed to differences in the non-specific binding; firstly because there was no statistically significant sex difference in cerebellum AUC, secondly we failed to identify any correlation between hippocampal 5-HT<sub>4</sub> receptor binding (where we saw the most solid sex difference) and cerebellum AUC. Firm conclusions on sex differences in the 5-HT<sub>4</sub> receptor availability will require studies of larger groups. Several studies have examined sex differences in the serotonin system. For the 5-HT<sub>1A</sub> receptor, larger *in vivo* binding in females has been reported (Jovanovic et al., 2008; Parsey et al., 2002), while a *post mortem* study find no differences (Palego et al., 1997). Lower binding to the serotonin transporter in females was also observed (Jovanovic et al., 2008), while studies of 5-HT<sub>2A</sub> receptors show no sex differences (Adams et al., 2004). Possible sex differences in 5-HT<sub>4</sub> binding are of interest, not the least because of the involvement of the serotonin system in affective and anxiety disorders, that both are more prevalent in females.

The data on inter- and intrasubject variability of 5-HT<sub>4</sub> receptor binding show that in order to detect a 15% difference between two groups, the required group size varies depending on the brain

region of interest, and is between 11 and 39. For a repeat study in the same subject, a 15% difference would require between only 4 and 14 subjects, again depending on the brain region. The reason for the large region-dependency is that brain regions with limited 5-HT<sub>4</sub> receptor binding, such as sensorimotor and occipital cortex, return noisy estimates, whereas the opposite is true for receptor rich regions. In addition, in spite of their high 5-HT<sub>4</sub> receptor binding amygdala and hypothalamus volumes are small and those regions therefore show a larger variance. In comparison to the power analysis for an imaging study of the 5-HT<sub>2A</sub> receptor binding with [<sup>18</sup>F]altanserin (Haugbol et al., 2007), [<sup>11</sup>C]SB207145 comes out more favorably.

We found that [<sup>11</sup>C]SB207145 binding as measured with PET is insensitive to endogenously released serotonin. Based on the confidence intervals depicted in figure 6, we could have overlooked a decrease in [<sup>11</sup>C]SB207145 binding smaller than 5%, but given the presumably large increases in cerebral 5-HT levels invoked by the pharmacological treatment, we consider that at more physiological (smaller) alterations in cerebral 5-HT levels, a change in binding below 5% is irrelevant in the context of neuroimaging. The lack of susceptibility to 5-HT changes means that [<sup>11</sup>C]SB207145 can be used for stably quantifying 5-HT<sub>4</sub> receptors *in vivo* without taking acute fluctuations in serotonin levels into account. The mechanism behind the occasionally observed reduction in *in vivo* radiotracer binding in conjunction with a stimulus that increases the endogenous release of neurotransmitter is still disputed. Suggested explanations for this sensitivity, so far most consistently observed with some D<sub>2</sub> receptor radioligands, include neurotransmitter competition at the receptor-ligand level, internalization of the receptor and/or radioligand selective binding to different affinity states of the receptor. The 5-HT<sub>4</sub> receptor is known to undergo rapid uncoupling in neurons, independent of the splice variant (Barthet et al., 2005) and an agonist induced uncoupling could theoretically have been associated with changes in the 5-HT<sub>4</sub> receptor affinity state, and thus with a change in radioligand binding.

Although acute changes did not seem to influence binding of [ $^{11}\text{C}$ ]SB207145, subacute or chronic changes in cerebral serotonin levels are shown to have a profound effect on the 5-HT<sub>4</sub> receptor levels (Compan et al., 1996) (Licht, personal communication). Accordingly, it will be interesting to investigate if more chronic alterations in cerebral 5-HT levels are associated with inverse changes in [ $^{11}\text{C}$ ]SB207145 binding *in vivo*. Given the absence of a non-invasive and robust methodology for measuring *in vivo* concentrations of cerebral 5-HT levels in humans, [ $^{11}\text{C}$ ]SB207145 PET here offers an interesting potential as an indirect measure.

In conclusion, [ $^{11}\text{C}$ ]SB207145 is a valuable tool for quantification of the 5-HT<sub>4</sub> receptor in human brain. The estimates of  $BP_{\text{ND}}$  exhibit low inter-subject variation, especially in the high-binding brain regions: Striatum, temporal cortex, and hippocampus. Our data provide an excellent basis for conduction of accordingly designed *in vivo* studies of the state of the 5-HT<sub>4</sub> receptor in, e.g., cognitive function and in Alzheimer's disease, depression (Lucas et al., 2007), epilepsy (Compan et al., 2004), or eating disorders (Compan et al., 2004; Jean et al., 2007). We anticipate that the use of [ $^{11}\text{C}$ ]SB207145 PET in occupancy studies will be a superior tool for dose selection in future clinical trials of drugs acting on the 5-HT<sub>4</sub> receptor.

## **Acknowledgements**

Bente Høy, Anita Dole, Blerta Shuka, and Kirsten Honsyld are thanked for invaluable technical assistance. The authors thank Paul Cumming for constructive contributions to the manuscript. The precursor for [ $^{11}\text{C}$ ]SB207145 was kindly supplied by GlaxoSmithKline; and we are grateful for the financial support from The Lundbeck Foundation, Rigshospitalet, and the Danish Medical Research Council. The John and Birthe Meyer Foundation is gratefully acknowledged for the donation of the Cyclotron and PET-scanner.

## References

- Adams,K.H., Pinborg,L.H., Svarer,C., Hasselbalch,S.G., Holm,S., Haugbol,S., Madsen,K., Frokjaer,V., Martiny,L., Paulson,O.B., and Knudsen,G.M. (2004). A database of [(18)F]-altanserin binding to 5-HT(2A) receptors in normal volunteers: normative data and relationship to physiological and demographic variables. *Neuroimage*. 21, 1105-1113.
- Barthet,G., Gaven,F., Framery,B., Shinjo,K., Nakamura,T., Claeysen,S., Bockaert,J., and Dumuis,A. (2005). Uncoupling and endocytosis of 5-hydroxytryptamine 4 receptors. Distinct molecular events with different GRK2 requirements. *J Biol. Chem*. 280, 27924-27934.
- Blier,P. (2003). The pharmacology of putative early-onset antidepressant strategies. *Eur. Neuropsychopharmacol*. 13, 57-66.
- Bonaventure,P., Hall,H., Gommeren,W., Cras,P., Langlois,X., Jurzak,M., and Leysen,J.E. (2000). Mapping of serotonin 5-HT(4) receptor mRNA and ligand binding sites in the post-mortem human brain. *Synapse*. 36, 35-46.
- Cachard-Chastel,M., Lezoualc'h,F., Dewachter,I., Delomenie,C., Croes,S., Devijver,H., Langlois,M., Van,L.F., Sicsic,S., and Gardier,A.M. (2007). 5-HT4 receptor agonists increase sAPPalpha levels in the cortex and hippocampus of male C57BL/6j mice. *Br. J. Pharmacol*. 150, 883-892.
- Cho,S., and Hu,Y. (2007). Activation of 5-HT4 receptors inhibits secretion of beta-amyloid peptides and increases neuronal survival. *Exp. Neurol*. 203, 274-278.
- Compan,V., Daszuta,A., Salin,P., Sebben,M., Bockaert,J., and Dumuis,A. (1996). Lesion study of the distribution of serotonin 5-HT4 receptors in rat basal ganglia and hippocampus. *Eur. J Neurosci*. 8, 2591-2598.
- Compan,V., Zhou,M., Grailhe,R., Gazzara,R.A., Martin,R., Gingrich,J., Dumuis,A., Brunner,D., Bockaert,J., and Hen,R. (2004). Attenuated response to stress and novelty and hypersensitivity to seizures in 5-HT4 receptor knock-out mice. *J. Neurosci*. 24, 412-419.
- De Maeyer,J.H., Aerssens,J., Verhasselt,P., and Lefebvre,R.A. (2008). Alternative splicing and exon duplication generates 10 unique porcine 5-HT 4 receptor splice variants including a functional homofusion variant. *Physiol Genomics*. 34, 22-33.
- Fagni,L., Dumuis,A., Sebben,M., and Bockaert,J. (1992). The 5-HT4 receptor subtype inhibits K+ current in colliculi neurones via activation of a cyclic AMP-dependent protein kinase. *Br. J Pharmacol*. 105, 973-979.

- Gee,A.D., Martarello,L., Passchier,M., Wishart,C., Parker,J., Matthews,R., Comley,R., Hopper,R., and Gunn,R. (2008). Synthesis and Evaluation of [<sup>11</sup>C]SB207145 as the First *In Vivo* Serotonin 5-HT<sub>4</sub> Receptor Radioligand for PET Imaging in Man. *Current Radiopharmaceuticals 1*.
- Goldberg,S., Smith,G.S., Barnes,A., Ma,Y., Kramer,E., Robeson,K., Kirshner,M., Pollock,B.G., and Eidelberg,D. (2004). Serotonin modulation of cerebral glucose metabolism in normal aging. *Neurobiol. Aging. 25*, 167-174.
- Haugbol,S., Pinborg,L.H., Arfan,H.M., Frokjaer,V.M., Madsen,J., Dyrby,T.B., Svarer,C., and Knudsen,G.M. (2007). Reproducibility of 5-HT(2A) receptor measurements and sample size estimations with [(18)F]altanserin PET using a bolus/infusion approach. *Eur. J. Nucl. Med. Mol. Imaging. 34*, 910-915.
- Hjorth,S., Westlin,D., and Bengtsson,H.J. (1997). WAY100635-induced augmentation of the 5-HT-elevating action of citalopram: relative importance of the dose of the 5-HT1A (auto)receptor blocker versus that of the 5-HT reuptake inhibitor. *Neuropharmacology. 36*, 461-465.
- Jean,A., Conductier,G., Manrique,C., Bouras,C., Berta,P., Hen,R., Charnay,Y., Bockaert,J., and Compan,V. (2007). Anorexia induced by activation of serotonin 5-HT<sub>4</sub> receptors is mediated by increases in CART in the nucleus accumbens. *Proc. Natl. Acad. Sci. U. S. A. 104*, 16335-16340.
- Jovanovic,H., Lundberg,J., Karlsson,P., Cerin,A., Saijo,T., Varrone,A., Halldin,C., and Nordstrom,A.L. (2008). Sex differences in the serotonin 1A receptor and serotonin transporter binding in the human brain measured by PET. *Neuroimage. 39*, 1408-1419.
- King,M.V., Marsden,C.A., and Fone,K.C. (2008). A role for the 5-HT(1A), 5-HT(4) and 5-HT(6) receptors in learning and memory. *Trends Pharmacol. Sci.*
- Kornum,B.R., Lind,N.M., Gillings,N., Marner,L., Andersen,F., and Knudsen,G.M. (2008). Evaluation of the novel 5-HT(4) receptor PET ligand [(11)C]SB207145 in the Göttingen minipig. *J Cereb Blood Flow Metab.*
- Lucas,G., Rymar,V.V., Du,J., Mnie-Filali,O., Bisgaard,C., Manta,S., Lambas-Senas,L., Wiborg,O., Haddjeri,N., Pineyro,G., Sadikot,A.F., and Debonnel,G. (2007). Serotonin(4) (5-HT(4)) receptor agonists are putative antidepressants with a rapid onset of action. *Neuron. 55*, 712-725.
- Marner,L., Gillings,N., Comley,R., Baaré,W., Rabiner,E.A., Wilson,A.A., Laruelle,M., Houle,S., Hasselbalch,S.G., Svarer,C., Gunn,R.N., and Knudsen,G.M. (2008a). Kinetic Modeling of [<sup>11</sup>C]SB207145 binding to 5-HT<sub>4</sub> receptors in the human brain in vivo. *J. Nucl. Med. (submitted)*.

- Marner,L., Knudsen,G.M., Haugbol,S., Holm,S., Baaré,W., and Hasselbalch,S.G. (2008b). Longitudinal assessment of cerebral 5-HT<sub>2A</sub> receptors in healthy elderly volunteers: An [18F]-altanserin PET study. *Eur. J. Nucl. Med. Mol. Imaging.* (*in press*).
- Mikami,T., Sugimoto,H., Naganeo,R., Ohmi,T., Saito,T., and Eda,H. (2008). Contribution of active and inactive states of the human 5-HT<sub>4d</sub> receptor to the functional activities of 5-HT<sub>4</sub>-receptor agonists. *J Pharmacol. Sci.* *107*, 251-259.
- Mohler,E.G., Shacham,S., Noiman,S., Lezoualc'h,F., Robert,S., Gastineau,M., Rutkowski,J., Marantz,Y., Dumuis,A., Bockaert,J., Gold,P.E., and Ragozzino,M.E. (2007). VRX-03011, a novel 5-HT<sub>4</sub> agonist, enhances memory and hippocampal acetylcholine efflux. *Neuropharmacology.* *53*, 563-573.
- Muller-Gartner,H.W., Links,J.M., Prince,J.L., Bryan,R.N., McVeigh,E., Leal,J.P., Davatzikos,C., and Frost,J.J. (1992). Measurement of radiotracer concentration in brain gray matter using positron emission tomography: MRI-based correction for partial volume effects. *J. Cereb. Blood Flow Metab.* *12*, 571-583.
- Orsetti,M., Dellarole,A., Ferri,S., and Ghi,P. (2003). Acquisition, retention, and recall of memory after injection of RS67333, a 5-HT(4) receptor agonist, into the nucleus basalis magnocellularis of the rat. *Learn. Mem.* *10*, 420-426.
- Palego,L., Marazziti,D., Rossi,A., Giannaccini,G., Naccarato,A.G., Lucacchini,A., and Cassano,G.B. (1997). Apparent absence of aging and gender effects on serotonin 1A receptors in human neocortex and hippocampus. *Brain Res.* *758*, 26-32.
- Parsey,R.V., Oquendo,M.A., Simpson,N.R., Ogden,R.T., Van,H.R., Arango,V., and Mann,J.J. (2002). Effects of sex, age, and aggressive traits in man on brain serotonin 5-HT<sub>1A</sub> receptor binding potential measured by PET using [C-11]WAY-100635. *Brain Res.* *954*, 173-182.
- Pinborg,L.H., Adams,K.H., Yndgaard,S., Hasselbalch,S.G., Holm,S., Kristiansen,H., Paulson,O.B., and Knudsen,G.M. (2004). [18F]altanserin binding to human 5HT<sub>2A</sub> receptors is unaltered after citalopram and pindolol challenge. *J. Cereb. Blood Flow Metab.* *24*, 1037-1045.
- Rabiner,E.A., Messa,C., Sargent,P.A., Husted-Kjaer,K., Montgomery,A., Lawrence,A.D., Bench,C.J., Gunn,R.N., Cowen,P., and Grasby,P.M. (2002). A database of [(11)C]WAY-100635 binding to 5-HT(1A) receptors in normal male volunteers: normative data and relationship to methodological, demographic, physiological, and behavioral variables. *Neuroimage.* *15*, 620-632.
- Reynolds,G.P., Mason,S.L., Meldrum,A., De,K.S., Parnes,H., Eglen,R.M., and Wong,E.H. (1995). 5-Hydroxytryptamine (5-HT)<sub>4</sub> receptors in post mortem human brain tissue: distribution, pharmacology and effects of neurodegenerative diseases. *Br. J Pharmacol.* *114*, 993-998.

- Robert,S.J., Zugaza,J.L., Fischmeister,R., Gardier,A.M., and Lezoualc'h,F. (2001). The human serotonin 5-HT<sub>4</sub> receptor regulates secretion of non-amyloidogenic precursor protein. *J. Biol. Chem.* 276, 44881-44888.
- Smith,G.S., Ma,Y., Dhawan,V., Gunduz,H., Carbon,M., Kirshner,M., Larson,J., Chaly,T., Belakhleff,A., Kramer,E., Greenwald,B., Kane,J.M., Laghrissi-Thode,F., Pollock,B.G., and Eidelber,D. (2002). Serotonin modulation of cerebral glucose metabolism measured with positron emission tomography (PET) in human subjects. *Synapse.* 45, 105-112.
- Svarer,C., Madsen,K., Hasselbalch,S.G., Pinborg,L.H., Haugbol,S., Frokjaer,V.G., Holm,S., Paulson,O.B., and Knudsen,G.M. (2005). MR-based automatic delineation of volumes of interest in human brain PET images using probability maps. *Neuroimage.* 24, 969-979.
- Tauscher,J., Verhoeff,N.P., Christensen,B.K., Hussey,D., Meyer,J.H., Kecojevic,A., Javanmard,M., Kasper,S., and Kapur,S. (2001). Serotonin 5-HT<sub>1A</sub> receptor binding potential declines with age as measured by [<sup>11</sup>C]WAY-100635 and PET. *Neuropsychopharmacology.* 24, 522-530.
- Terry,A.V., Jr., Buccafusco,J.J., Jackson,W.J., Prendergast,M.A., Fontana,D.J., Wong,E.H., Bonhaus,D.W., Weller,P., and Eglen,R.M. (1998). Enhanced delayed matching performance in younger and older macaques administered the 5-HT<sub>4</sub> receptor agonist, RS 17017. *Psychopharmacology (Berl).* 135, 407-415.
- Turner,P.R., O'Connor,K., Tate,W.P., and Abraham,W.C. (2003). Roles of amyloid precursor protein and its fragments in regulating neural activity, plasticity and memory. *Prog. Neurobiol.* 70, 1-32.
- Varnas,K., Halldin,C., and Hall,H. (2004). Autoradiographic distribution of serotonin transporters and receptor subtypes in human brain. *Hum. Brain Mapp.* 22, 246-260.
- Varnas,K., Halldin,C., Pike,V.W., and Hall,H. (2003). Distribution of 5-HT<sub>4</sub> receptors in the postmortem human brain--an autoradiographic study using [<sup>125</sup>I]SB 207710. *Eur. Neuropsychopharmacol.* 13, 228-234.

	<b>Males (n=8)</b>	<b>Females (n=8)</b>
<b>Age (years)</b>	27.2 ±7.16	29.8 ±8.90
<b>Body Weight (kg)</b>	85.2 ±8.28	65.1 ±7.85***
<b>BMI (kg m<sup>-2</sup>)</b>	24.9 ±1.99	23.1 ±1.64
<b>Years of Education<sup>1</sup></b>	15.9 ±3.00	16.1 ±2.70
<b>Injected Dose (MBq)</b>	412 ±178	421 ±128
<b>Injected Mass (nmol)</b>	10.7 ±6.53	13.7 ±7.56
<b>Cerebellar AUC, normalized (g min mL<sup>-1</sup>)</b>	116 ±12.3	132 ±28.9
<b>Parent compound 32 min (%)</b>	16.4 ±2.28 (n=4)	16.9 ±3.66 (n=5)
<b>Parent compound 55 min (%)</b>	11.8 ±1.95 (n=6)	12.9 ±2.73 (n=6)
<b>Free fraction, <i>f<sub>p</sub></i></b>	0.27 ±0.032 (n=4)	0.32 ±0.086 (n=6)

Table 1. Demographic variables of the sixteen healthy subjects enrolled in the study. Injected mass is the amount of injected unlabelled tracer. Cerebellar AUC, normalized is the area under the curve of the cerebellar time-activity curve, normalized to injected dose per unit body mass.

\*\*\* p<0.001.

<sup>1</sup>Started but not yet completed education counts as finished for younger subjects.

Region	Without PV correction				With PV correction			
	Males (n=8) $BP_{ND}$ ( $\pm SD$ )	Females (n=8) $BP_{ND}$ ( $\pm SD$ )	All (n=16) $BP_{ND}$ ( $\pm SD$ )	Sample Size 2-sample (n=16) 15%	Sample Size Paired (n=6) 15%	Males (n=8) $BP_{ND}$ ( $\pm SD$ )	Females (n=8) $BP_{ND}$ ( $\pm SD$ )	
Temporal cortex	0.58±0.05	0.49±0.09*	0.54±0.08	18	4	0.83±0.07	0.77±0.08	
Parietal cortex	0.43±0.03	0.39±0.09	0.41±0.07	20	5	0.96±0.10	0.89±0.10	
Occipital cortex	0.35±0.03	0.31±0.08	0.33±0.06	27	4	0.61±0.10	0.57±0.07	
Sensorimotor cortex	0.25±0.04	0.22±0.06	0.24±0.05	39	9	0.73±0.11	0.67±0.07	
Prefrontal cortex	0.38±0.03	0.35±0.06	0.36±0.05	14	4	0.81±0.07	0.79±0.06	
Insula	0.71±0.06	0.62±0.11	0.66±0.10	17	7	0.72±0.10	0.65±0.10	
Thalamus	0.48±0.03	0.44±0.08	0.46±0.06	13	6	0.54±0.05	0.50±0.08	
Anterior Cingulate	0.54±0.05	0.47±0.11	0.51±0.09	24	14	0.71±0.11	0.64±0.12	
Putamen	2.37±0.10	2.14±0.32	2.26±0.26	11	4	2.77±0.17	2.53±0.33	
Hippocampus	0.87±0.05	0.69±0.13**	0.78±0.13	21	5	0.83±0.10	0.69±0.14*	
Posterior Cingulate	0.55±0.06	0.47±0.10	0.51±0.09	24	3	0.72±0.08	0.66±0.09	
Caudate Nucleus	2.34±0.31	2.17±0.38	2.25±0.34	18	4	3.27±0.21	3.05±0.31	
Amygdala	0.71±0.09	0.57±0.09**	0.64±0.12	24	8	0.75±0.13	0.61±0.17	
Hypothalamus	0.57±0.10	0.50±0.12	0.53±0.11	33	12	1.11±0.21	1.01±0.18	

Table 2. [ $^{11}C$ ]SB207145  $BP_{ND}$  ordered in very large ( $>50\text{ cm}^3$ ), large ( $10\text{-}50\text{ cm}^3$ ), intermediate ( $5\text{-}10\text{ cm}^3$ ), and small regions ( $<5$

$\text{cm}^3$ ). Sample size estimates for group wise comparisons (2-sample) were based on mean and standard deviation ( $SD$ ) of all 16

subjects, a power of 0.80 and a group difference of 15%, while the estimates for paired tests were based on mean and  $SD$  of the

difference between first and second scan for the 6 subjects with test-retest data. \* $p<0.05$ , \*\* $p<0.01$  (Student's t-test).

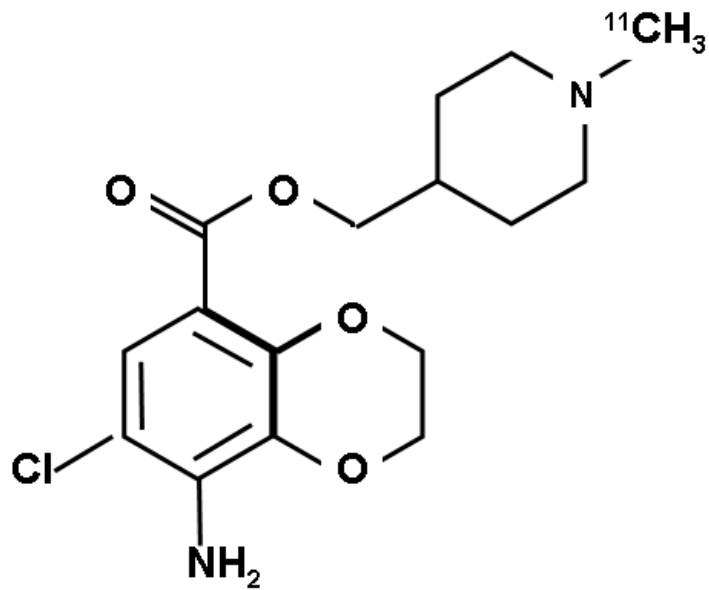


Figure 1. Chemical structure of the high affinity 5-HT<sub>4</sub> receptor antagonist [<sup>11</sup>C]SB207145. When tested against more than 40 brain receptors, the selectivity of [<sup>11</sup>C]SB207145 for the 5-HT<sub>4</sub> receptor was high with only limited binding to the 5-HT<sub>3</sub> receptor and even smaller binding to dopamine receptors D<sub>1</sub>, D<sub>2</sub>, D<sub>4</sub>, histamine H<sub>2</sub>, and adrenoceptor α<sub>2B</sub> (GSK internal report).

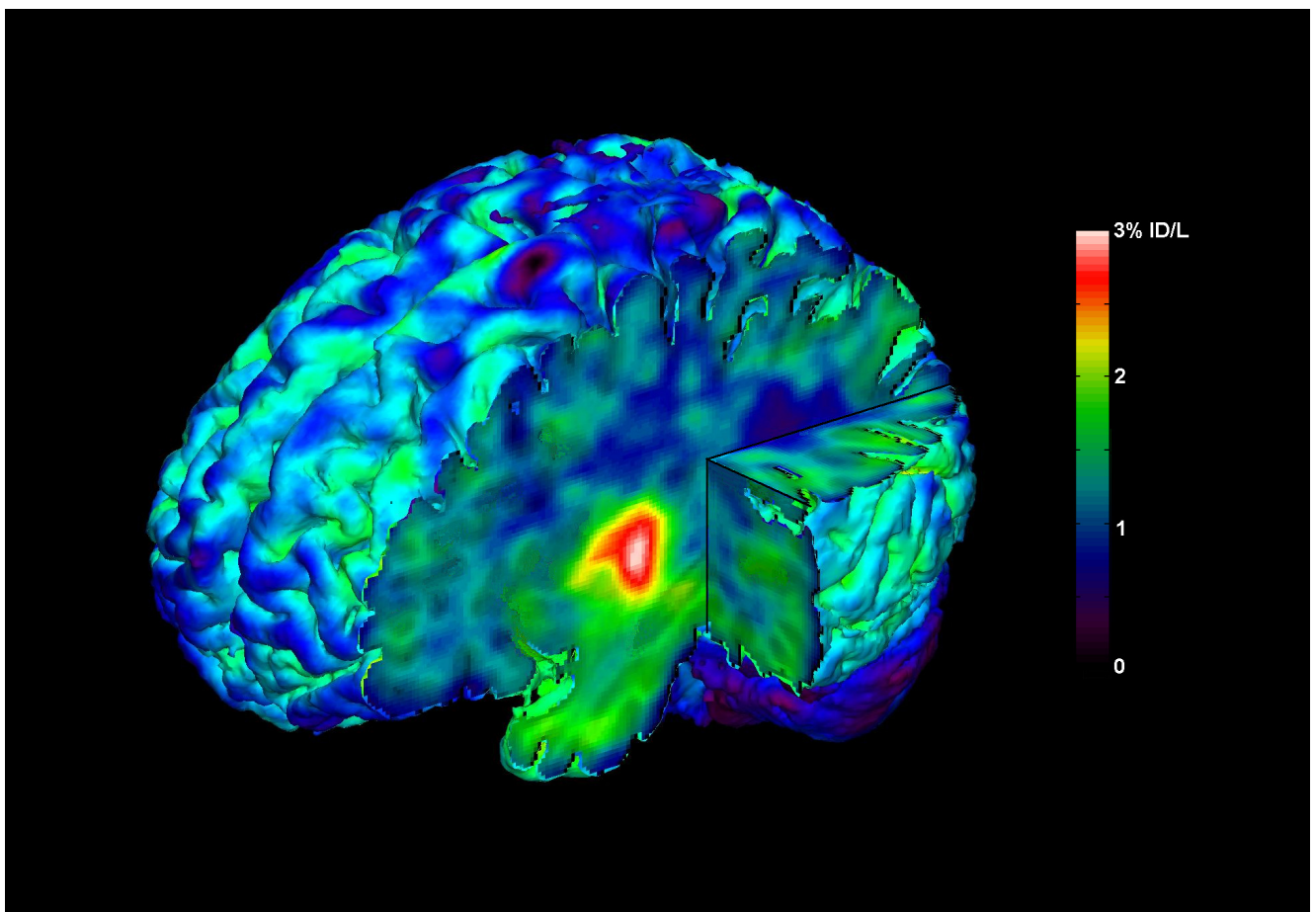


Figure 2. Cerebral 5-HT<sub>4</sub> receptor distribution in a healthy male, measured with [<sup>11</sup>C]SB207145-PET and coregistered with MRI. The image scale is given as Standard Uptake Values, integrated from 60 to 120 min after injection, and normalized by the injected dose (ID). The highest binding in the image is seen in the lateral part of striatum and intermediate binding in hippocampus. Cerebellum is deep blue, and represents non-displaceable binding only.

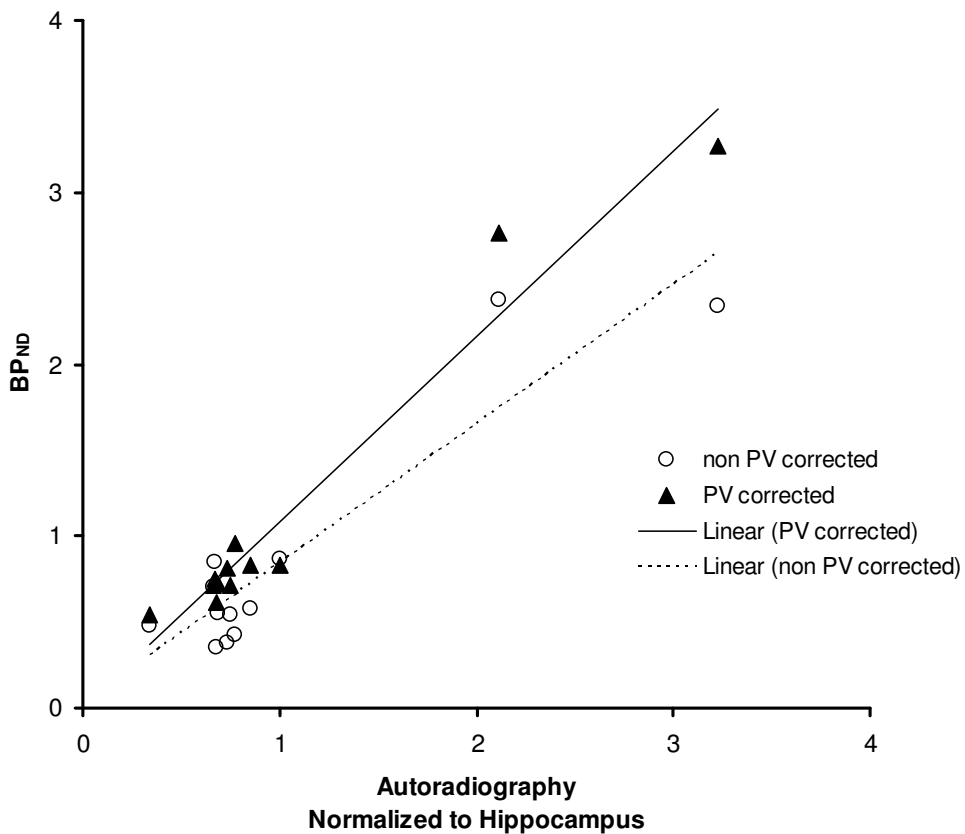


Figure 3. Cerebral 5-HT<sub>4</sub> receptor binding, as assessed *in vivo* with [<sup>11</sup>C]SB207145-PET in comparison to autoradiography in twelve selected regions: occipital cortex, frontal cortex, temporal cortex, parietal cortex, insula, anterior cingulate, posterior cingulate, amygdala, hippocampus, thalamus, putamen, and caudate nucleus. Autoradiographic data are averaged from three *post mortem* studies of the human brain with [<sup>125</sup>I]SB207710 (Varnas et al., 2004) (mean of cortical layers, n=3-7), [<sup>3</sup>H]Prucalopride and [<sup>3</sup>H]R116712 (Bonaventure et al., 2000) (n=3), and [<sup>3</sup>H]R116712 (Reynolds et al., 1995), normalized to the hippocampal binding. The [<sup>11</sup>C]SB207145 binding potential values are averaged for eight males both with and without PV correction (Spearman rank correlation, non-PV corrected: r= 0.50, p=0.095, PV corrected: r= 0.86, p=0.0003).

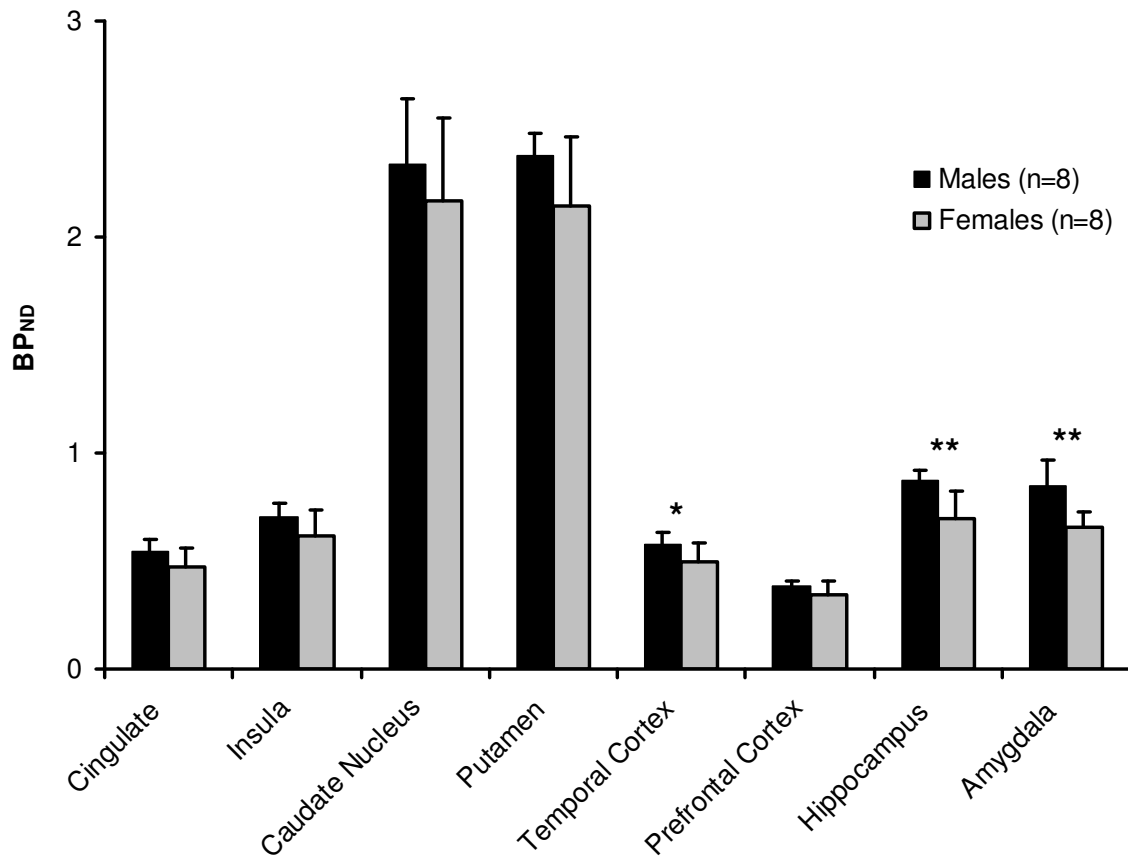


Figure 4. Mean  $BP_{ND} \pm 1 SD$  for males (n=8) and females (n=8) in eight selected regions. Statistically significant sex differences are indicated as: \* $p < 0.05$ , \*\* $p < 0.005$ .

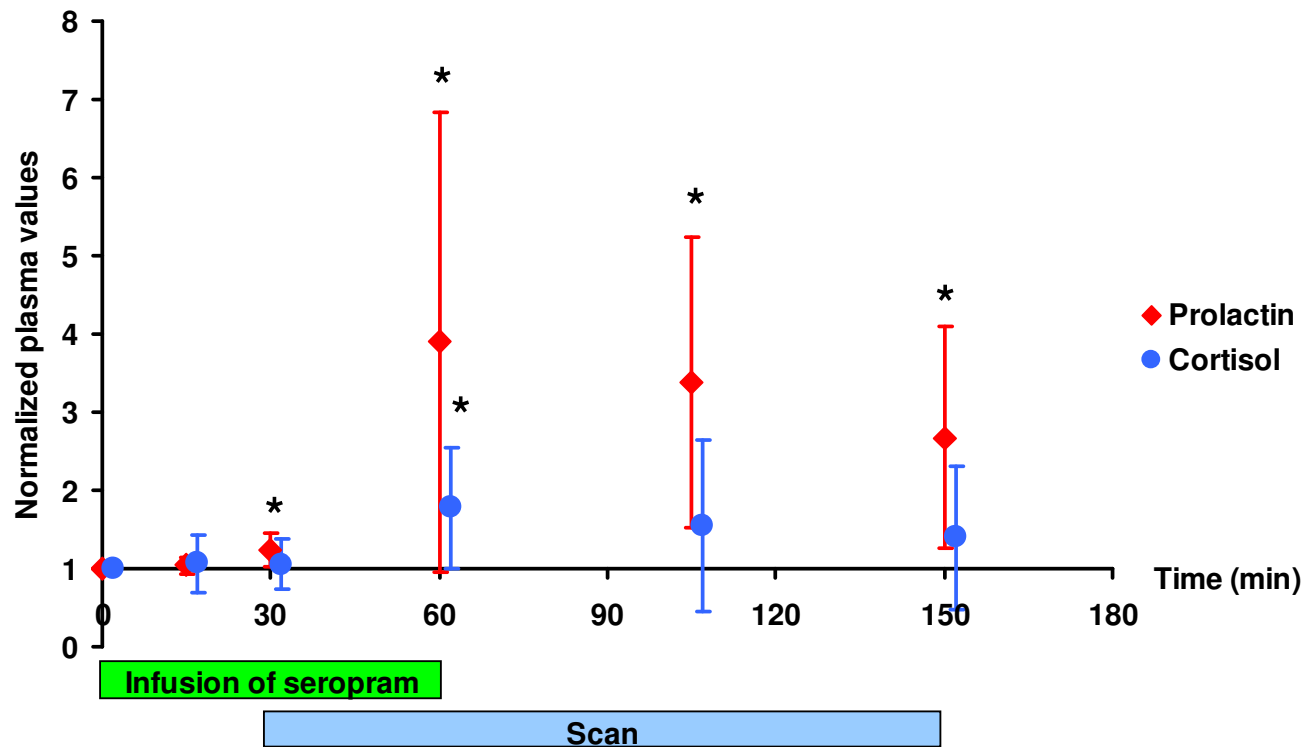


Figure 5. Plasma prolactin and cortisol concentrations as biomarkers of hypothalamic serotonin release in response to Citalopram infusion. Plasma prolactin values (range 77-1655 mIU/L) are normalized to baseline plasma prolactin concentration. Significant, but highly varying increases in plasma prolactin and cortisol levels were observed. Error bars represent one standard deviation. \*  $p < 0.05$ .

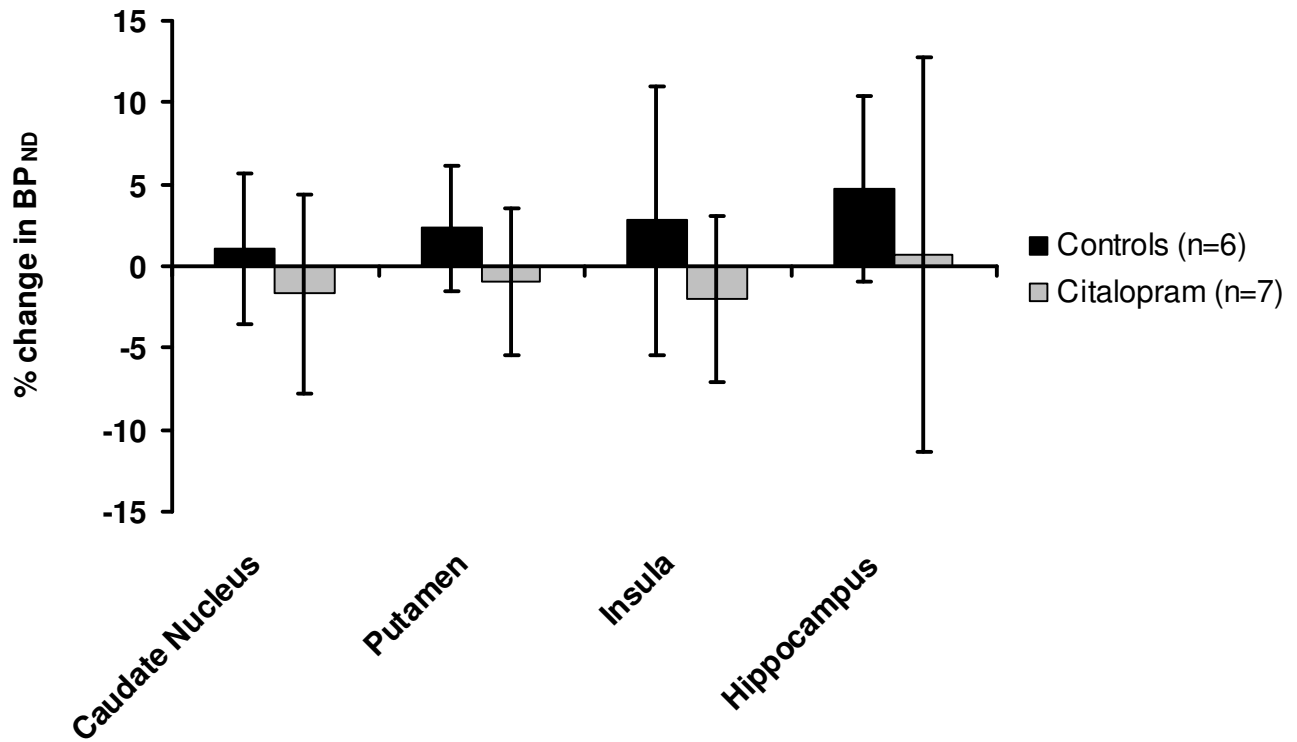


Figure 6. The relative change in  $BP_{ND}$  between first and second scan in untreated test-retest subjects (black) and in citalopram-treated subjects (gray). Error bars indicate 95% confidence intervals.